# Electrospun Separator for Structural Battery Applications

By

**Wisawat Keaswejjareansuk**

*A Dissertation Submitted to the Faculty of the*
**WORCESTER POLYTECHNIC INSTITUTE**
*in partial fulfillment of the requirements for the*
Degree of Doctor of Philosophy
*in*
Mechanical Engineering

April 2019

APPROVED:

_____

Professor Jianyu Liang, Research Advisor

_____

Professor Richard D. Sisson, Jr., ME Graduate Committee Representative

# ABSTRACT

Lithium-ion battery (LIB) is widely utilized in many modern applications as energy sources. Numerous efforts have been dedicated to increasing electrochemical performances, but improvement on battery safety remains a visible challenge. While new electrode materials have been developed, advancement in new separator for LIB has remained relatively slow. Separator is the polymeric porous material that physically separates electrodes and allows free flow of ions through its structure. It is electrochemically inactive but essential for avoiding thermal runaway conditions. Besides its crucial functions, separator has been known as the mechanically weakest component. Structural battery is a new approach that employs multifunctional material concept to use LIB as load-bearing material to minimize the weight of the complete system and maximize the efficiency. Separator materials are required to have good thermal stability, battery chemistry, and mechanical performance. This work aims at creating electrospun membranes with improved thermal resistance, structural integrity and moderate ionic conductivity as the next generation LIB separators. Electrospinning process is known as a versatile and straightforward technique to fabricate continuous fibers at nano- and micro- scales. The electrospinning process employs an electrostatic force to control the production of fibers from polymer solutions. Solution and process parameters, including type of polymer and solvent system, concentration of polymer solution, acceleration voltage, and solution feed rate, have been studied to achieve the desirable membrane properties. In this report, the electrospinning parameters affecting morphology and corresponding properties of electrospun membranes, electrospun polymer composite and polymer-metal oxide composite membranes for structural battery applications will be discussed.

# ACKNOWLEDGEMENT

# TABLE OF CONTENTS

# TABLE OF FIGURES

# TABLE OF TABLES

# CHAPTER 1 INTRODUCTION

## 1. BACKGROUND

The most common commercial lithium-ion batteries are in forms of cylindrical cell, pouch cell or coin cells. These batteries are generally rigid structures and account for significant portion of weight of the devices they power. For example, battery capacity and vehicle mass in the developments of electric vehicle is visualized in Figure 1. In addition to the mass and battery capacity concerns, rapid developments of electronic and information technologies moving toward high integration, high power and multifunctionality demand high capacity batteries with flexibility in shape, size and structure/safety integrations. Beside the demands of higher capacity, Figure 2 presents the projecting increment of the U.S. lithium-ion battery market revenue by product from 2014 - 2025.
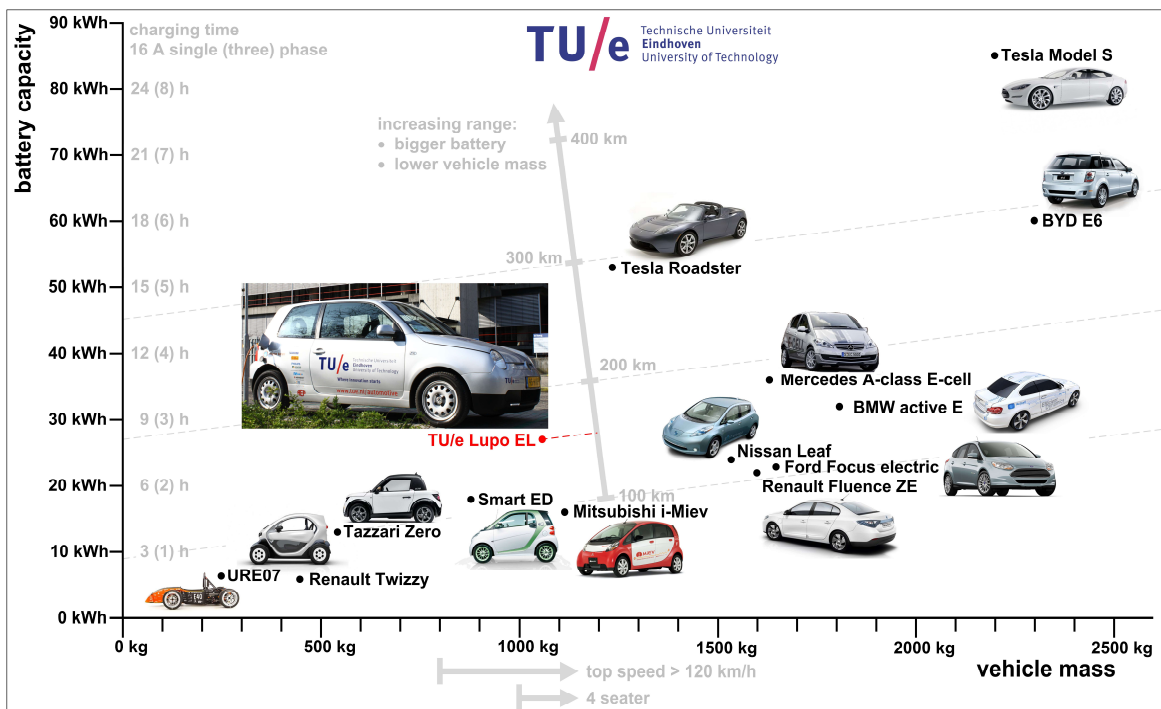


Figure 1 Overview of electric vehicle: battery capacity vs. vehicle mass [1]
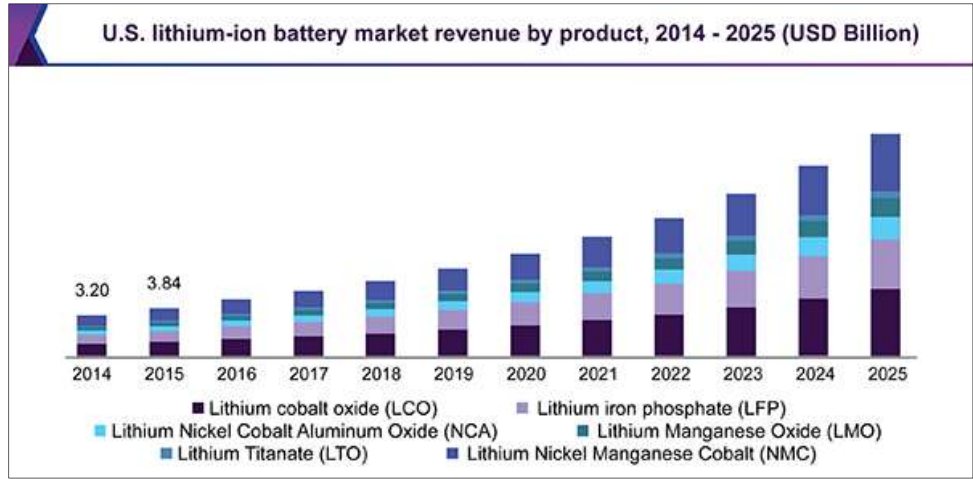
Figure 2 U.S. lithium-ion battery market revenue by product, 2014 - 2025 [2]

Lithium-ion batteries consist of a positive electrode (also called intercalation compounds), a negative electrode and a separator. The current mainstream commercial separator is a porous membrane that is soaked with electrolyte to allow ions transport through its structure and prevent electrons to pass through or direct physical contact between electrodes. Lithium-ions transport between negative and positive electrodes internally, whereas electrons transport externally. The separator for liquid electrolyte lithium-ion battery does not participate in electrochemical reactions. It is considered to be a crucial component for avoiding thermal runaway conditions. In the *discharge stage*, ions transport from negative electrode (oxidation reaction, called anode) to positive electrode (reduction reaction, called cathode) and reverse transportation in *charge state*.
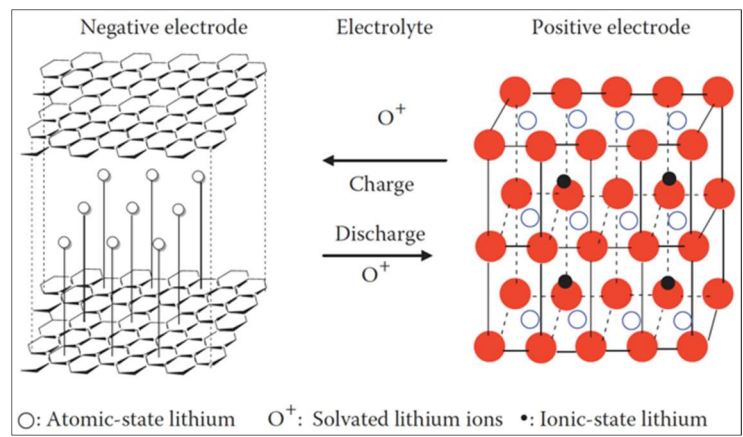


Figure 3 Schematic illustration of lithium-ion battery operation [3]

## 1.1 Commercialized separator materials for lithium-ion battery

In commercial lithium-ion batteries, anode materials include carbons, nitrides, silicon-based materials, carbon nanotubes, tin-based materials, nano-oxide and other alloys. Cathode materials are transition metal oxides that able to reversibly intercalate lithium at a high potential difference to anode materials. Table 1 shows materials and design of commercial separators from major manufacturers. While there are many developments of electrode materials, polyolefin has been used as the primary separator materials.

Table 1 Major separator manufacturers [4]

| Manufacturer | Materials | Design |
|---|---|---|
| Asahi Kasei chemicals | Polyolefin, ceramic-filled polyolefin | Biaxial oriented |
| Celgard LLC | PE, PP and PP/PE/PP | Uniaxial oriented |
| Entek membranes | Ceramic-filled UHMW PE | Biaxial oriented |
| ExxonMobil/Tonen | PE and PE/PP mixture | Biaxial oriented |
| SK energy | PE | Biaxial oriented |
| Ube industries | PP/PE/PP | Uniaxial oriented |

Three types of separator for liquid electrolyte system are (1) porous separator - the common type of commercial separator, (2) non-woven mat and (3) composite/ceramic-enhanced separator.

- Commercial separators are porous and created by semi-crystalline polyolefin. Regardless of separator design, *polyolefin is anisotropic*. The commercial separators have excellent mechanical properties in transverse direction and poor in machine direction. Tensile tests are performed on polypropylene (Celgard 2400) and polyethylene (Celgard 2500) separators (1-inch by 4-inch) at a strain rate of 0.4 mm/min. Surprisingly, tensile strength in transverse direction are 115-130 MPa, however, only 9-12 MPa in machine direction. The tensile tests confirm that the separators are easily damaged by dendrite growth, external puncture forces and tension force. Those damages allow internal short circuits that lead to batteries catching fire.
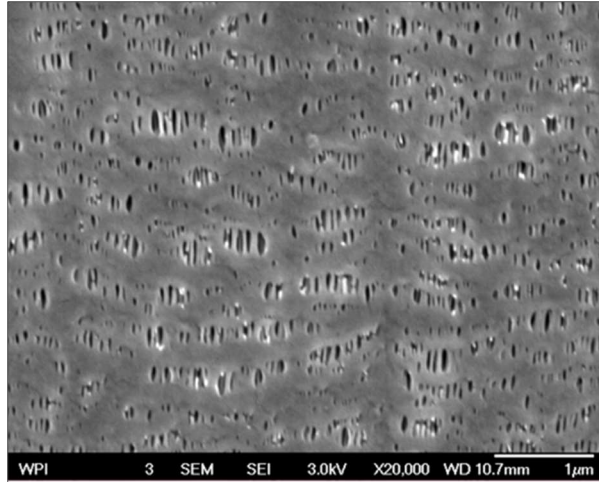
Figure 4 Porous commercial polypropylene separators, Celgard 2400
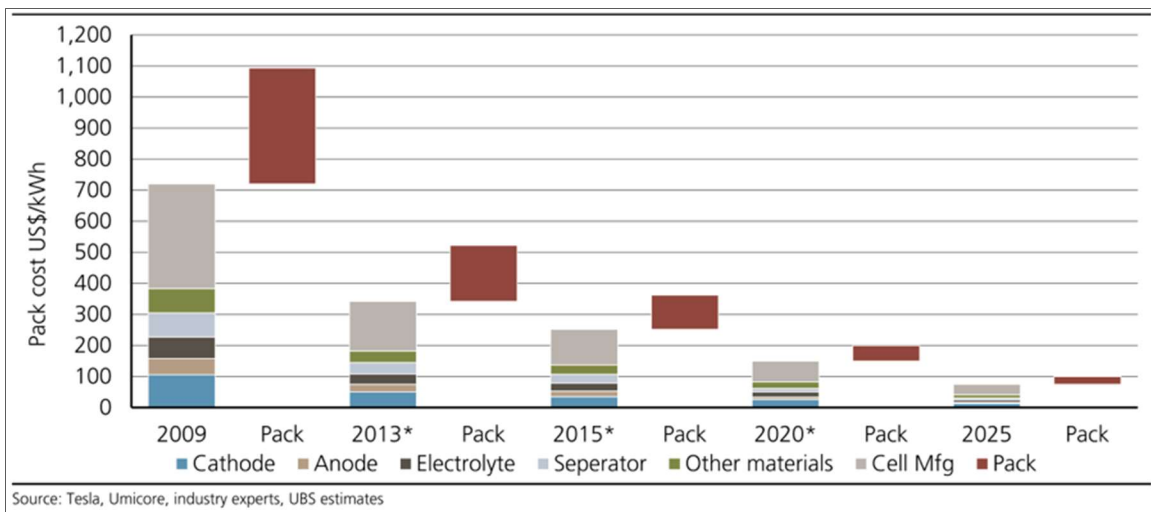


Figure 5 Costs of battery pack and breakdown: costs of separator continue to decrease [5]

- Non-woven mat separators are created by various processes, for examples wet-laid, air-laid, melt blowing and electrospinning/electrospraying. Advantages of non-woven mat are high porosity, lightweight and low process cost. Different organic and inorganic mats can be fabricated to provide high heat resistance and good mechanical properties. Non-woven mat usually has large pore size, therefore, thicker non-woven mat is required to prevent dendrites from penetrating through the pores. Currently, non-woven mats are used as supports for porous separators.
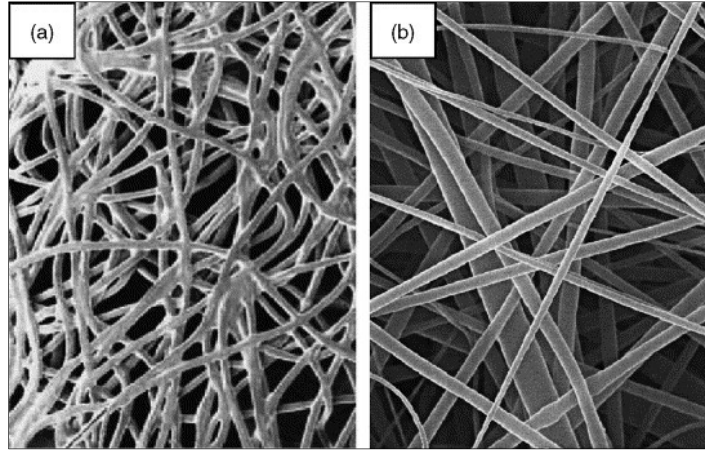
Figure 6 Non-woven mats made by (a) wet-laid and (b) electrospinning methods [5]

- Composite separators can be produced by (1) using different polymers with high melting temperatures, (2) coating a supporting porous polyolefin or nonwoven structure with a layer of inorganic particle or (3) incorporating inorganic fillers (less than micro size) into the porous or nonwoven membrane. In general, composite/ceramic-enhanced separator has excellent wettability, thermal stability and thermal conductivity for fast dissipation of heat. On another hand, it has low tensile strength and higher weight than the polymeric separator. Electrochemical stability of ceramic and ceramic binding in highly oxidizing and reducing stages is currently unknown.
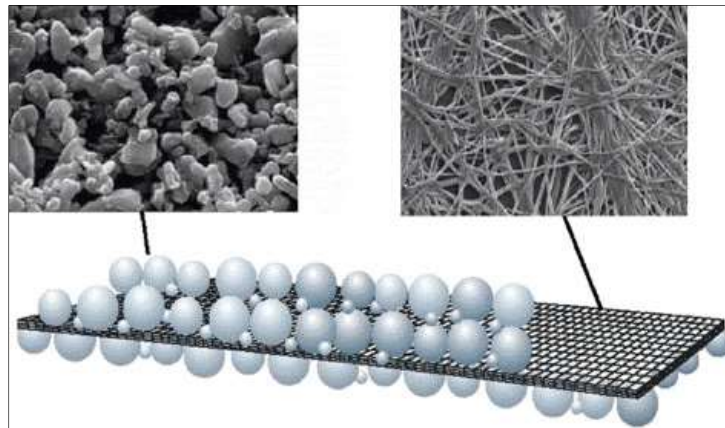


Figure 7 Schematic of polymer/ceramic composite separator [5]

**1.2 Research on separator materials for lithium-ion battery**

Figure 8 visualizes research trends by the percent of publications on lithium-ion battery from 2007-2018. Anode materials are the majority proportions followed by cathode materials. Because of the high-energy demands of lithium-ion batteries and electrochemical inactive nature of separators, the majority of research works focus on improving electrodes to have higher energy capability (in a unit of watts-hour per gram) and materials stability [6]–[43]. Consequently, the separator has had much less advancements than those of electrode materials. According to the number of research publications, the separator accounts for less than 10% and exhibits tendency to decrease during last decade. Further research on separators includes:

- Realize low cost fabrication process
- Create separator with high thermal stability and improved mechanical properties
- Increase understanding of separator behaviors during operation
- Achieve multifunctional separator to improve the battery performance and ensure safety.
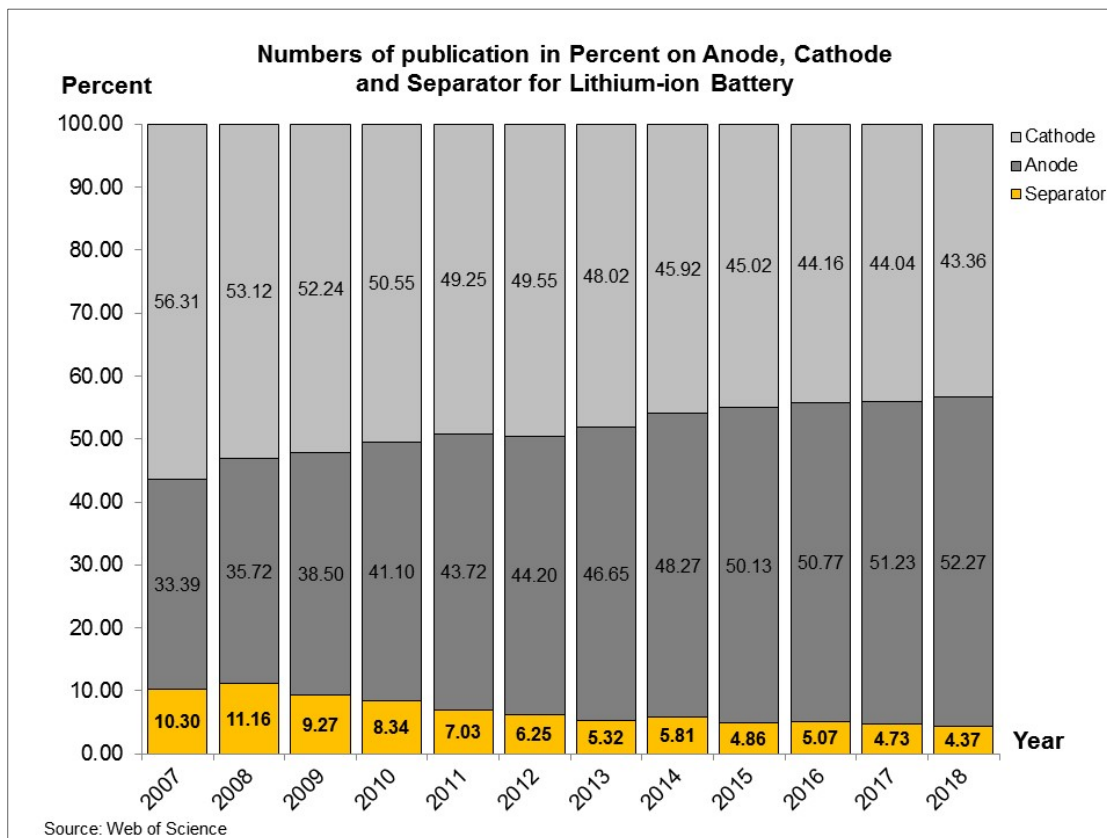


Figure 8 Lithium-ion battery research trends by percent of publications from 2007-2018
(Source: Web of Sciences)

## 2. RESEARCH OBJECTIVES

This work is aimed to improve the thermal, mechanical and electrochemical properties of separators for the structural purposes of LIBs by using electrospinning process for creating porous continuous, fibrous membranes to serve as next generation separators for LIBs. The objectives include:

1) understanding the controls of the electrospinning parameters for customized membranes' morphology and corresponding properties.

2) developing separators with controlled property in forms of

      (1) polymer layer-by-layer structure and

      (2) polymer-metal oxide composites

These two forms of electrospun membranes will be defined as strategies for creating the electrospun separators with the controlled structural properties.

# 3 RESEARCH PLAN

This research plan has three phases: 1) gains the understanding of electrospinning process, 2) fabricate the layer-by-layer structure with controlled properties and the composite membranes with polymer and metal oxide, and 3) characterize the properties of the fabricated membranes. Overall expectations of this research are to create porous membranes with mechanical, thermal and chemical integrations and promote battery multifunctionality.

*The first phase* aims to gain the understanding of the electrospinning process. Poly(bisphenol a-co-epichlorohydrin) (PBE) is chosen in the studies of the electrospinning process as a model thermoplastic resin due to its versatile applications. PBE has a good miscibility with various polymers [44][45][46]. It has been used to increase tensile strength and elongation [47], elastic modulus [48] and flexural strength of thermoplastics [49], improves storage modulus of carbon nanotube composites [50][51] and increase glass transition temperature of functional polymer blends [52][53]. Process parameters in these studies are acceleration potential, tip-to-collector distance and solution feed rate. Solution parameters in terms of solution concentration and solvent system are examined under the controlled process parameters.

*The second phase* uses the electrospinning process to 1) fabricate the membranes with layer-by-layer structure and 2) fabricate the composite membranes with metal oxide. Materials are polyethylene oxide (PEO), poly(vinylidene difluoride-co-hexafluoropropylene) (PVdF-HFP) and titanium dioxide (commercial grades) nanofillers. PEO is a semi-crystalline (70-82% [54]), hydrophilic and low toxic polymer with good thermal properties, high dielectric constant, strong $Li^+$ solvating abilities and interfacial stable with Li electrode. In additional to amorphous phase, ethylene oxide units are promoting ions transportation due to having a high donor number for $Li^+$ and high chain flexibility [55]. PVdF-HFP is a common semi-crystalline polymer, being used as material for separators due to good chemical stability, high solubility in various organic solvents and high anodic stability. Although PVdF-HFP has low crystallinity, the crystalline VdF provides sufficient mechanical supports whereas the amorphous HFP assists higher ionic conduction [56][57][58]. Metal oxide nanofillers depress the crystallinity of polymer and increase the electrolyte uptake [59][60]. The metal oxide nanofillers is expected to improve ionic conductivity and mechanical properties of the fabricated membranes.

*The third phase* characterizes the properties of the fabricated membranes with extensive characterization methods, including SEM, XRD, DSC, TGA, tensile test and AC impedance spectroscopy. Microstructure

and corresponding tensile strength and elastic modulus are analyzed. Thermal stability was characterized by the DSC and TGA analysis. Ionic conductivity of the fabricated membranes is examined by the AC impedance spectroscopy method.

## 4. DISSERTATION ORGANIZATION

There are 4 parts included in this dissertation. Firstly, an introduction provides readers with motivation, objectives, and research plan for this study. The second part is a literature reviews on structural battery and electrospun separator to summarize its current advancement toward structural applications, and the characterization of electrospun separator. The third part is a compilation of articles submitted or to be submitted to peer-reviewed journals. Finally, the forth part makes a conclusion of experimental works and perspective of electrospun separator for structural applications.

# REFERENCES

[1]     I. Besselink, "Overview of Full Electric Vehicles, Battery Capacity vs Weight," 2012. [Online]. Available: https://steinbuch.wordpress.com/2012/09/10/overview-of-full-electric-vehicles-battery-capacity-vs-weight/. [Accessed: 16-Apr-2019].

[2]     Grand View Research, "Lithium-Ion Battery Market Analysis By Product (Lithium Cobalt Oxide, Lithium Iron Phosphate, NCA, LMO, LTO, Lithium Nickel Manganese Cobalt (NMC)), By Application, And Segment Forecasts, 2018 - 2025," 2017.

[3]     F. A. Silva, *Lithium-Ion Batteries: Fundamentals and Applications [Book News]*, vol. 10, no. 1. London: CRC Press, 2016.

[4]     X. Huang, "Separator technologies for lithium-ion batteries," *Journal of Solid State Electrochemistry*, vol. 15, no. 4. Springer-Verlag, pp. 649–662, 30-Apr-2011.

[5]     S. S. Zhang, "A review on the separators of liquid electrolyte Li-ion batteries," *Journal of Power Sources*, vol. 164, no. 1. pp. 351–364, 2007.

[6]     L. Wang, X. He, W. Sun, J. Wang, Y. Li, and S. Fan, "Crystal Orientation Tuning of LiFePO$_4$ Nanoplates for High Rate Lithium Battery Cathode Materials," *Nano Lett.*, vol. 12, no. 11, pp. 5632–5636, 2012.

[7]     Y. Da Li, S. X. Zhao, C. W. Nan, and B. H. Li, "Electrochemical performance of SiO2-coated LiFePO4cathode materials for lithium ion battery," *J. Alloys Compd.*, vol. 509, no. 3, pp. 957–960, Jan. 2011.

[8]     K. Amine *et al.*, "Nanostructured anode material for high-power battery system in electric vehicles," *Adv. Mater.*, vol. 22, no. 28, pp. 3052–3057, 2010.

[9]     A. S. Prakash, P. Manikandan, K. Ramesha, M. Sathiya, J. M. Tarascon, and A. K. Shukla, "Solution-combustion synthesized nanocrystalline Li4Ti 5O12 as high-rate performance li-ion battery anode," *Chem. Mater.*, vol. 22, no. 9, pp. 2857–2863, 2010.

[10]    H. Song *et al.*, "A bottom-up synthetic hierarchical buffer structure of copper silicon nanowire hybrids as ultra-stable and high-rate lithium-ion battery anodes," *J. Mater. Chem. A*, vol. 6, no. 17, pp. 7877–7886, May 2018.

[11]    J. Han *et al.*, "Creating graphene-like carbon layers on SiO anodes via a layer-by-layer strategy for lithium-ion battery," *Chem. Eng. J.*, vol. 347, no. January, pp. 273–279, Sep. 2018.

[12]    X. Sun, C. Shao, F. Zhang, Y. Li, Q.-H. Wu, and Y. Yang, "SiC Nanofibers as Long-Life Lithium-Ion Battery Anode Materials," *Front. Chem.*, vol. 6, p. 166, May 2018.

[13]    D. Liao, X. Kuang, J. Xiang, and X. Wang, "A Silicon Anode Material with Layered Structure for the Lithium-ion Battery," *J. Phys. Conf. Ser.*, vol. 986, no. 1, p. 012024, 2018.

[14] J. Qin *et al.*, "Graphene networks anchored with Sn@Graphene as lithium ion battery anode," *ACS Nano*, vol. 8, no. 2, pp. 1728–1738, 2014.

[15] X. Zhu, Y. Zhu, S. Murali, M. D. Stoller, and R. S. Ruoff, "Nanostructured Reduced Graphene Oxide/Fe$_2$O$_3$ Composite As a High-Performance Anode Material for Lithium Ion Batteries," *ACS Nano*, vol. 5, no. 4, pp. 3333–3338, 2011.

[16] L. Fei *et al.*, "Reduced graphene oxide wrapped fes nanocomposite for lithium-ion battery anode with improved performance," *ACS Appl. Mater. Interfaces*, vol. 5, no. 11, pp. 5330–5335, 2013.

[17] Y. Sun, X. Hu, W. Luo, and Y. Huang, "Self-assembled hierarchical MoO2/graphene nanoarchitectures and their application as a high-performance anode material for lithium-ion batteries," *ACS Nano*, vol. 5, no. 9, pp. 7100–7107, 2011.

[18] A. Pan *et al.*, "Template free synthesis of LiV$_3$O$_8$ nanorods as a cathode material for high-rate secondary lithium batteries," *J. Mater. Chem.*, vol. 21, no. 4, pp. 1153–1161, 2011.

[19] G. Zhou *et al.*, "Graphene-wrapped Fe3O4anode material with improved reversible capacity and cyclic stability for lithium ion batteries," *Chem. Mater.*, vol. 22, no. 18, pp. 5306–5313, 2010.

[20] Z. S. Wu, W. Ren, L. Xu, F. Li, and H. M. Cheng, "Doped graphene sheets as anode materials with superhigh rate and large capacity for lithium ion batteries," in *ACS Nano*, 2011, vol. 5, no. 7, pp. 5463–5471.

[21] Y. Shi *et al.*, "Hollow structured Li3VO4wrapped with graphene nanosheets in situ prepared by a one-pot template-free method as an anode for lithium-ion batteries," *Nano Lett.*, vol. 13, no. 10, pp. 4715–4720, 2013.

[22] B. Li, H. Cao, J. Shao, G. Li, M. Qu, and G. Yin, "Co3O4@graphene composites as anode materials for high-performance lithium ion batteries," *Inorg. Chem.*, vol. 50, no. 5, pp. 1628–1632, 2011.

[23] S. H. Lee *et al.*, "Graphene-nanotube-iron hierarchical nanostructure as lithium ion battery anode," *ACS Nano*, vol. 7, no. 5, pp. 4242–4251, 2013.

[24] H. Wang *et al.*, "Mn3O4-graphene hybrid as a high-capacity anode material for lithium ion batteries," *J. Am. Chem. Soc.*, vol. 132, no. 40, pp. 13978–13980, 2010.

[25] Y. P. Wu, E. Rahm, and R. Holze, "Carbon anode materials for lithium ion batteries," *J. Power Sources*, vol. 114, no. 2, pp. 228–236, Mar. 2003.

[26] C. S. Wang, G. T. Wu, and W. Z. Li, "Lithium insertion in ball-milled graphite," *J. Power Sources*, vol. 76, no. 1, pp. 1–10, Nov. 1998.

[27] A. K. Shukla and T. Prem Kumar, "Materials for next-generation lithium batteries," *Current Science*, vol. 94, no. 3. IOP Publishing, pp. 314–331, 15-Apr-2008.

[28] K. Evanoff *et al.*, "Ultra strong silicon-coated carbon nanotube nonwoven fabric as a

multifunctional lithium-ion battery anode," *ACS Nano*, vol. 6, no. 11, pp. 9837–9845, 2012.

[29]   A. Pan *et al.*, "Nanosheet-structured LiV3O8 with high capacity and excellent stability for high energy lithium batteries," *J. Mater. Chem.*, vol. 21, no. 27, p. 10077, 2011.

[30]   C. K. Chan *et al.*, "High-performance lithium battery anodes using silicon nanowires," *Nat. Nanotechnol.*, vol. 3, no. 1, pp. 31–35, Jan. 2008.

[31]   C. De Las Casas and W. Li, "A review of application of carbon nanotubes for lithium ion battery anode material," *Journal of Power Sources*, vol. 208. Elsevier, pp. 74–85, 15-Jun-2012.

[32]   T. Shen, Z. Yao, X. Xia, X. Wang, C. Gu, and J. Tu, "Rationally Designed Silicon Nanostructures as Anode Material for Lithium-Ion Batteries," *Advanced Engineering Materials*, vol. 20, no. 1. 2018.

[33]   M. Kakunuri and C. S. Sharma, "Resorcinol-formaldehyde derived carbon xerogels: A promising anode material for lithium-ion battery," *Journal of Materials Research*, vol. 33, no. 9, pp. 1074–1087, 2018.

[34]   E. Hosono, T. Kudo, I. Honma, H. Matsuda, and H. Zhou, "Synthesis of single crystalline spinel LiMn2O4 nanowires for a lithium ion battery with high power density," *Nano Lett.*, vol. 9, no. 3, pp. 1045–1051, 2009.

[35]   R. Ruffo, S. S. Hong, C. K. Chan, R. A. Huggins, and Y. Cui, "Impedance analysis of silicon nanowire lithium ion battery anodes," *J. Phys. Chem. C*, vol. 113, no. 26, pp. 11390–11398, 2009.

[36]   B. Varghese *et al.*, "Fabrication of NiO nanowall electrodes for high performance lithium ion battery," *Chem. Mater.*, vol. 20, no. 10, pp. 3360–3367, 2008.

[37]   Y. Xia, J. Zheng, C. Wang, and M. Gu, "Designing principle for Ni-rich cathode materials with high energy density for practical applications," *Nano Energy*, vol. 49, pp. 434–452, Apr. 2018.

[38]   S. Sarkar, H. Banda, and S. Mitra, "High capacity lithium-ion battery cathode using LiV3O8nanorods," *Electrochim. Acta*, vol. 99, pp. 242–252, Jun. 2013.

[39]   X. Li, F. Cheng, B. Guo, and J. Chen, "Template-synthesized LiCoO2, LiMn2O4, and LiNi0.8Co0.2O2 nanotubes as the cathode materials of lithium ion batteries," *Journal of Physical Chemistry B*, vol. 109, no. 29. pp. 14017–14024, 2005.

[40]   S. Jouanneau, D. D. MacNeil, Z. Lu, S. D. Beattie, G. Murphy, and J. R. Dahn, "Morphology and Safety of Li[Ni[sub x]Co[sub 1−2x]Mn[sub x]]O[sub 2] (0≤x≤1/2)," *J. Electrochem. Soc.*, vol. 150, no. 10, p. A1299, 2003.

[41]   J. Y. Luo, H. M. Xiong, and Y. Y. Xia, "LiMn2O4 nanorods, nanothorn microspheres, and hollow nanospheres as enhanced cathode materials of lithium ion battery," *J. Phys. Chem. C*, vol. 112, no. 31, pp. 12051–12057, 2008.

[42]   D. K. Kim *et al.*, "Spinel LiMn 2O 4 nanorods as lithium ion battery cathodes," *Nano Lett.*, vol. 8,

no. 11, pp. 3948–3952, 2008.

[43]  Y. Q. Wang *et al.*, "Rutile-TiO2nanocoating for a high-rate Li4Ti5O12anode of a lithium-ion battery," *J. Am. Chem. Soc.*, vol. 134, no. 18, pp. 7874–7879, 2012.

[44]  M. A. Iriarte, J. J. Iruin, and J. I. Eguiazábal, "Thermal decomposition of miscible phenoxy/poly(ethylene oxide) blends," *J. Mater. Sci.*, vol. 24, no. 3, pp. 1021–1024, Mar. 1989.

[45]  R. Zhang, X. Luo, and D. Ma, "Miscibility of polyhydroxy ether of bisphenol-A with ethylene terephthalate-caprolactone copolyesters," *Eur. Polym. J.*, vol. 31, no. 10, pp. 1011–1014, Oct. 1995.

[46]  B. K. Kim and C. H. Choi, "Melt blends of poly(methyl methacrylate) with a phenoxy," *Polymer (Guildf).*, vol. 37, no. 5, pp. 807–812, Jan. 1996.

[47]  T. Yilmaz, Ö. Özarslan, E. Yildiz, A. Kuyulu, E. Ekinci, and A. Güngör, "Effects of nonreactive resins on the properties of a UV-curable methacrylated urethane resin," *J. Appl. Polym. Sci.*, vol. 69, no. 9, pp. 1837–1845, Aug. 1998.

[48]  G. Qipeng, H. Jinyu, L. Binyao, C. Tianlu, Z. Hongfang, and F. Zhiliu, "Blends of phenolphthalein poly(ether ether ketone) with phenoxy and epoxy resin," *Polymer (Guildf).*, vol. 32, no. 1, pp. 58–65, Jan. 1991.

[49]  H. Wu, C. M. Ma, and J. Lin, "Processability and Properties of Phenoxy Resin Toughened Phenolic Resin Composites," *J. Appl. Polym. Sci.*, vol. 63, no. March 1996, pp. 911–917, Feb. 1997.

[50]  B.-X. Yang, J.-H. Shi, K. P. Pramoda, and S. H. Goh, "Enhancement of stiffness, strength, ductility and toughness of poly(ethylene oxide) using phenoxy-grafted multiwalled carbon nanotubes," *Nanotechnology*, vol. 18, no. 12, p. 125606, Mar. 2007.

[51]  H. W. Goh, S. H. Goh, G. Q. Xu, K. P. Pramoda, and W. D. Zhang, "Dynamic mechanical behavior of in situ functionalized multi-walled carbon nanotube/phenoxy resin composite," *Chem. Phys. Lett.*, vol. 373, no. 3–4, pp. 277–283, May 2003.

[52]  Q. Guo, "Effect of curing agent on the phase behaviour of epoxy resin/phenoxy blends," *Polymer (Guildf).*, vol. 36, no. 25, pp. 4753–4760, Jan. 1995.

[53]  H. M. Jeong, B. K. Ahn, and B. K. Kim, "Miscibility and shape memory effect of thermoplastic polyurethane blends with phenoxy resin," *Eur. Polym. J.*, vol. 37, no. 11, pp. 2245–2252, Nov. 2001.

[54]  G. Wypych, *Handbook of Polymers*, 2nd ed. ChemTec Publishing, 2016.

[55]  Z. Xue, D. He, and X. Xie, "Poly(ethylene oxide)-based electrolytes for lithium-ion batteries," *J. Mater. Chem. A*, vol. 3, no. 38, pp. 19218–19253, 2015.

[56]  S. Abbrent, J. Plestil, D. Hlavata, J. Lindgren, J. Tegenfeldt, and Å. Wendsjö, "Crystallinity and

morphology of PVdF-HFP-based gel electrolytes," *Polymer (Guildf).*, vol. 42, no. 4, pp. 1407–1416, Feb. 2001.

[57]     H. Xie, Z. Tang, Z. Li, Y. He, Y. Liu, and H. Wang, "PVDF-HFP composite polymer electrolyte with excellent electrochemical properties for Li-ion batteries," *J. Solid State Electrochem.*, vol. 12, no. 11, pp. 1497–1502, Nov. 2008.

[58]     M. Stolarska, L. Niedzicki, R. Borkowska, A. Zalewska, and W. Wieczorek, "Structure, transport properties and interfacial stability of PVdF/HFP electrolytes containing modified inorganic filler," *Electrochim. Acta*, vol. 53, no. 4, pp. 1512–1517, Dec. 2007.

[59]     A. Manuel Stephan, K. S. Nahm, T. Prem Kumar, M. A. Kulandainathan, G. Ravi, and J. Wilson, "Nanofiller incorporated poly(vinylidene fluoride–hexafluoropropylene) (PVdF–HFP) composite electrolytes for lithium batteries," *J. Power Sources*, vol. 159, no. 2, pp. 1316–1321, Sep. 2006.

[60]     C. G. Wu, M. I. Lu, C. C. Tsai, and H. J. Chuang, "PVdF-HFP/metal oxide nanocomposites: The matrices for high-conducting, low-leakage porous polymer electrolytes," *J. Power Sources*, vol. 159, no. 1 SPEC. ISS., pp. 295–300, Sep. 2006.

## CHAPTER 2 LITERATURE REVIEW

## 2.1 Structural Battery

### 2.1.1 Early development and design

By the year of publications, "structural battery" was first conceptually introduced in 1998 by Panetta *et al.* [1] for NASA's nano-satellite technology development with requirements of compact, lightweight, thermal resistance and structural integrity to survivable in a space radiation environment. The earliest generation of the NASA's structural battery is in a form of nickel-hydrogen battery cells inside the honeycomb core. Five years later - 2003, Queheillalt *et al.* [2] emphasized "multifunctional structure" concept to the structural battery for nickel-metal hybrid and fiber based solid-state system. Multifunctional structure has capability to perform one or more functions simultaneously [3], for example combine load-bearing support in addition to distribute electrochemical energy supply, mechanical actuation or thermal management [2]. Different approaches have been utilized for designing structural lithium-ion battery including multifunctional structure, power fiber and laminated structural battery [4]. Shalouf *et al.* [3] fabricated the first-generation lithium structural battery by embedded rechargeable lithium polymer battery cells into carbon fiber/epoxy matrix composite laminates and tested for tensile, flexural and compressive loading. In 2006, Wetzel *et al.* [5] reported the design of structural battery concept consists of thin, planar architecture in analogue to laminated, fiber-reinforce composite materials. In this report, the synthesis of electrolytes those required both ion-conductive and mechanically robust were emphasized. Afterward, the developments of the structural battery have been using lithium-ion chemistry because of high energy density and cyclability [5]. Wong *et al.* [6] fabricated composite structural battery based on carbon fabric anode, glass fabric separator and stainless steel cathode, then performed the tensile test (Figure 11). Later, Liu *et al.* [7] proposed the modern design of structural lithium ion battery (Figure 12) consists of: (1) carbon fiber, cathode active material and structural binder as cathode material, (2) carbon fiber, anode active material as anode material and (3) insulating glass fiber separator. On the contrary modern design proposed by Liu *et al.*, the structural battery developments were still based on carbon fiber anode mat, functional polymer matrix layer and glass fiber/conventional lithium-ion battery separator. Timeline on the structural battery study and development efforts is listed in Table 2.
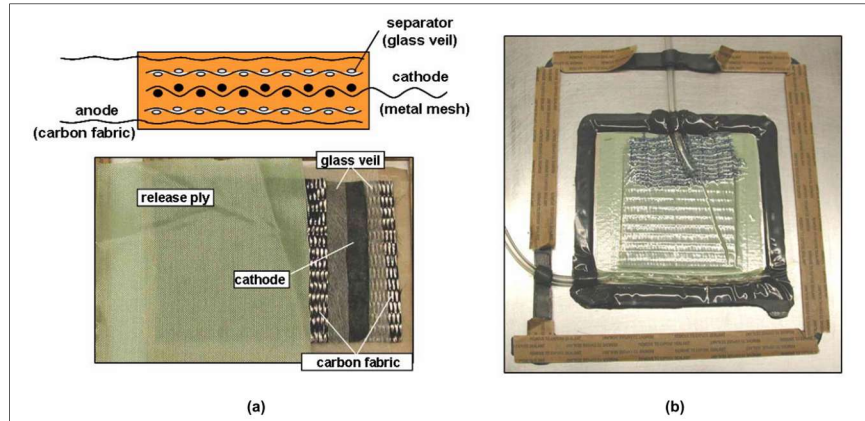
Figure 9 Composite structural battery in Wetzel *et al*. design [5] (a) Schematic and preform arrangement, and (b) preform undergoing vacuum infusion of electrolyte resin
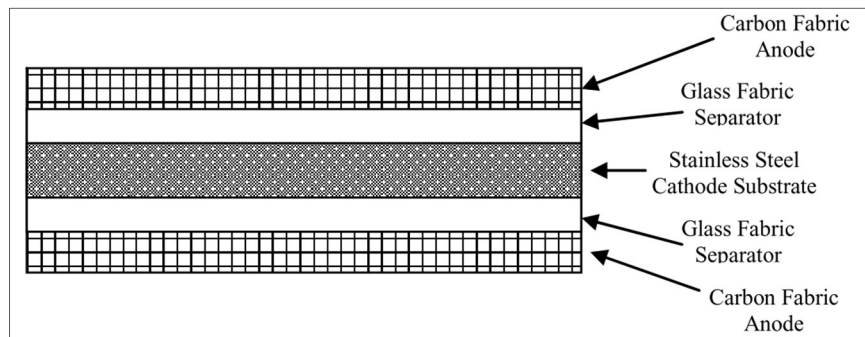


Figure 10 Composite structural battery based on carbon fabric anode, glass fabric separator and stainless steel cathode with LiFePO$_4$ chemistry in Wong *et al.* design [6]
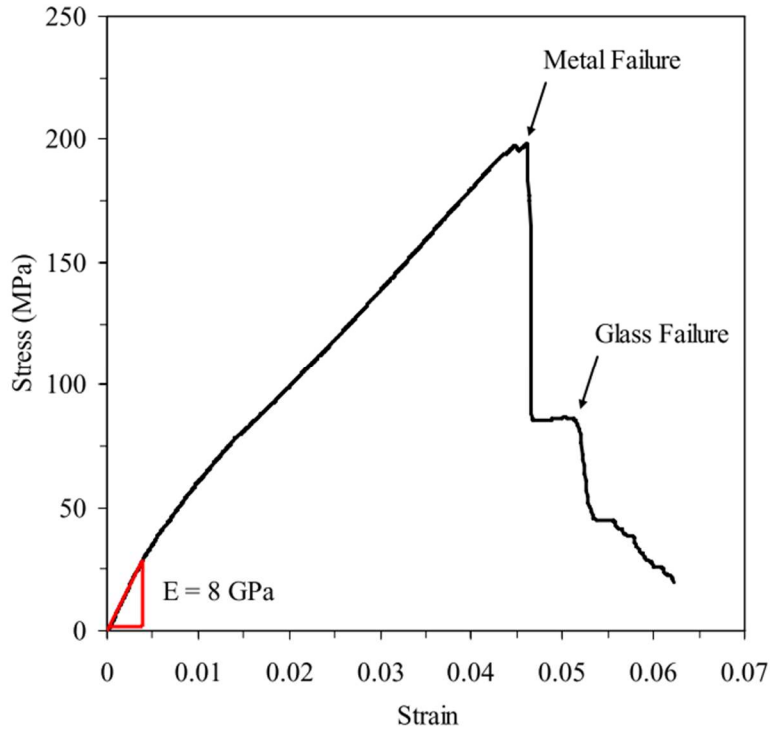
Figure 11 Stress-strain curve of composite structural battery used carbon fabric anode, glass fabric separator and stainless steel cathode with LiFePO$_4$ chemistry in Wong *et al.* [6] design
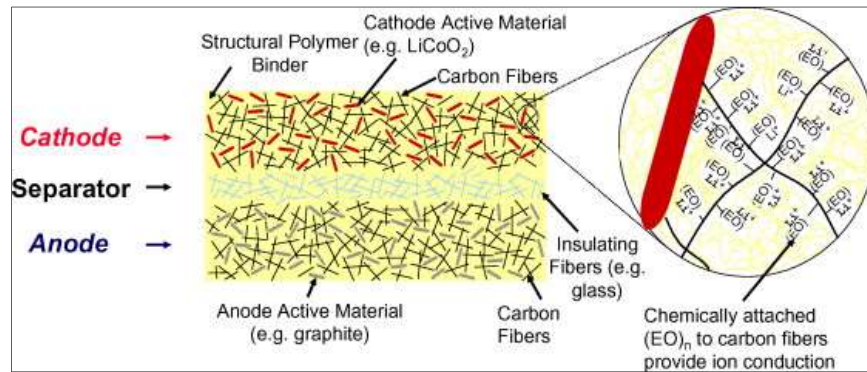


Figure 12 Modern design of structural lithium ion battery proposed by Liu *et al.* [7]

## 2.2.2 Structural electrode materials

Carbon fiber (CF) and carbon fiber reinforced plastic (CFRP) have been using in structural anode materials to the present because of many characteristics [8]: (1) high tensile strength, (2) high tensile stiffness-to-weight ratio, (3) have graphitic microstructure that enables reversible lithium-ion intercalation with carbon content higher than 90%. A study of lithium-ion intercalation to the mechanical property conducted by Jacques *et al.* [9] shows that tensile stiffness remained unchanged over time whereas the tensile strength partly irreversible dropped about 20% after lithiated and delithiated at varied C-rate. A study on CF LIB structural electrode [10] shows that the fiber stiffness was controlled by crystallite size and orientation, for example large crystallites and high ordered results in high stiffness. In recent development, vertically aligned multiwall carbon nanotubes and graphene-carbon nanotubes were grown on fabric electrodes from methane by chemical vapor deposition (Figure 13) [11]. The novel CNT-CF and graphene-CNT-CF were tested with impedance spectroscopy method using CNT-CF, graphene-CNT-CF and pristine-CF as working electrode; lithium metal as counter electrode; and, glass fiber separator in 1 M $LiPF_6$/1:1 EC:DMC (v/v) liquid electrolyte. The CNT-CF exhibited the minimum interfacial resistance in this study (Figure 14).
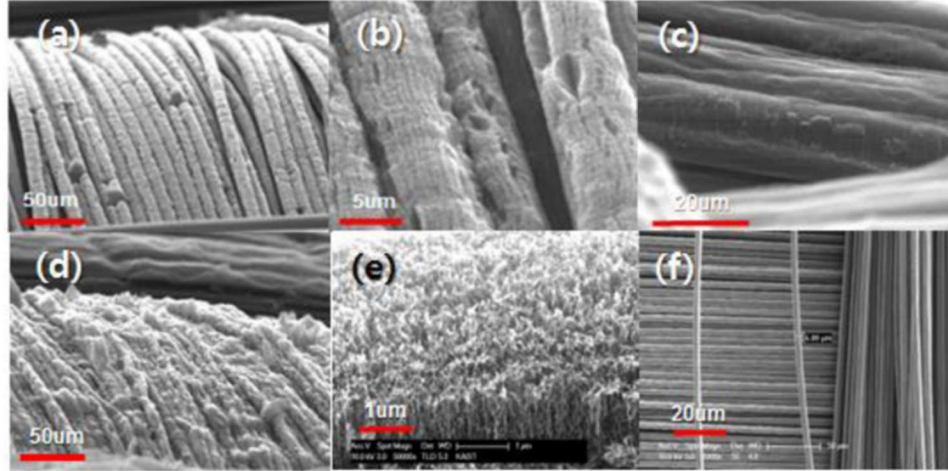


Figure 13 SEM micrograph showing the CNTs deposited on the carbon fabric, (d) G-CNTs deposited on the carbon fabric, (e) 50,000× magnification of CNTs deposited on the carbon fabrics, and (f) pristine carbon fabric in novel nonwoven fabric electrode reported by Park *et al.* [11]
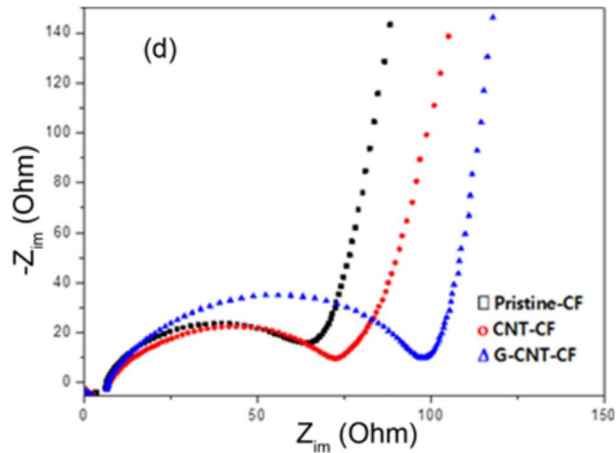
Figure 14 EIS spectra of CNT-CF, G-CNT- CF, and pristine-CF electrodes
in novel nonwoven fabric electrode reported by Park *et al.* [11]

### 2.2.3 Structural separator/electrolyte

Separator/electrolyte for structural battery has relatively less advancements than the structural electrodes. Polymers for structural battery separator/electrolyte were required to provide stiffness, strength and environmental durability through high crosslink density and low chain mobility [5]. Structural polymers/electrolytes were created by physical blending, synthesis of block copolymers and formation of partially crosslinked polymer networks [5]. In early development, Synder *et al*. [12] studied vinyl ester derivatives of poly(ethylene glycol) (PEG) solid polymer electrolyte for electrochemical and mechanical behaviors. Ihrner *et al.* [13] prepared structural lithium-ion battery electrolyte (ionic conductivity = 0.21 mS/cm and elastic modulus = 530 MPa) consists of a liquid phase and a stiff thermoset phase using reaction induced phase separation. In addition, diglycidylether of bisphenol-A (DGEBA) was mixed with $LiClO_4$/PC at different weight percent to form a polymer electrolyte [4]. The DGEBA-based polymer electrolytes with the highest ionic conductivity (1.58 mS/cm) exhibited extremely poor tensile strength (0.23 MPa) and elastic modulus (1.45 MPa). At the different weight percent that produced the polymer electrolyte with a tensile strength of 82 MPa and elastic modulus of 1.35 GPa, the ionic conductivity decreased to 0.81 µS/cm. Thus, both functionalities (ionic conductivity and mechanical property) have a tread-off relationship with each other.

Table 2 Timeline of structural battery study and development efforts by year of publications

| Year | Author | Developments |
|---|---|---|
| 1998 | Panetta et al. [1] | Conceptual introduced for nano-satellite technology development |
| 2003 | Queheillalt et al. [2] | Introduced multifunctional structure concept |
| 2003 | Shalouf et al. [3] | Embedded lithium polymer battery cell into carbon fiber/epoxy matrix |
| 2006 | Wetzel et al. [5] | Proposed the design of structural battery concept using lithium-ion chemistry |
| 2007 | Synder et al. [12] | Extensively studied the electrochemical and mechanical behavior of vinyl ester derivatives of poly(ethylene glycol) (PEG) |
| 2007 | Wong et al. [6] | Fabricated fiber-matrix composite |
| 2008 | Pereira et al. [14] | Embedded commercial thin film lithium cell in structural composites |
| 2009 | Liu et al. [7] | Re-design the multifunctional structure battery |
| 2012 | Kjell et al. [15] | Evaluated electrochemical property and performance of commercial PAN-based carbon fiber |
| 2013 | Jacques et al. [8][9] | Investigated performance of lithium-intercalated carbon fiber |
| 2014 | Asp et al. [16] | First presented state of the art in structural power composites |
| 2015 | Wang et al. [17] | Reported the thermal analysis of multifunctional structural battery for satellite applications |
| 2017 | Yu et al. [18] | Reported structural liquid/epoxy electrolyte in CFRP composite |
| 2017 | Ihrner et al. [13] | Prepared structural electrolyte used liquid electrolyte in stiff vinyl based thermoset matrix |
| 2018 | Calsted et al. [19] | Proposed a new conceptual design framework for laminated structural battery composites |
| 2018 | Fredi et al. [10] | Reported lithium-ion insertion mechanism in carbon fiber structural electrode |
| 2018 | Park et al. [11] | Reported carbon fabric, CNT-CF and graphene-CNT-CF fabricated by plasma-enhanced chemical vapor deposition |

## 2.2 Research Trends in Conventional Lithium-ion Battery Materials

Unlike the developments of structural battery, conventional lithium-ion battery has been being developed for energy density, safety and functionality. Studies of LIB rapidly increases in the last decade. Research on LIB materials by the numbers of publication from 2007-2018 are collected from the Web of Science and visualized in Figure 15. Similar to the development of structural battery, the percentage of advancements in separator for the conventional LIB materials that presented in the previous chapter (figure 7) clearly shows much slow progress than electrode materials.
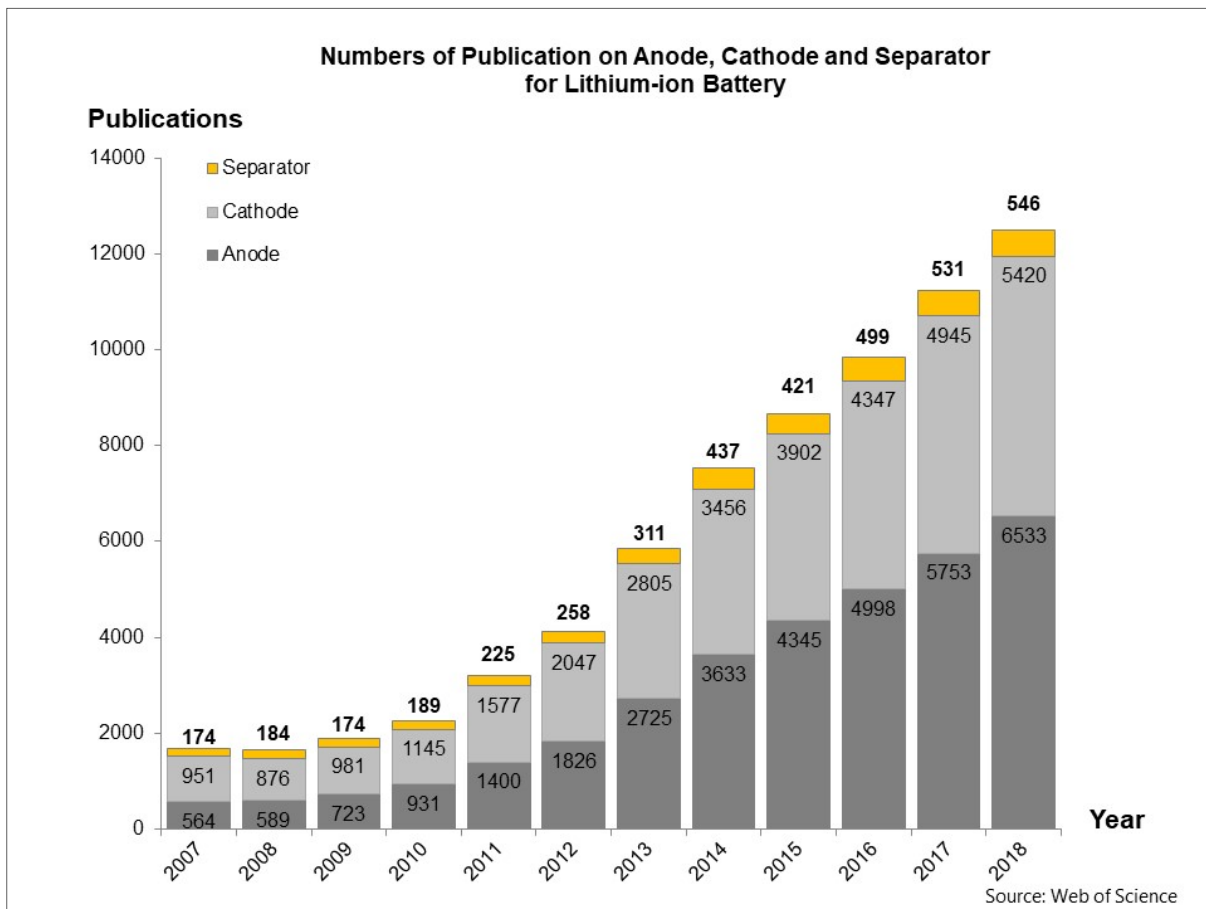


Figure 15 Numbers of publication on anode, cathode and separator for lithium-ion battery (2007-2018)

(Source: Web of Science)

## 2.3 Electrospinning method

### 2.3.1 Electrospinning and typical setups

*Electrospinning method (ES)* is a less complex process to create continuous fibers in micro- and nano- sizes diameter. High porosity, fiber structured membrane can be created by deposition of the electrospun fibers on a substrate. The electrospun membrane is lightweight and high surface area to volume ratio. A typical electrospinning setup consist of high electric potential supply, spinneret (needle), syringe, syringe pump and ground substrate (collector). High electric potential is applied at a spinneret equipped with polymer solution syringe. The polymer solution is fed into a generated electric field at a working distance from a collector (tip-to-collector distance). ES has been studies in many applications, biomaterials [20][21][22], catalysts [23][24], electrochemical energy [25][26][27][28][29] and filtration [30][31].
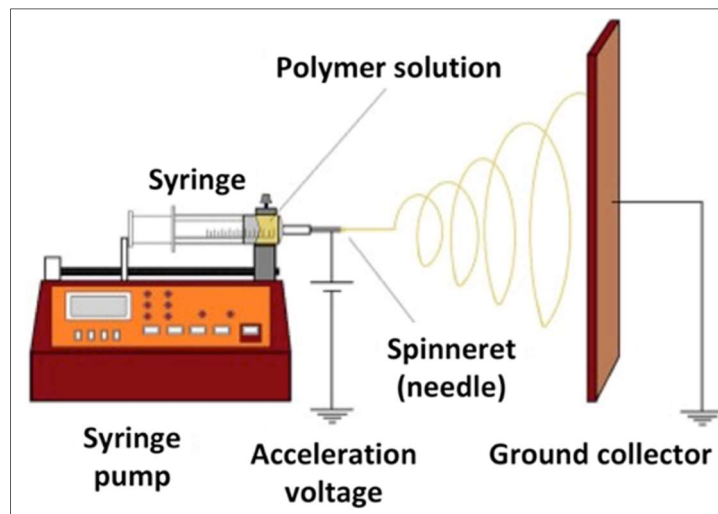


Figure 16 Typical setups of electrospinning experiments [32]

### 2.3.2 Parameters and controls of the electrospinning process

The electrospinning process consists of solution and process parameters. Solution parameters are polymer, concentrations, and solvents system. Process parameters consist of acceleration voltage, solution feed rate, tip-to-collector distance, including the temperature and relative humidity (sometimes, called environmental

parameters). In creating electrospun membranes with customized structures, for example consistent fibers structure, all parameters are controlled simultaneously.

- *Solvents* are not only used for preparing polymer into solution, but also used as a mechanism to control the morphology. In mixed solvents system, the different boiling points of solvents make the spun jets reduce the diameters prior to being collected. Polymer solutions with different solvents have different dielectric constants. Higher dielectric constant results in thicker fibers and more deposition on the collector.
- *Solution concentration* is an important parameter to control the spun structure. Extremely low concentrations produce bead structures. The spun structure transforms from beads to bead-fibers with the increasing concentration. At a proper range of concentrations, the spun structures have consistent fiber diameters.
- *Acceleration voltage* is applied to the spinning chamber in order to generate electric field. Charged, spun jets move faster in higher acceleration voltage setups and result to cylindrical fibers with high bead density structures. At low acceleration voltage, fibers are straight and cylindrical, defect free structures.
- *Collector* is an electrically grounded substrate. The charged, spun jets are randomly deposited on the ground collector. Collectors are using in two forms, stationary and rotating collectors. Stationary collectors yield non-woven membranes, whereas rotating collectors give aligned fabrics.
- *Syringe pump* is a component that hosts the solution syringe. The pump continuously supplies the solution into the generated electric field, also, controls the solution feeding rates of spun solution.
- *Tip-to-collector distance or working distance* is a distance between spinneret and collector. Tip-to-collector distance is an important parameter that allows the charged spun jets to elongate (reduction in its diameters) and the solvents to evaporate.

In electrospinning experiments, either solution feed rate or tip-to-collector distance is regulated. Adjusting the solution feed rate is changing the volume of the spun jets. On one hand, larger fiber diameters are obtained at higher solution feed rates. On another hand, changing the tip-to-collector distance is more complicated. The spun jets have more flight time, more solvents evaporation and reduced diameters due to more elongation.

According to prior studies of structural battery, lightweight fiber structured material is preferred for separators because of structural integrity [8][33][18]. Hence, the electrospun membrane is a promising candidate for LIB separator because of its structures those will enhance the liquid electrolyte

accommodation. Figure 17 shows the utilizations of the electrospinning among other methods in LIB separator research from 2007-2018.
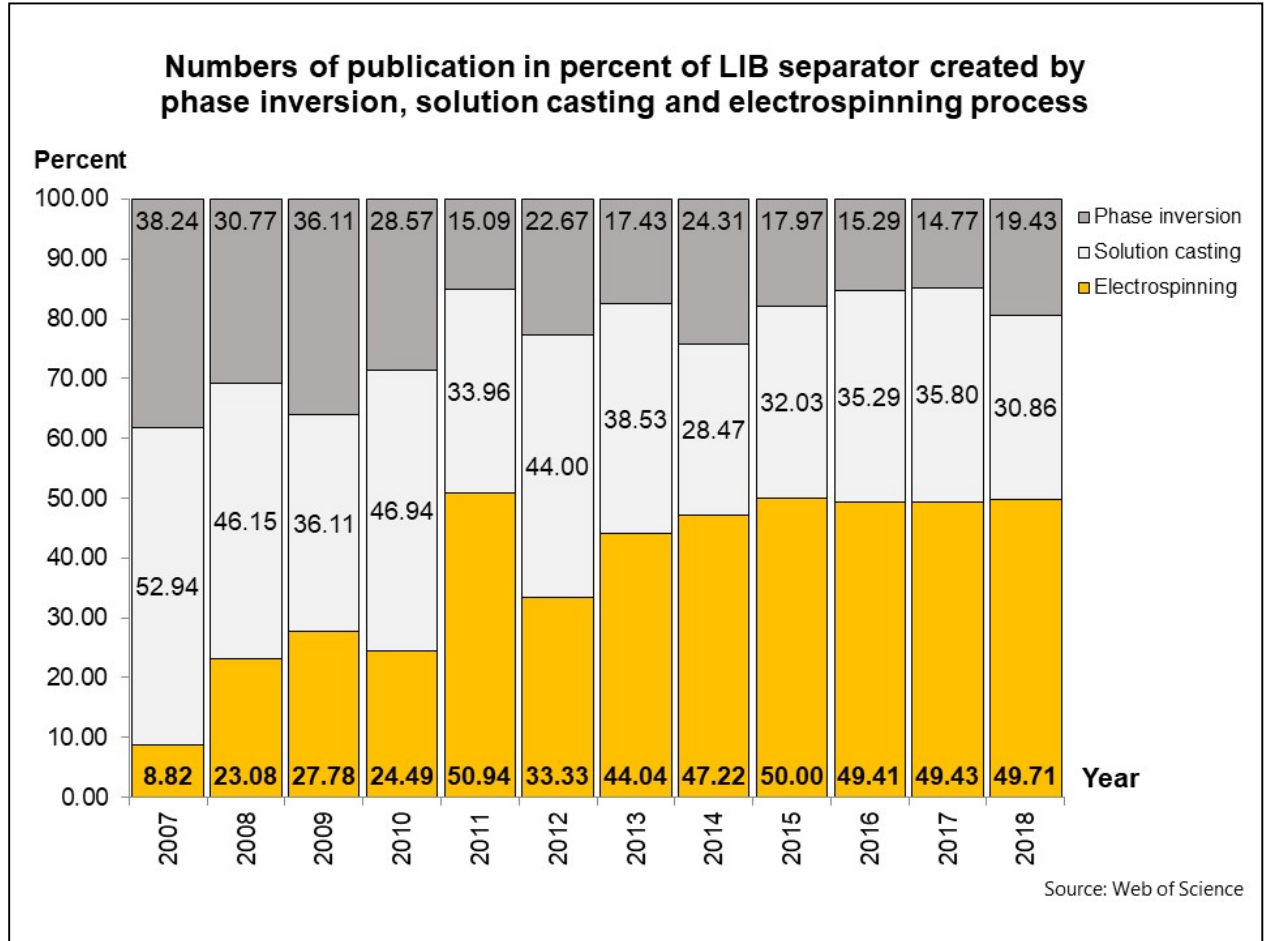


Figure 17 Publications in percent of fabrication methods for LIB separator

## 2.4 Electrospun Separator

To create the separator suitable for structural battery, comprehensive literature survey on electrospun separator for conventional LIBs focusing on multifunctional in addition to the electrochemical storage. The standalone electrospun separators can be categorized into three groups: (1) electrospun single polymer solution membrane (Table 3), (2) electrospun polymer blends/composites (Table 4) and (3) electrospun polymer-ceramic composites (Table 5).

### 2.4.1 Electrospun single polymer solution membrane

The most studied electrospun separator is the electrospinning with one type of polymer. In earlier studies of electrospun separator, its slowly developments focused on one characteristic at a time. Choi *et al.* [34] reported the electrospun PVdF with a wide range of fiber diameter (100-800 nm, average 400 nm). The tensile strength, strain-at-break and elastic modus of the electrospun separator were increased after thermal treated at 150-160ºC for 2 h. Gao *et al.* [35] studied the effects of the acceleration potential (8-15 kV) to the structure of the electrospun PVdF membrane. In this study, the higher acceleration potentials result to the decrease in crystallinity (calculated by DSC data), fiber diameter and less diameter distribution (Figure 18).
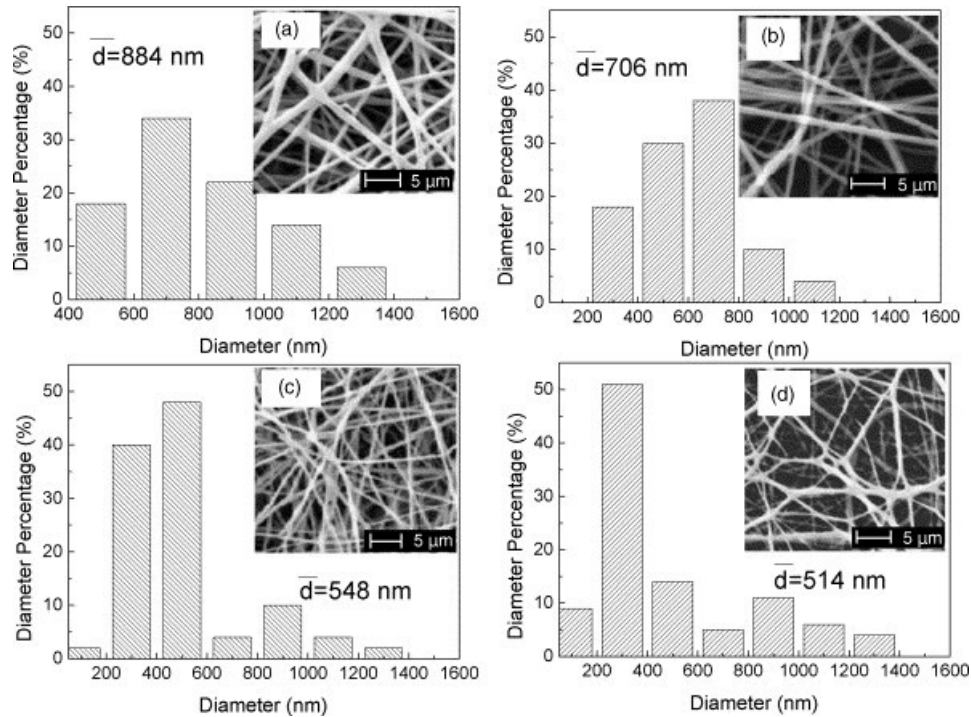
Figure 18 Fiber diameter and its distribution of electrospun PVdF *vs.* acceleration potential in Gao *et al*. study [35]: (a) 8 kV, (b) 10 kV and (c) 12 kV, (d) 15 kV

Characteristics of electrospun polymer membrane are mostly contributed by the properties of materials. For example, melting temperatures of the electrospun polyimide (PI) those synthesized by different methods [36][37] exhibited thermally stable to 500 °C. Similarly, the melting temperature of the electrospun polyacrylonitrile (PAN) [38] and partially oxidized polyacrylonitrile (oxy-PAN) [39] were reported as ~300 °C. Owing the properties of material, an electrospun nylon 6,6 performance separator had tensile strength of 10 MPa and exhibited dimensional stability up to 190 °C for 5 h [40]. Yanilmaz *et al.* [41] reported the electrospun pristine nylon 6,6 with a high tensile strength (18 MPa), electrolyte uptake (270%) and ionic conductivity (2.8 mS/cm). Although the characteristics of the electrospun membrane are dominated by the material, process parameters of the electrospinning and post-treatments also alter the characteristics of the electrospun separator. A study conducted by Ma *et al.* [38] showed variation of ionic conductivity with different pressing pressures in the hot-pressing treatment. The electrospun PAN separator with a small fiber diameter range (200-300 nm) treated with a high pressing pressure (20 MPa, 3 min.) demonstrated an ionic conductivity as high as 1.06 mS/cm and an electrolyte uptake 336%. In another experiment conducted by Lee *et al.* [39], the as-spun PAN membrane was calendared at 110 °C followed by heat treated at 230 °C for 30-120 minutes to creates the partially oxidized electrospun PAN separator. The highest ionic

conductivity, electrolyte uptake and tensile strength in this experiment were 49.6 MPa, 300% and 0.935 mS/cm, respectively. The electrospinning parameters and treatments in these two studies (18 kV, 25 cm in Ma *et al.* [38] *vs* 13 kV, 11 cm in Lee *et al.* [39]) could be noted for smaller fiber diameter in Ma *et al.* [38] experiment. Surface morphology before and after treatments in these studies are shown in Figure 19 and Figure 20. The quick hot-pressing treatment made the electrospun membrane thinner and maintained the fiber shape. On another hand, the calendaring flatted the electrospun fiber. The flatten fibers were then melted during the long heat treatment. Hence, the electrospun PAN membrane in Ma *et al.* [38] experiment was not only much smaller fiber diameter than those of Lee *et al.* [39], but also have more space to accommodate the electrolyte.
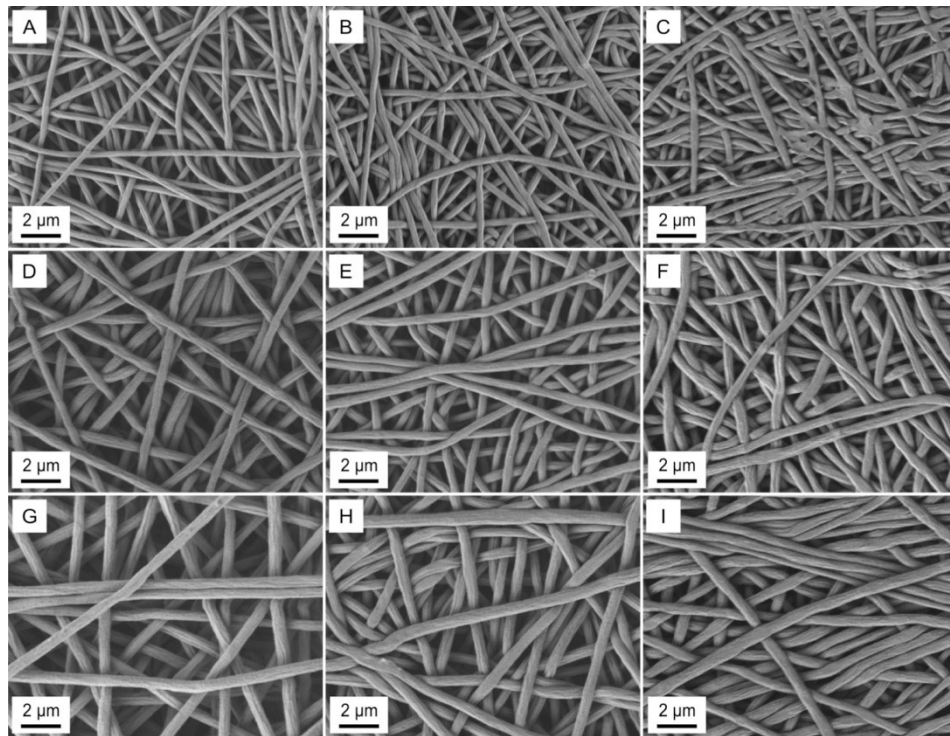


Figure 19 Surface morphology of electrospun PAN with thermal treated in Ma *et al.* experiment [38]
(a)-(c) small diameter range, (d)-(f) medium diameter range, (g)-(i) large diameter range;
(a),(d),(g) - low pressing pressure, (b),(e),(h) - medium pressing pressure, and
(c)(f)(i) - high pressing pressure
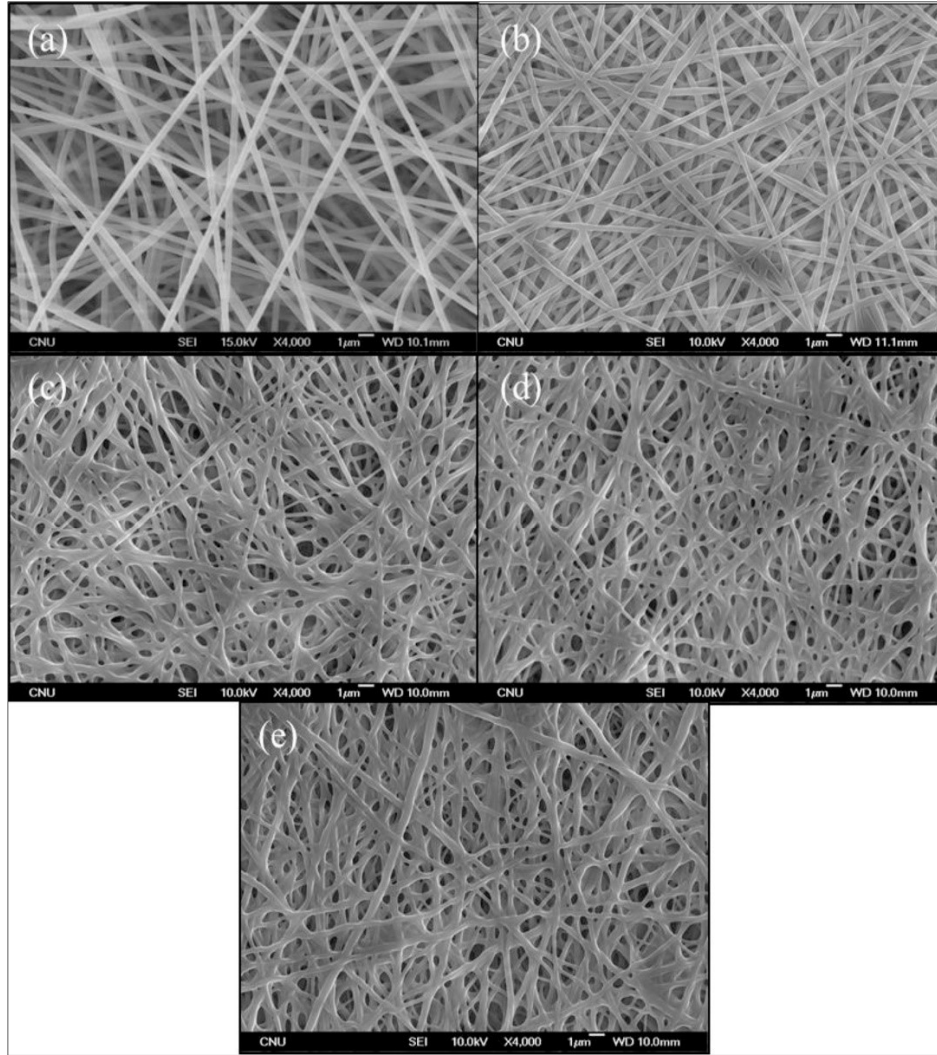
Figure 20 Surface morphology of electrospun PAN and oxy-PAN membranes in Lee *et al.* experiment [39] (a) as-spun PAN, (b) calendared PAN, (c) oxy-PAN treated for 30 min., (d) oxy-PAN treated for 60 min. and (e) oxy-PAN treated for 120 min.

Table 3 Electrospun single polymer solution membrane (group 1)

List of abbreviations shows in Appendix 1.

*Symbols*: d – thickness; EU – electrolyte uptake; φ – porosity (%); σ – ionic conductivity (mS/cm); $T_m$ – melting temperature (°C); $T_{decomp}$ – decomposition temperature (°C); TS – tensile strength, ε – tensile strain (%), E – elastic modulus

| Materials | Electrospinning conditions | d (μm) | EU (%) | φ (%) | Thermal | Mechanical | σ (mS/cm) | Ref. |
|---|---|---|---|---|---|---|---|---|
| PVdF | 10 kV, 15 cm | 20 | - | - | $T_m$ 170 °C | TS 5.3 kg$_f$/g, E 110.5 kg$_f$/g, ε 23.4 | 1.6-2.0 | [34] 2004 |
| PVdF | 8 kV, 0.1 mL/h, 10 cm | - | - | - | $T_m$ 166.7 °C | TS 15.9 MPa, E 153.4 MPa, | - | [35] 2006 |
| PI | 18-25 kV, 0.25 mL/h, 20 cm | 40-100 | - | - | $T_m$ 240 °C, $T_{decomp}$ 500 °C | - | - | [42] 2012 |
| PI | 30 kV, 0.2 mL/h, 20 cm | - | 509 | 79 | $T_{decomp}$ 500 °C | - | 0.7 | [37] 2016 |
| Nylon 6,6 | 20 kV, 0.35 mL/h, 20 cm | 20 | - | - | $T_{decomp}$ 400 °C, Dimensional stable 190 °C | TS 10 MPa | - | [40] 2016 |
| Nylon 6,6 | 20 kV, 1 mL/h, 12 cm | 65 | 260 | 67 | Dimensional stable 150 °C | TS 18 MPa | 2.8 | [41] 2014 |
| PAN | 18 kV, 0.5 mL/h, 25 cm | 22-29.4 | 280-378 | 50.8-63.5 | $T_m$ 303 °C | - | 0.59-1.06 | [38] 2017 |
| oxy-PAN | 13 kV, 1 mL/h, 11 cm | 20-26 | 138-238 | 60 | $T_m$ 300 °C, Dimensional stable 180 °C | TS 49.6 MPa E 1.30 GPa | 0.45-0.93 | [39] 2015 |
| PBz | 8.5 kV, 1.5 mL/h, 15 cm | 80 | 820 | 150 | $T_{decomp}$ 300 °C, fire retardant | TS 10 MPa | 2.92 | [43] 2016 |
| PTFE | 15 kV, 0.6 mL/h, 15 cm | 30 | 330 | 80 | $T_m$ 327 °C, $T_{decomp}$ 500 °C, Dimensional stable 170 °C | TS 7.2 MPa, ε 62 | 1.87` | [44] 2018 |
| PI | 18 kV, 0.6 mL/h, 20 cm | 25 | 2522 | 92 | $T_{decomp}$ 550 °C, Dimensional stable 500 °C | TS 11 MPa, ε 32.5 | - | [45] 2016 |

## 2.4.2 Electrospun polymer blends/composites (group 2)

The electrospinning method in creating polymer blends/composites separators can be categorized into three routes: (1) polymer blends, (2) electrospinning layer-by-layer polymer composites and (3) polymer coating on the electrospun membrane.

*Route 1: Polymer blends* is a convenience route to combines preferred properties of different polymers [46]. For examples, PAN is one of the typical electrospun separators materials because of its excellent electrolyte uptake, good ionic conductivity and considerable thermal solidity [47]. However, electrospun PAN separator shows the ionic conductivity in a range of 0.45-1.63 mS/cm [38][39]. Zhu *et al.* [48] blended the PVdF with PAN at different weight ratios followed by doped with PVdF dilute solution. The electrospun blended polymer membrane exhibited a high tensile strength over 20 MPa and a high ionic conductivity of 1.45 mS/cm, those contributed to the thermal solidity of PAN material and the high ionic conductivity of the electrospun PVdF separator [34], respectively. In different blending polymers, Kang *et al.* [49] mixed cellulose acetate (CA) into PVdF, due to its high hydrophilicity. Hence, water contact angles of the electrospun CA/PVdF blends decreased as presented in Figure 21. Another study conducted by Yvonne *et al.* [50], PVdF, CA and PMMA were blended for the electrospinning solution to increase the porosity from 88.3% (electrospun PVdF separator) to 94.2% (electrospun composite separator). Another work reported by Monaca *et al.* [51], PEO ($T_m \sim$ 61-64 °C) was blended with PVdF to create the electrospun blend separator with an ionic conductivity of 3.23 mS/cm. Because PEO and PVdF were phase separated which visualized by different endothermic peaks in DSC thermogram (Figure 22), the melting temperature of PEO was used as the shutdown mechanism by initiated the pore closure.
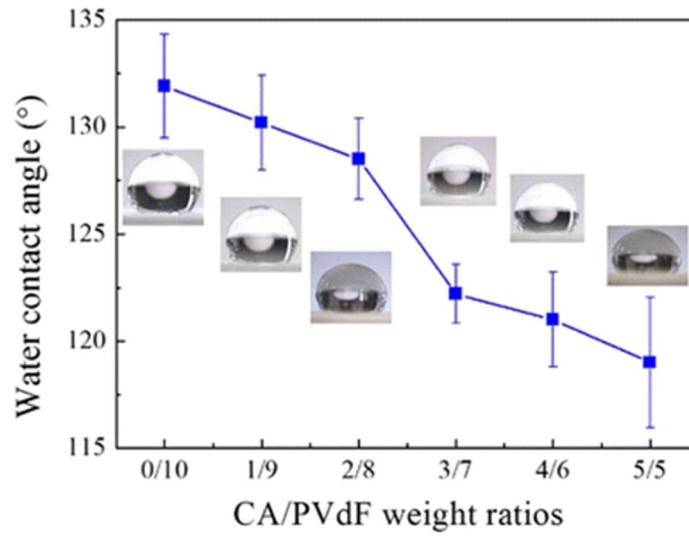
Figure 21 Water contact angles of the electrospun CA/PVdF blends separator reported in Kang *et al.* study [49]
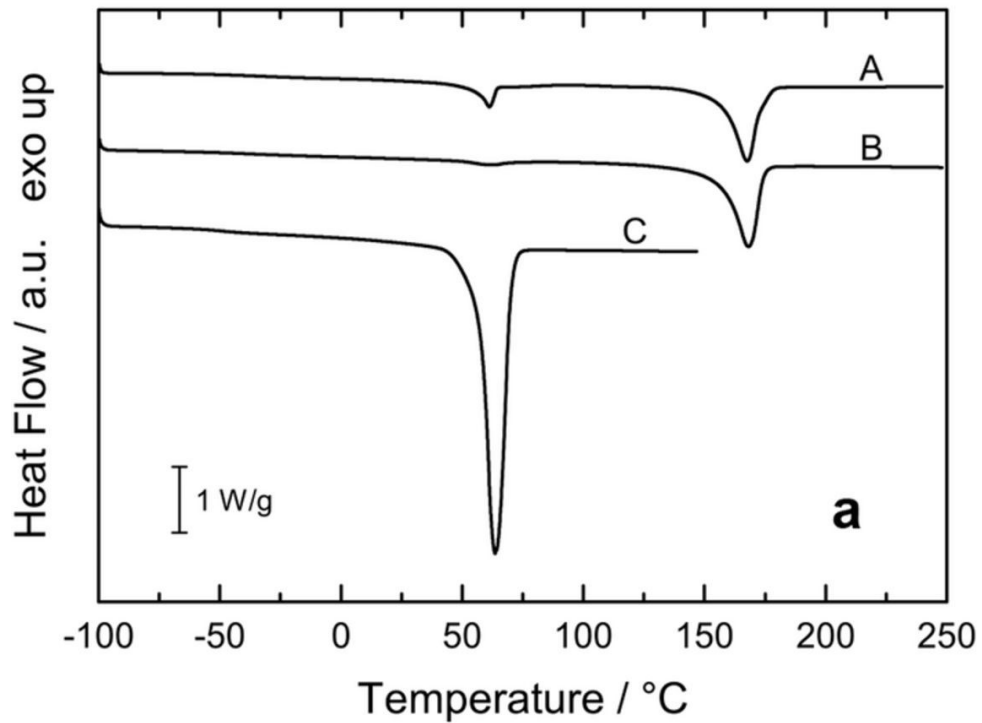


Figure 22 DSC thermogram of PVdF-PEO blend (a), PVdF (b) and PEO (c) in Monaca *et al.* study [51]

*Route 2: Electrospinning layer-by-layer polymer composites,* two or more polymer solutions are sequentially electrospun onto the same collector. Common configuration of the electrospun layer-by-layer separator is a tri-layer composite separator, (A/B/A where A and B are two different polymers, Figure 23 as an example). Material behavior in each layer separately exhibits with its own characteristics. Lu *et al*. [52] fabricated an electrospun tri-layer PPESK/PVdF/PPESK separator. PPESK ($T_m$ ~263-305 °C) was anticipated to promotes wettability and thermal dimensionality. The PPESK/PVdF/PPESK composite separator achieved the high ionic conductivity of ~7 mS/cm. Special care must be taken when choosing the polymer for each layer. Because the PPESK and PVdF were phase separated and $T_m$ of PVdF much lower than that of PPESK, PVdF caused the shrinkage to the composite when the temperature reaches its melting temperature. Similar tri-layer PVdF/PMIA/PVdF fabricated by Zhai *at el.* [53] reported a high tensile strength of 13.9 MPa.
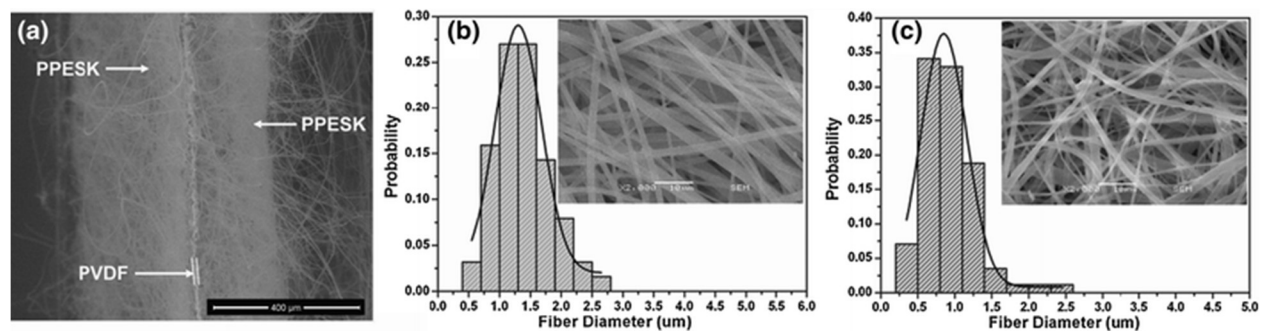


Figure 23 Common configuration of PPESK/PVdF/PPESK tri-layer polymer composite separator as reported by Lu *et al.* [52] (a) SEM micrograph, (b) fiber diameter distribution of PPESK and (c) fiber diameter distribution of PVdF

*Route 3: Polymer coating on the electrospun membrane*, the electrospun membrane is coated with a thin adherent polymer film to modify or functionalize the surface of the electrospun fiber, thus, the surface of the membrane. Liang *et al.* [54] quickly dip coated PEO on the electrospun PI membrane. Although the PEO coated PI membrane lost its porosity and electrolyte uptake ~10% and 50%, respectively, the ionic conductivity was as high as 3.83 mS/cm. Xie *et al.* [55] immersed the electrospun PES into dopamine (DA) solution for 24 h resulted to double the tensile strength. Like others, the DA coated PES separator lost its porosity ~15%. Beside the coating of polymer solution onto surface of the electrospun membrane, Shi *et al.* [56] prepared the electrospun PVdF-HFP, then followed by dip-coated in the DA solution for 48 h. The

composite PVdF-HFP-PDA membrane exhibited core (PVdF-HFP) - shell (PDA) fiber structure with improved tensile strength (20 MPa) and dimensional stable up to 220 °C.

Table 4 Electrospun polymer blends/composites (group 2)

List of abbreviations shows in Appendix 1.

*Symbols*: d – thickness; EU – electrolyte uptake; φ – porosity (%); σ – ionic conductivity (mS/cm); $T_m$ – melting temperature (°C); $T_{decomp}$ – decomposition temperature (°C); TS – tensile strength, ε – tensile strain (%), E – elastic modulus

| Materials | Additives | Electrospinning conditions | d (µm) | EU (%) | φ (%) | Thermal | Mechanical | σ (mS/cm) | Ref. |
|---|---|---|---|---|---|---|---|---|---|
| PVdF | PAN | 15 kV | | 320 | | $T_{decomp}$ 290 °C, Dimensional stable 200 °C | TS 20.4 MPa | 1.45 | [57] 2017 |
| PVdF | CA | 20 kV, 1 mL/h, 15 cm | 20-52 | 768.2 | 88 | $T_m$ 162.2 °C | TS 11.1 MPa, ε 119.63 | 3.23 | [49] 2016 |
| PVdF | PEO | 20 kV, 0.4 mL/h, 22 cm | 60-100 | 527 | | - | TS 8.9 MPa, E 38 MPa | - | [58] 2017 |
| PVdF | PMMA/CA | 16 kV, 0.8 mL/h, 20 cm | - | 315 | 94 | $T_m$ 160 °C | - | - | [50] 2014 |
| PVdF | PI | 10 kV, 10 cm, 0.125 mL/h (PVdF), 0.1 mL/h (PI) | 50 | 476 | 83 | $T_m$ 170 °C, Dimensional stable 180 °C | | 3.46 | [59]2015 |
| PVdF | PMIA | 30 kV, 25 cm, 2 mL/h (PVdF), 0.1 mL/h (PMIA) | - | - | 83.97 | $T_m$ 172 °C, Dimensional stable 180 °C | TS 13.9 MPa, ε 46.09 | 0.81 | [53] 2014 |
| PVdF | PPESK | PVdF: 23 kV, 2.8 mL/h, 10 cm; PPESK: 25 kV, 2.8 mL/h, 15 cm | 150-195 | 928-1140 | - | $T_m$ 160 °C, Dimensional stable 180 °C | - | 5.42-7.35 | [52]2013 |
| PVdF-g-PMASS | MA-SS | 10 kV, 1 mL/h, 15 cm | - | - | 67.4 | $T_{decomp}$ 430 °C, Dimensional stable 170 °C | - | 1.48 | [60] 2017 |
| PVdF-HFP | PMMA | 30 kV, 0.3 mL/h, 15 cm | 150-250 | 337 | - | - | TS 8.5 MPa, ε ~55 | 1.99 | [61] 2009 |

| | | | | | | | | | |
|---|---|---|---|---|---|---|---|---|---|
| PVdF-HFP | PI | multi-syringes<br>30 kV, 20 cm, 1 mL/h<br>(PVdF-HFP), 2 mL/h (PI) | 21 | 350 | 73 | $T_m$ 135 °C (PVdF-HFP),<br>$T_m$ 235 °C (PI),<br>shutdown function | TS 7.5 MPa,<br>$\varepsilon$ ~70 | 1.46 | [62] 2014 |
| PVdF-HFP | TPP | 13 kV | 40 | - | - | $T_{decomp}$ 200 °C, fire retardant | TS 4.5 MPa,<br>E 20 GPa | - | [63] 2017 |
| PVdF-HFP | PDA | 10 kV, 7.5 mL/h. 10 cm | 40 | 254 | 72.80 | Dimensional stable 160 °C | TS 7.1 MPa | 1.40 | [56] 2016 |
| PAN | PU | multi-syringes<br>25 kV,1 mL/h, 15 cm | 50 | 714.50-776.09 | 80-92 | $T_m$ 275 °C,<br>Dimensional stable 170 °C | TS 10 MPa,<br>$\varepsilon$ 40 | 1.30-2.07 | [47] 2016 |
| PI | PEO | 15-25 kV, 0.3 mL/h, 30 cm | 80 | 170 | 90 | - | - | 3.83 | [54] 2016 |
| PES | DA | 18 kV, 3.6 µL/h, 20 cm | 38 | 1581 | 75 | Dimensional stable 220 °C | TS 20.07 MPa,<br>E 154.20 MPa,<br>$\varepsilon$ 74.86 | - | [55] 2016 |
| PLA | PBS | 15 kV, 15 cm,<br>0.74 mL/h (PLA)<br>1.68 mL/h (PBS) | - | 969 | - | Dimensional stable 170 °C | - | 1.65 | [64] 2017 |
| PVA | Lignin | 26 kV, 1.2 mL/h, 25 cm | 90 | 508 | - | $T_{decomp}$ 220 °C,<br>Dimensional stable 150 °C | | - | [65] 2017 |

## 2.4.3 Electrospun polymer-metal oxide composites (group 3)

Metal oxide particle has high surface area and high hydrophilicity. The addition of metal oxide into polymer membrane is anticipated to increases amorphous phase and wettability (hence, enhances electrolyte uptake and ionic conductivity). Studies show the metal oxide particles improve thermal stability and mechanical strength to the composite membrane [66] [67] [68] [69]. There are three routes to incorporate the metal oxide particles into the electrospun separator: (1) combined electrospinning with sol-gel method; (2) interpenetrate the metal oxide colloid solution to the electrospun separator; and (3) direct dispersion of metal oxide particles in the polymer solution.

*Route 1) Combined electrospinning with sol-gel method* is the most effective route to adds the metal oxide particles into the electrospun fibers. Zhang *et al.* [70] and Yanilmaz *et al.* [71] reported the $SiO_2$ composite separator prepared by the mixture of the $SiO_2$ sol and polymer solution. The $SiO_2$ sol was hydrolyzed tetraethoxysilane (TEOS) similar to typical $SiO_2$ synthesized by sol-gel method. Ratio of the $SiO_2$ sol to the PVdF solution (9:1 and 10:1 wt./wt.) was studied in Zhang *et al.* [70] experiment. The highest ionic conductivity and electrolyte uptake were 7.47 mS/cm and 646%, respectively. Figure 24 shows TEM micrograph of the PVdF/$SiO_2$ composite separator. Similarly, the $SiO_2$ contents in the electrospun composite membrane corresponding to the ratios of PAN to TEOS were investigated in Yanilmaz *et al.* [71] study. The tensile strength was reported ~4.3 MPa with 16 wt. % $SiO_2$.
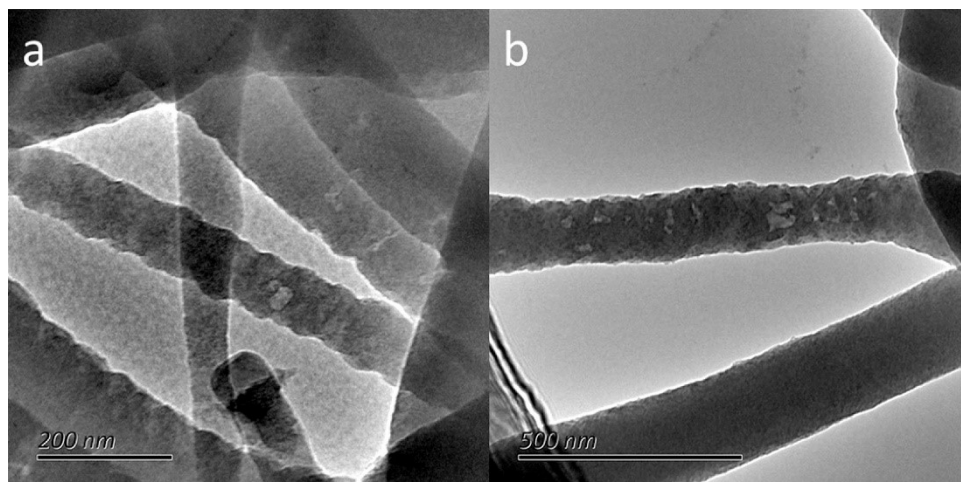
Figure 24 TEM micrograph of electrospun PVdF/SiO2 separator prepared by Zhang *et al.* [70]

*Route 2) Interpenetrate the metal oxide colloid solution to the electrospun separator*, metal-oxide particles are dispersed into organic solvent to obtains a colloid solution. The colloid solution is then penetrated to the electrospun membrane (by dip-coat or vacuum filtration method). Zheng *et al.* [66] prepared the electrospun PVdF/PAN membrane and dispersed $SiO_2$ in PVdF/acetone solution separately. The $SiO_2$ colloid solution was then filtered through the nanofiber membrane to form the composite separator. The PVdF-PAN/$SiO_2$ had high tensile strength of 10 MPa and ionic conductivity of 1.68 mS/cm. Interesting, this $SiO_2$ composite separator with interpenetration method exhibited dimensional stable to a high temperature of 200 ºC, shown in Figure 25. Zhai *et al.* [67] dip-coated the electrospun PEI-PU membrane into $SiO_2$ colloid solution. The electrospun PEI-PU/$SiO_2$ composite exhibited high tensile strength (15.6 MPa) and flame-retardant behavior. Figure 26 demonstrated the flame suppression of PEI-PU and the effect of the $SiO_2$ to decreases the dimension shrinkage. Although the porosity and electrolyte uptake after the $SiO_2$ addition decreased from 82.15% to 59.14% and 664.34% to 188.38%, respectively, the composite separator improved the ionic conductivity from 1.47 to 2.33 mS/cm. In additional to the filtration and dip-coating process, cross-linked vinyl-functionalized $SiO_2$ to the electrospun PAN separator with thermal initiator (azobisisobutyronitrile) provided a high tensile strength (7.7 MPa) and a high ionic conductivity (2.1 mS/cm) [72]. It could note on the metal oxide colloid solution interpenetration. Although adhesive agents (for examples PVdF [66], PVdF-HFP [67] and TEGDA [72]) were added into the colloid solution to enhances the adhesion between the particles and the electrospun fiber, effectiveness of particle adhesion and distribution of the particle in the penetration are questionable. The fiber structure membrane also lost the porosity at some degree due to coating of the adhesion agent.
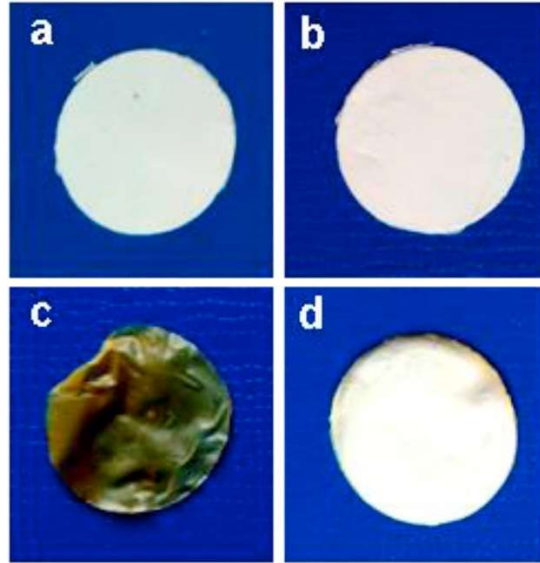
Figure 25 Dimensional stable of PVdF-PAN/SiO$_2$ before and after thermal treated at 200 ºC investigated by Zheng *et al.* [66] (a,c): PVdF-PAN, (b,d): PVdF-PAN/SiO$_2$
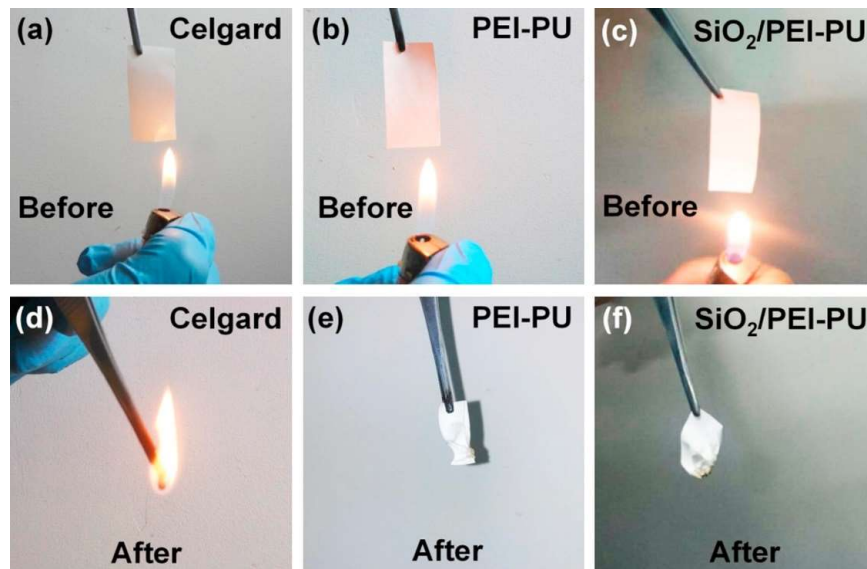


Figure 26 Combustion test of PEI-PU/SiO$_2$ in Zhai *et al.* experiment [67]

*Route 3: Direct dispersion of metal oxide particle in the polymer solution* is the simplest route to create the electrospun membrane. The metal oxide particles are ultrasonicate agitated to dispersed in the polymer solution. The dispersed colloid solution is, then used in the electrospinning process. A common problem occurs in this route is the metal oxide particles tend to aggregate and do not well distribute in the spun fibers. Direct dispersion of $SiO_2$ and $TiO_2$ in the nylon 6,6 solution without adding of dispersant in Yanilmaz *et al.* [41][73] experiment shown the improvements of tensile strength, elastic modulus, ionic conductivity (3.3 mS/cm $TiO_2$ and 3.6 mS/cm $SiO_2$) and dimensional stable up to 150 °C. Dispersion of $SiO_2$ into specially prepared polymers reported to have high electrolyte uptake and ionic conductivity. For examples, synthesized PI in Wang *et al.* [69], PMMA-grafted electrospun PVdF in Yang *et al.* [74] and synthesized PMIA in Li *et al.* [68] archived the ionic conductivity of 2.27, 2.31 and 3.23 mS/cm, respectively. Li *et al.* [68] varied the amount of $SiO_2$ particles in the preparation of electrospun PMIA/$SiO_2$ separator. Wettability of the composite separator was increasing with the increasing amount of $SiO_2$ particle. However, the tensile strength and ionic conductivity dropped down at the amount of $SiO_2$ loadings higher than 6 wt. %. The ionic conductivity decreased at higher loadings of $SiO_2$ particle because the interactions among $SiO_2$ particles, PMIA groups and lithium salt those affect ion agglomeration in amorphous phase of organic-inorganic composite polymer [68].
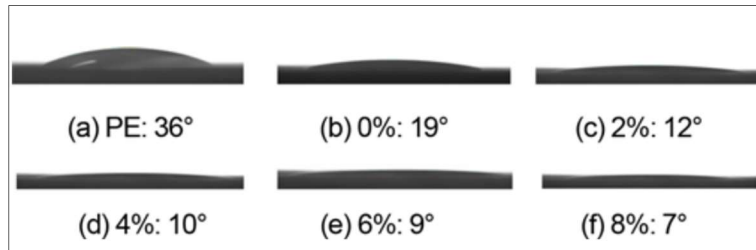


Figure 27 Contact angles at different weight % loadings of $SiO_2$ in electrospun PMIA/SiO $_2$ membrane reported by Li *et al.* [68]

Table 5 Electrospun polymer-metal oxide composites (group 3)

List of abbreviations shows in Appendix 1.

*Symbols*: d – thickness; EU – electrolyte uptake; φ – porosity (%); σ – ionic conductivity (mS/cm); $T_m$ – melting temperature (°C); $T_{decomp}$ – decomposition temperature (°C); TS – tensile strength, ε – tensile strain (%), E – elastic modulus

| Materials | Metal oxide | Electrospinning conditions | d (µm) | EU (%) | φ (%) | Thermal | Mechanical | σ (mS/cm) | Ref. |
|---|---|---|---|---|---|---|---|---|---|
| PVdF | $SiO_2$ sol | 29 kV, 3 mL/h, 20 cm | 83 | 646 | 85 | $T_m$ 161 °C, $T_{dcomp}$ 400 °C, Dimensional stable 150 °C | - | 7.47 | [75] 2014 |
| PVdF/PAN | $SiO_2$ | 15 kV, 15 cm | - | 440 | - | Dimensional stable 200 °C | TS 10 MPa, ε 100 | 1.68 | [66] 2017 |
| PVdF-g-PMMA | $SiO_2$ | 28 kV, 20 cm | 100 | - | 68 | $T_m$ 163.2 °C, Dimensional stable 120 °C | TS 6.24 MPa | 2.31 | [74] 2015 |
| PAN | $SiO_2$ sol | 16 kV, 0.75 mL/h, 25 cm | 65 | 377 | 77 | Dimensional stable 150 °C | TS ~4.3 MPa | 2.6 | [71] 2016 |
| PAN | f-$SiO_2$ | 15 kV, 0.8 mL/h, 16 cm | 35 | - | 49.3 | Dimensional stable 200 °C | TS 7.7 MPa | 2.1 | [72] 2017 |
| PAN | GO | 15 kV, 0.75 mL/h | 65 | 303 | 72 | - | - | 1.36 | [76] 2016 |
| PU | GO | 9-10 kV, 13 cm | - | 733 | 90.7 | $T_m$ 400 °C | TS 0.9-3 MPa | 3.73 | [77] 2018 |
| PEI/PU | $SiO_2$ | 30 kV, 1 mL/h, | 35 | - | 59.14 | Dimensional stable 180 °C, fire retardant | TS 15.6 MPa | 2.33 | [67] 2015 |
| PMIA | $SiO_2$ | 25 kV, 0.2 mL/h, 16 cm | - | 850 | 89 | Dimensional stable 280 °C | TS 18.14 MPa, ε 19.50 | 3.23 | [68] 2017 |
| PI (synt.) | $SiO_2$ | 15 kV, 15 cm | 20 | 2400 | 90 | $T_{decomp}$ 500 °C, Dimensional stable 250 °C | TS 7.75 MPa | 2.27 | [69] 2017 |
| Nylon 6,6 | $TiO_2$, $SiO_2$ | 20 kV, 1 mL/h, 12 cm | 65 | 310-350 | 71-75 | Dimensional stable 150 °C | TS 22 MPa | 3.3-3.6 | [73] 2017 |
| Nylon 6,6 | $SiO_2$ | 20 kV, 1 mL/h, 12 cm | 65 | 360 | 77 | Dimensional stable 150 °C | TS 22 MPa | 3.8 | [41] 2014 |

## 2.4 Characterization Methods of Electrospun Membranes

Characterizations are essential processes to understand and evaluate the basic chemical and physical properties of certain materials. The characterizations of micro- and nano- scales materials are performed at different levels. At micro- and nano- structures, morphology, size and shape are visualized by microscopy techniques, whereas chemical composition and composition variation are evaluated by spectroscopy techniques. Macroscopic testing procedures are used for testing mechanical, thermal and materials' intensive properties at bulk membrane.

### 2.4.1 Surface morphology: scanning electron microscopy (SEM)

Since the electrospinning process produces random spun fibers on the collector, surface morphology can represent the morphology of the membrane. Scanning electron microscopy (SEM) uses electrons scan over surface of materials to measure the scattered back electrons. Scanning electron micrograph provides information on morphology and shapes of the spun structure. Image processing techniques are required to measure the sizes of fiber diameters and void spaces between non-woven fibers. Micrographs are obtained at low acceleration voltage (2 kV) and low current (2 mA) operations due to beam sensitivity of polymer. Sputter coating (current of 25 mA, coated for 180 s) is required to increase electrical conductivity, improve edge resolution, and reduce sample charging and microscopic beam damage.

### 2.4.2 Membrane density

The electrospun membranes are porous with high volume-to-weight ratio. Membrane density is determined by an average of individual weight and volume from three specimens for each electrospun conditions. The spun membranes are punched into discs with a diameter of 7/32 inch. The weight of samples is measured by analytical balance. Sample thickness is measured to a precision of ±0.0005 inch with a flat tip digital micrometer. Special care must be taken to assure the samples are not distorted or crushed when making the measurement.

## 2.4.3 Membrane porosity

Image processing techniques of micrograph are common procedures to determine the porosity. The micrograph of surface morphology is a good representative of membrane structure; however, analysis of micrograph only represents information on the top layer. The spun fibers are randomly collected and can be visualized, *roughly*, like layer-by-layer with a fiber's diameter as a thickness of each layer. Hence, the pores information on each layer is difference. The spun membranes are punched into discs with a diameter of 3/4 inch. Samples are submerged into liquid (using *n*-butanol, *n*-BuOH) for 40 minutes, wiped out the excessed liquid and measured the weight as soaked. *Membrane porosity (%)* is a ratio of the voids space volume to the overall volume, as presents in Equation 1:

$$Porosity(\%) = \frac{\left( \dfrac{Mass_{soaked} - Mass_{dry}}{Density_{n-BuOH}} \right)}{\left( \dfrac{Mass_{soaked} - Mass_{dry}}{Density_{n-BuOH}} \right) + \left( \dfrac{Mass_{dry}}{Density_{polymer,as-received}} \right)} \times 100\% \qquad \text{Equation 1}$$

where,

$$\text{Volume of the void space} = \left( \frac{Mass_{soaked} - Mass_{dry}}{Density_{n-BuOH}} \right) \qquad \text{Equation 1a}$$

$$\text{Overall volume} = \left( \frac{Mass_{soaked} - Mass_{dry}}{Density_{n-BuOH}} \right) + \left( \frac{Mass_{dry}}{Density_{polymer,as-received}} \right) \qquad \text{Equation 1b}$$

## 2.4.4 Electrolyte uptake

Electrolyte uptake of the electrospun membranes is measured *as a function of dipping time* in the electrolyte (lithium hexafluorophosphate solution, 1M LiPF$_6$ EC/DMC) and calculated by Equation 2:

$$Electrolyte\ uptake\ (\%) = \left( \frac{Mass_{soaked} - Mass_{dry}}{Mass_{dry}} \right) \times 100\% \qquad \textbf{Equation 2}$$

where, $Mass_{soaked}$ and $Mass_{dry}$ are mass of the soaked and dry membranes, respectively.

## 2.4.5 Mechanical property: tensile strength and elastic modulus

The electrospun membranes are cut into strips of 0.25-inch width and 1-inch length with 0.5-inch gauge-length to avoid the imperfection of standard dog-bone sample preparations. Tensile strength and elastic modulus are measured by a universal testing machine (tensile mode) with a crosshead speed of 0.2 mm/min. Data points are post-processed by curve smoothing to minimize noises and fluctuations. Values of tensile strengths and elastic modulus are the averages of three of the processed data for each electrospinning conditions.

## 2.4.6 Powder x-ray diffraction spectroscopy

X-ray diffraction spectra are used to identify and evaluate the nanoparticles with reference data given in electronic database (such as, Inorganic Crystal Structure Database ICSD). X-ray diffraction is non-destructive technique, in brief, a monochromatic beam of x-rays is diffracted by crystalline phases in the specimen if Bragg's law Equation 3 is satisfied:

$$\lambda = 2d \ sin\theta \qquad\qquad \textbf{Equation 3}$$

where $d$ is the spacing between atomic planes in crystalline phase and $\lambda$ is the x-ray wavelength. Intensity of the diffracted x-rays is measured as a function of the diffraction angle $2\theta$. In addition to crystal structure and lattice parameter, information on crystallite size can be observed by the shape of XRD pattern. Figure 12 shows different peaks' shape on typical XRD patterns.
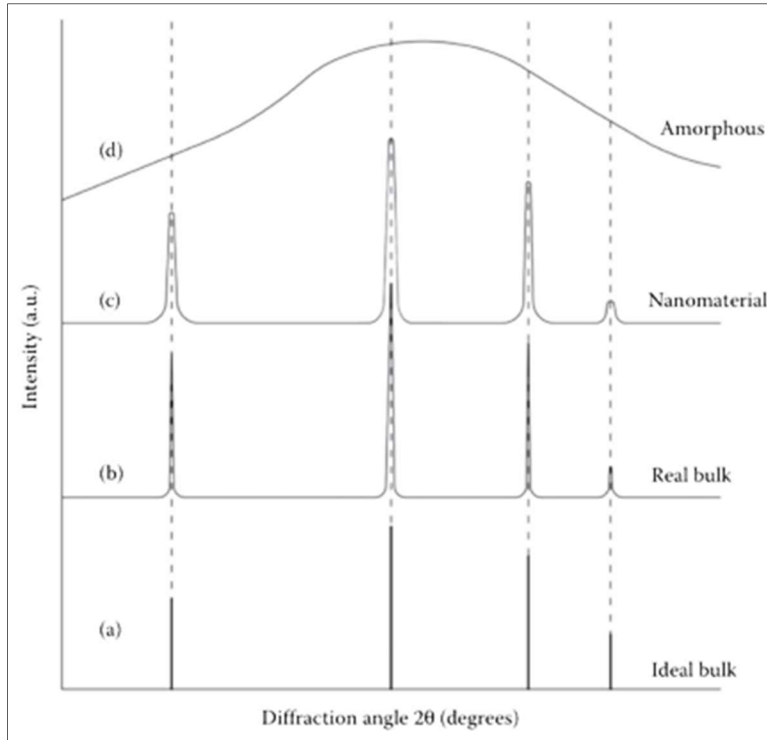
Figure 28 Typical x-ray diffraction patterns [78]

## 2.4.7 Thermal analysis: dimensional stabile, glass transition temperature, melting temperature and thermal stability

Lithium-ion batteries can be damaged by water or high moisture content. Typically, materials to be fabricated into the cells are dried at 80 °C under vacuum. The samples must not shrink or wrinkle significantly.

*Dimensional Stable* As the electrospun membranes are isotropic materials, the membranes are punched into circular samples with a diameter of 3/4 inch, then, placed in vacuum oven at 90°C for 60 minutes. Shrinkage in the diameter of the samples must less than 5% is a reasonable generalization.

*Differential scanning calorimetry (DSC)* is an effective analytical tool to determine specific heat, glass transition temperature, melting temperature, curing/decomposition characteristics and the corresponding enthalpy/ entropy changes of the polymers. DSC has two sample positions, one for investigating sample and another for reference sample. Calorimeters are scanned at a constant heating or cooling rates and

recorded the heat flow rate (function of time) as outputs. Typical data represents as heat flow rate *vs* temperature [79][80].
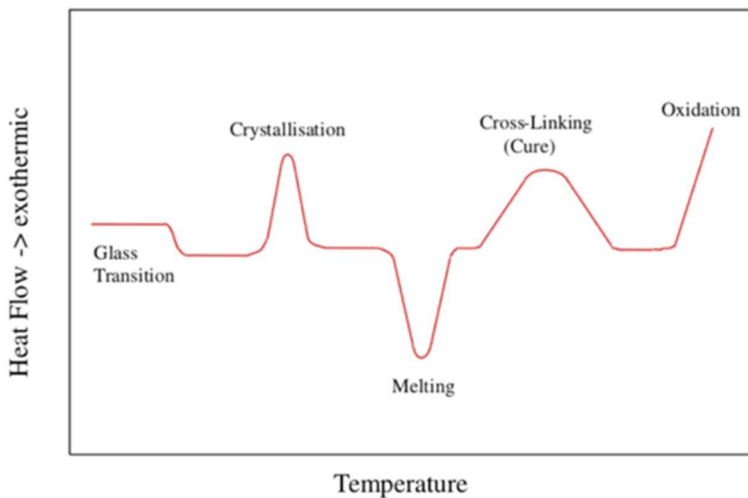


Figure 29 Typical DSC thermogram

*Glass transition temperature (T$_g$)* and *melting temperature (T$_m$)* are determined from differential scanning calorimeter from 25°C – 450°C with a scanning rate of 10°C/min. Average mass of samples for thermal analysis is 2 mg. The T$_g$ can be determined at the first change (drop) in Figure 29, (endothermic plots) by the midpoint of the change in slopes for heat capacity plot. The T$_m$ is the temperature at the minimum peak of endothermic plot.

*Thermogravimetric analysis (TGA)* is a general method for comparing the thermal stability of polymers. Mass of sample is continuously recorded while the temperature is increased at a constant rate, accurately. The weight loss occurs when (1) volatiles absorbed by the membrane are driven off and (2) degradation of polymer at higher temperature. In addition to comparison of the thermal stability of polymers, TGA can be used as an indirect technique to determine the amount of metal oxide nanoparticles in the electrospun polymer-metal oxide composites owing the high accuracy of mass measurements.

## 2.4.8 Electrochemical characterizations

Ionic conductivity and interfacial electrochemical stability were measured by AC impedance spectroscopy with an AC amplitude of 5 mV and a frequency range of 1 Hz to 100 kHz.
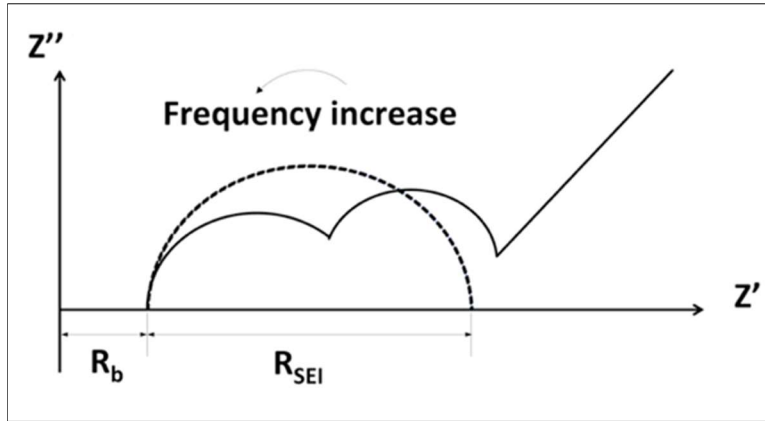


Figure 30 Typical impedance spectra (Nyquist plot)

Typical impedance spectra are shown in Figure 30. $R_b$ is the bulk resistance, the real part of impedance (z' axis intercept) at the highest frequency. $R_{SEI}$ is the resistance of solid electrolyte interface on the electrode surface.

*Ionic conductivity* is measured by the AC impedance spectroscopy. The electrospun samples are sandwiched between SS/SS or Li/Li symmetry cells. With this configuration, the bulk resistance $R_b$ represents the membrane resistance and is used in ionic conductivity calculation.

$$\sigma = \frac{d}{R_b \cdot S} \qquad\qquad \text{Equation 4}$$

where $\sigma$ is ionic conductivity per thickness of the separator (S/cm), $d$ is thickness of separator (cm), $R_b$ is the bulk resistance (ohm) and $S$ is surface area of electrode (cm$^2$).

*Interfacial electrochemical stability* is measured like ionic conductivity. However, the cell configuration is either half- or full- battery cells. Interfacial resistance can be simple estimated by (semi-cycle) subtracting the bulk resistance from the complex impedance spectra.

**REFERENCES**

[1]     P. V. Panetta *et al.*, "NASA-GSFC Nano-Satellite Technology Development," Logan, 1998.

[2]     D. T. Queheillalt, D. D. Hass, and H. N. G. Wadley, "Electron-beam-directed vapor deposition of multifunctional structures for electrochemical storage," in *Smart Structures and Materials 2002: Industrial and Commercial Applications of Smart Structures Technologies*, 2003, vol. 4698, pp. 201–211.

[3]     S. Shalouf, J. Zhang, C. Wang, and L. Wackett, "THE EFFECTS OF MECHANICAL DEFORMATION ON THE PERFORMANCE OF COMPOSITE STRUCTURES EMBEDDED WITH POLYMER BATTERIES," in *International Conference on Composite Materials-ICCM19*, 2003.

[4]     A. Javaid and M. Z. Ali, "Multifunctional structural lithium ion batteries for electrical energy storage applications," *Mater. Res. Express*, vol. 5, no. 5, p. 55701, 2018.

[5]     E. D. Wetzel, D. J. O. Brien, J. F. Snyder, R. H. Carter, and J. T. South, "Multifunctional Structural Power and Energy Composites for U.S Army Applications," *Multifunct. Struct. / Integr. Sensors Antennas*, no. 2006, pp. 2–14, 2006.

[6]     E. L. Wong, D. M. Baechle, K. Xu, R. H. Carter, J. F. Snyder, and E. D. Wetzel, "Design and Processing of Structural Composite Batteries," Aberdeen Proving Ground, 2007.

[7]     P. Liu, E. Sherman, and A. Jacobsen, "Design and fabrication of multifunctional structural batteries," *J. Power Sources*, vol. 189, no. 1, pp. 646–650, 2009.

[8]     E. Jacques, H. Kjell, D. Lindbergh, and G. Behm, "PERFORMANCE OF LITHIUM-INTERCALATED CARBONFIBRES FOR STRUCTURAL ELECTRODE APPLICATIONS," in *ICCM 19, 19th international conference on composites materials*, 2013, pp. 1–8.

[9]     E. Jacques, M. H. Kjell, D. Zenkert, and G. Lindbergh, "The effect of lithium-intercalation on the mechanical properties of carbon fibres," *Carbon N. Y.*, vol. 68, pp. 725–733, 2014.

[10]    G. Fredi *et al.*, "Graphitic microstructure and performance of carbon fibre Li-ion structural battery electrodes," *Multifunct. Mater.*, vol. 1, pp. 1–32, 2018.

[11]    M. Y. Park, J. H. Kim, D. K. Kim, and C. G. Kim, "Perspective on Carbon Fiber Woven

Fabric Electrodes for Structural Batteries," *Fibers Polym.*, vol. 19, no. 3, pp. 599–606, 2018.

[12]   J. F. Snyder, R. H. Carter, and E. D. Wetzel, "Electrochemical and mechanical behavior in mechanically robust solid polymer electrolytes for use in multifunctional structural batteries," *Chem. Mater.*, vol. 19, no. 15, pp. 3793–3801, 2007.

[13]   N. Ihrner, W. Johannisson, F. Sieland, D. Zenkert, and M. Johansson, "Structural lithium ion battery electrolytes: Via reaction induced phase-separation," *J. Mater. Chem. A*, vol. 5, no. 48, pp. 25652–25659, Dec. 2017.

[14]   T. Pereira, Z. Guo, S. Nieh, J. Arias, and H. T. Hahn, "Embedding thin-film lithium energy cells in structural composites," *Compos. Sci. Technol.*, vol. 68, no. 7–8, pp. 1935–1941, 2008.

[15]   M. H. Kjell, E. Jacques, D. Zenkert, M. Behm, and G. Lindbergh, "PAN-based carbon fibers for structural lithium-ion batteries," *ECCM 2012 - Compos. Venice, Proc. 15th Eur. Conf. Compos. Mater.*, no. June, pp. 24–28, 2012.

[16]   L. E. Asp and E. S. Greenhalgh, "Structural power composites," *Compos. Sci. Technol.*, vol. 101, pp. 41–61, 2014.

[17]   Y. Wang, C. Peng, and W. Zhang, "Thermal analysis of multifunctional structural battery for satellite applications," *Appl. Therm. Eng.*, vol. 78, pp. 209–216, 2015.

[18]   Y. Yu and B. Zhang, "multifunctional structural batteries based on carbon fiber reinforced plastic composites: investigation on mechanical and electrochemical properties," in *21st International Conference on Composite Materials*, 2017.

[19]   D. Carlstedt, W. Johannisson, D. Zenkert, P. Linde, and L. E. Asp, "Conceptual Design Framework for Laminated Structural Battery Composites," in *ECCM18 - 18th European Conference on Composite Materials*, 2018, pp. 24–28.

[20]   H. Yoshimoto, Y. M. Shin, H. Terai, and J. P. Vacanti, "A biodegradable nanofiber scaffold by electrospinning and its potential for bone tissue engineering," *Biomaterials*, vol. 24, no. 12, pp. 2077–2082, May 2003.

[21]   Z. M. Huang, Y. Z. Zhang, S. Ramakrishna, and C. T. Lim, "Electrospinning and mechanical characterization of gelatin nanofibers," *Polymer (Guildf).*, vol. 45, no. 15, pp. 5361–5368, Jul. 2004.

[22]   J. A. Matthews, G. E. Wnek, D. G. Simpson, and G. L. Bowlin, "Electrospinning of collagen nanofibers," *Biomacromolecules*, vol. 3, no. 2, pp. 232–238, 2002.

[23] E. Formo, E. Lee, D. Campbell, and Y. Xia, "Functionalization of electrospun TiO 2 nanofibers with Pt nanoparticles and nanowires for catalytic applications," *Nano Lett.*, vol. 8, no. 2, pp. 668–672, 2008.

[24] A. C. Patel, S. Li, C. Wang, W. Zhang, and Y. Wei, "Electrospinning of porous silica nanofibers containing silver nanoparticles for catalytic applications," *Chem. Mater.*, vol. 19, no. 6, pp. 1231–1238, 2007.

[25] S. W. Choi, S. M. Jo, W. S. Lee, and Y. R. Kim, "An electrospun poly(vinylidene fluoride) nanofibrous membrane and its battery applications," *Adv. Mater.*, vol. 15, no. 23, pp. 2027–2032, Dec. 2003.

[26] Y.-T. Peng and C.-T. Lo, "Electrospun porous carbon nanofibers as lithium ion battery anodes," *J. Solid State Electrochem.*, vol. 19, no. 11, pp. 3401–3410, Nov. 2015.

[27] P. Ramakrishnan and S. Shanmugam, "Electrochemical Performance of Carbon Nanorods with Embedded Cobalt Metal Nanoparticles as an Electrode Material for Electrochemical Capacitors," *Electrochim. Acta*, vol. 125, pp. 232–240, Apr. 2014.

[28] F. Zhang, C. Yuan, J. Zhu, J. Wang, X. Zhang, and X. W. Lou, "Flexible films derived from electrospun carbon nanofibers incorporated with Co3O4hollow nanoparticles as self-supported electrodes for electrochemical capacitors," *Adv. Funct. Mater.*, vol. 23, no. 31, pp. 3909–3915, Aug. 2013.

[29] S. Hosogai and H. Tsutsumi, "Electrospun nickel oxide/polymer fibrous electrodes for electrochemical capacitors and effect of heat treatment process on their performance," *J. Power Sources*, vol. 194, no. 2, pp. 1213–1217, Dec. 2009.

[30] R. Gopal, S. Kaur, Z. Ma, C. Chan, S. Ramakrishna, and T. Matsuura, "Electrospun nanofibrous filtration membrane," *J. Memb. Sci.*, vol. 281, no. 1–2, pp. 581–586, Sep. 2006.

[31] X. H. Qin and S. Y. Wang, "Filtration properties of electrospinning nanofibers," *J. Appl. Polym. Sci.*, vol. 102, no. 2, pp. 1285–1290, Oct. 2006.

[32] K. Riazi *et al.*, "Polystyrene comb architectures as model systems for the optimized solution electrospinning of branched polymers," *Polym. (United Kingdom)*, vol. 104, pp. 240–250, Nov. 2016.

[33] National Aeronautics and Space Administration, "Development of Lightweight CubeSat with Multi-Functional Structural Battery Systems Composite Housing Enables Structure to Store Power and Save Weight of Batteries," Moffett Field, 2017.

[34] S. G. Lee, K.-S. Han, C. W. Joo, J. K. Park, S.-S. Choi, and Y. S. Lee, "Electrospun PVDF nanofiber web as polymer electrolyte or separator," *Electrochim. Acta*, vol. 50, no. 2–3, pp. 339–343, Nov. 2004.

[35] K. Gao, X. Hu, C. Dai, and T. Yi, "Crystal structures of electrospun PVDF membranes and its separator application for rechargeable lithium metal cells," *Mater. Sci. Eng. B Solid-State Mater. Adv. Technol.*, vol. 131, no. 1–3, pp. 100–105, Jul. 2006.

[36] Y. E. Miao, G. N. Zhu, H. Hou, Y. Y. Xia, and T. Liu, "Electrospun polyimide nanofiber-based nonwoven separators for lithium-ion batteries," *J. Power Sources*, vol. 226, pp. 82–86, 2013.

[37] A. Maceiras *et al.*, "Effect of cyano dipolar groups on the performance of lithium-ion battery electrospun polyimide gel electrolyte membranes," *J. Electroanal. Chem.*, vol. 778, pp. 57–65, Oct. 2016.

[38] X. Ma *et al.*, "Electrospun polyacrylonitrile nanofibrous membranes with varied fiber diameters and different membrane porosities as lithium-ion battery separators," *Electrochim. Acta*, vol. 236, pp. 417–423, May 2017.

[39] J. H. Lee, J. Manuel, H. Choi, W. H. Park, and J. H. Ahn, "Partially oxidized polyacrylonitrile nanofibrous membrane as a thermally stable separator for lithium ion batteries," *Polymer (Guildf).*, vol. 68, pp. 335–343, Jun. 2015.

[40] H. Wang *et al.*, "A heatproof separator for lithium-ion battery based on nylon66 nanofibers," *Ionics (Kiel).*, vol. 22, no. 5, pp. 731–734, May 2016.

[41] M. Yanilmaz, M. Dirican, and X. Zhang, "Evaluation of electrospun SiO2/nylon 6,6 nanofiber membranes as a thermally-stable separator for lithium-ion batteries," *Electrochim. Acta*, vol. 133, pp. 501–508, Jul. 2014.

[42] G.-N. Zhu, T. Liu, Y.-E. Miao, Y.-Y. Xia, and H. Hou, "Electrospun polyimide nanofiber-based nonwoven separators for lithium-ion batteries," *J. Power Sources*, vol. 226, pp. 82–86, Mar. 2012.

[43] H. Y. Li, G. A. Li, Y. Y. Lee, H. Y. Tuan, and Y. L. Liu, "A Thermally Stable, Combustion-Resistant, and Highly Ion-Conductive Separator for Lithium-Ion Batteries Based on Electrospun Fiber Mats of Crosslinked Polybenzoxazine," *Energy Technol.*, vol. 4, no. 4, pp. 551–557, Apr. 2016.

[44] J. Li *et al.*, "Electrochemical performance and thermal stability of the electrospun PTFE nanofiber separator for lithium-ion batteries," *J. Appl. Polym. Sci.*, vol. 135, no.

29, p. 46508, 2018.

[45] L. Cao, P. An, Z. Xu, and J. Huang, "Performance evaluation of electrospun polyimide non-woven separators for high power lithium-ion batteries," *J. Electroanal. Chem.*, vol. 767, pp. 34–39, Apr. 2016.

[46] C. Koning, M. Van Duin, C. Pagnoulle, and R. Jerome, "Strategies for compatibilization of polymer blends," *Prog. Polym. Sci.*, vol. 23, no. 4, pp. 707–757, Jan. 1998.

[47] G. Zainab *et al.*, "Electrospun polyacrylonitrile/polyurethane composite nanofibrous separator with electrochemical performance for high power lithium ion batteries," *Mater. Chem. Phys.*, vol. 182, pp. 308–314, Oct. 2016.

[48] Y. Zhu *et al.*, "Modification and characterization of electrospun poly (vinylidene fluoride)/poly (acrylonitrile) blend separator membranes," *Compos. Part B Eng.*, vol. 112, pp. 31–37, Mar. 2017.

[49] W. Kang *et al.*, "Electrospun cellulose acetate/poly(vinylidene fluoride) nanofibrous membrane for polymer lithium-ion batteries," *J. Solid State Electrochem.*, vol. 20, no. 10, pp. 2791–2803, Oct. 2016.

[50] T. Yvonne, C. Zhang, C. Zhang, E. Omollo, and S. Ncube, "Properties of electrospun PVDF/PMMA/CA membrane as lithium based battery separator," *Cellulose*, vol. 21, no. 4, pp. 2811–2818, Aug. 2014.

[51] A. La Monaca, F. De Giorgio, M. L. Focarete, D. Fabiani, M. Zaccaria, and C. Arbizzani, "Polyvinylidene Difluoride–Polyethyleneoxide Blends for Electrospun Separators in Li-Ion Batteries," *J. Electrochem. Soc.*, vol. 164, no. 1, pp. A6431–A6439, Feb. 2017.

[52] J. Xu *et al.*, "Electrochemical performance and thermal property of electrospun PPESK/PVDF/PPESK composite separator for lithium-ion battery," *J. Appl. Electrochem.*, vol. 43, no. 7, pp. 711–720, Jul. 2013.

[53] Y. Zhai *et al.*, "Sandwich-structured PVdF/PMIA/PVdF nanofibrous separators with robust mechanical strength and thermal stability for lithium ion batteries," *J. Mater. Chem. A*, vol. 2, no. 35, pp. 14511–14518, Aug. 2014.

[54] X. Liang, Y. Yang, X. Jin, and J. Cheng, "Polyethylene Oxide-Coated Electrospun Polyimide Fibrous Seperator for High-Performance Lithium-Ion Battery," *J. Mater. Sci. Technol.*, vol. 32, no. 3, pp. 200–206, Mar. 2016.

[55] M. Xie *et al.*, "The high performance of polydopamine-coated electrospun poly(ether sulfone) nanofibrous separator for lithium-ion batteries," *Macromol. Res.*, vol. 24, no. 11, pp. 965–972, Nov. 2016.

[56] C. Shi *et al.*, "A simple method to prepare a polydopamine modified core-shell structure composite separator for application in high-safety lithium-ion batteries," *J. Memb. Sci.*, vol. 518, pp. 168–177, Nov. 2016.

[57] Y. Zhu *et al.*, "Modification and characterization of electrospun poly (vinylidene fluoride)/poly (acrylonitrile) blend separator membranes," *Compos. Part B Eng.*, vol. 112, pp. 31–37, Mar. 2017.

[58] D. Fabiani, F. De Giorgio, C. Arbizzani, M. L. Focarete, A. La Monaca, and M. Zaccaria, "Polyvinylidene Difluoride–Polyethyleneoxide Blends for Electrospun Separators in Li-Ion Batteries," *J. Electrochem. Soc.*, vol. 164, no. 1, pp. A6431–A6439, 2017.

[59] C. Shi *et al.*, "Electrospun Nanofibers for Sandwiched Polyimide/Poly (vinylidene fluoride)/Polyimide Separators with the Thermal Shutdown Function," *Electrochim. Acta*, vol. 176, pp. 727–734, Sep. 2015.

[60] Y. Y. Lee and Y. L. Liu, "Crosslinked electrospun poly(vinylidene difluoride) fiber mat as a matrix of gel polymer electrolyte for fast-charging lithium-ion battery," *Electrochim. Acta*, vol. 258, pp. 1329–1335, Dec. 2017.

[61] Y. Ding, P. Zhang, Z. Long, Y. Jiang, F. Xu, and W. Di, "The ionic conductivity and mechanical property of electrospun P(VdF-HFP)/PMMA membranes for lithium ion batteries," *J. Memb. Sci.*, vol. 329, no. 1–2, pp. 56–59, Mar. 2009.

[62] W. Chen, Y. Liu, Y. Ma, J. Liu, and X. Liu, "Improved performance of PVdF-HFP/PI nanofiber membrane for lithium ion battery separator prepared by a bicomponent cross-electrospinning method," *Mater. Lett.*, vol. 133, pp. 67–70, Oct. 2014.

[63] K. Liu *et al.*, "Electrospun core-shell microfiber separator with thermal-triggered flame-retardant properties for lithium-ion batteries," *Sci. Adv.*, vol. 3, no. 1, p. e1601978, Jan. 2017.

[64] X. Jiang, L. Xiao, X. Ai, H. Yang, and Y. Cao, "A novel bifunctional thermo-sensitive poly(lactic acid)@poly(butylene succinate) core-shell fibrous separator prepared by a coaxial electrospinning route for safe lithium-ion batteries," *J. Mater. Chem. A*, vol. 5, no. 44, pp. 23238–23242, Nov. 2017.

[65]    M. J. Uddin, P. K. Alaboina, L. Zhang, and S. J. Cho, "A low-cost, environment-friendly lignin-polyvinyl alcohol nanofiber separator using a water-based method for safer and faster lithium-ion batteries," *Mater. Sci. Eng. B Solid-State Mater. Adv. Technol.*, vol. 223, pp. 84–90, Sep. 2017.

[66]    W. Zheng *et al.*, "Hybrid silica membranes with a polymer nanofiber skeleton and their application as lithium-ion battery separators," *Compos. Sci. Technol.*, vol. 144, pp. 178–184, May 2017.

[67]    Y. Zhai, K. Xiao, J. Yu, and B. Ding, "Fabrication of hierarchical structured SiO2/polyetherimide-polyurethane nanofibrous separators with high performance for lithium ion batteries," *Electrochim. Acta*, vol. 154, pp. 219–226, Feb. 2015.

[68]    Y. Li *et al.*, "Electrospun SiO2/PMIA nanofiber membranes with higher ionic conductivity for high temperature resistance lithium-ion batteries," *Fibers Polym.*, vol. 18, no. 2, pp. 212–220, Feb. 2017.

[69]    Y. Wang, S. Wang, J. Fang, L. X. Ding, and H. Wang, "A nano-silica modified polyimide nanofiber separator with enhanced thermal and wetting properties for high safety lithium-ion batteries," *J. Memb. Sci.*, vol. 537, pp. 248–254, Sep. 2017.

[70]    F. Zhang, X. Ma, C. Cao, J. Li, and Y. Zhu, "Poly(vinylidene fluoride)/SiO2 composite membranes prepared by electrospinning and their excellent properties for nonwoven separators for lithium-ion batteries," *J. Power Sources*, vol. 251, pp. 423–431, Apr. 2014.

[71]    M. Yanilmaz, Y. Lu, J. Zhu, and X. Zhang, "Silica/polyacrylonitrile hybrid nanofiber membrane separators via sol-gel and electrospinning techniques for lithium-ion batteries," *J. Power Sources*, vol. 313, pp. 205–212, May 2016.

[72]    S. R. Park, Y. C. Jung, W. K. Shin, K. H. Ahn, C. H. Lee, and D. W. Kim, "Cross-linked fibrous composite separator for high performance lithium-ion batteries with enhanced safety," *J. Memb. Sci.*, vol. 527, pp. 129–136, Apr. 2017.

[73]    Y. Ge, X. Zhang, M. Yanilmaz, Y. Lu, and J. Zhu, "High-strength, thermally stable nylon 6,6 composite nanofiber separators for lithium-ion batteries," *J. Mater. Sci.*, vol. 52, no. 9, pp. 5232–5241, May 2017.

[74]    C. L. Yang *et al.*, "Batwing-like polymer membrane consisting of PMMA-grafted electrospun PVdF-SiO2 nanocomposite fibers for lithium-ion batteries," *J. Memb. Sci.*, vol. 495, pp. 341–350, 2015.

[75]   F. Zhang, X. Ma, C. Cao, J. Li, and Y. Zhu, "Poly(vinylidene fluoride)/SiO2 composite membranes prepared by electrospinning and their excellent properties for nonwoven separators for lithium-ion batteries," *J. Power Sources*, vol. 251, pp. 423–431, Apr. 2014.

[76]   J. Zhu *et al.*, "Highly porous polyacrylonitrile/graphene oxide membrane separator exhibiting excellent anti-self-discharge feature for high-performance lithium-sulfur batteries," *Carbon N. Y.*, vol. 101, pp. 272–280, May 2016.

[77]   X. Liu *et al.*, "Electrospun PU@GO separators for advanced lithium ion batteries," *J. Memb. Sci.*, vol. 555, pp. 1–6, Jun. 2018.

[78]   R. K. Goyal, *Nanomaterials and nanocomposites : synthesis, properties, characterization techniques, and applications*. Boca Raton: Taylor & Francis Group, 2018.

[79]   N. R. Choudhury, P. P. De, and N. K. . Dutta, *Thermal Analysis of Rubbers and Rubbery Materials*. Shropshire, UK: Smithers Rapra Technology Ltd, 2010.

[80]   C. Schick, "Differential scanning calorimetry (DSC) of semicrystalline polymers," *Analytical and Bioanalytical Chemistry*, vol. 395, no. 6. pp. 1589–1611, 2009.

# CHAPTER 3 ELECTROSPINNING STUDY

## Paper 1: Electrospun Poly(Bisphenol A-co-Epichlorohydrin) Membrane

Wisawat Keaswejjareansuk[1], Xiang Wang[2], Richard D. Sisson[1] and Jianyu Liang[1*]

[1]*Worcester Polytechnic Institute, Worcester, MA, USA*

[2]*Wuhan University of Technology, Hubei Province, P.R. China*

[*]Corresponding author.

Address: Worcester Polytechnic Institute 100 Institute Road, Materials Science and Engineering, Mechanical Engineering Department. Worcester, MA 01609

E-mail address: jianyul@wpi.edu

## ABSTRACT

Porous poly(Bisphenol A-co-Epichlorohydrin) PBE membranes are created by an electrospinning process. Morphology of the electrospun membrane is controlled by adjusting solution and process parameters. Different concentrations of polymer solutions are prepared in various ratios of acetone to N,N-dimethylformamide. In order to study the stimulated effects of solution parameters and process parameters, acceleration voltages were varied between 20kV and 25 kV while keeping the solution feed rate and tip-to-collector distance at certain values. The highest elastic modulus, tensile strength and density with consistent fiber morphology obtained in this study was $9.125 \pm 2.573$ GPa, $1.260 \pm 0.195$ MPa and $0.043 \pm 0.006$ mg/cm$^3$, respectively. Mechanical properties (elastic modulus and tensile strength) are morphology dependent. Thermal analysis with differential scanning calorimetry shows no significant changes in glass transition and melting temperatures of the electrospun samples and the raw materials. Since PBE has been widely used as an adhesive, coating agent, additive and matrix to other functional materials, this study explores the use and control of

electrospinning process with PBE and its corresponding mechanical performance in a form of porous non-woven membrane.

## 1. INTRODUCTION

Thermoplastics are extensively used in many applications because of having flexible and linear chains structure. Examples of thermoplastics are polycarbonate PC, polyether ether ketone PEEK, polyetherimide PEI, polylactic acid PLA, polyvinyl chloride PVC, polyvinylidene fluoride PVDF, poly(methyl methacrylate) PMMA, polyethylene PE, polypropylene PP and polytetrafluoroethylene PTFE with applications in consumer products, biomedical materials, chemical sensors, filtration and separation, data storage and transmission, energy materials and manufacturing process [1]–[19]. They are softened and able to be processed into shapes when heating to temperatures those higher than glass transition temperature. In addition to the ease of processing, mechanical performance is an important factor for thermoplastic utilizations. Interestingly, fiber structured, and fiber composited thermoplastics show much improvements in the mechanical properties. Studies of Alexander *et al.* and Wanasekara *et al.* show the PP fibers have tensile strength as high as 200 MPa [20][21]. Ye *et al.* demonstrated the PE fibers have the tensile strength in a range of 26 MPa - 3.3 GPa, varies by production process, while injection-molded HDPE (non-fiber structure) has the tensile strength less than 50 MPa [22]. In Zhang *et al.* experiments, loadings of 5 wt.% and 15wt% cellulose fiber to PE composites increase elastic modulus to 15% and 40%, respectively [23]. Shubhra *et al.* reviewed the reinforced PP composites with 10 wt.% loading of various types natural fiber have tensile strengths more than 20 MPa [24]. Bledzki *et al.* fabricated PP composites by two-step extrusions coating and injection molding process loaded with 30 wt.% cellulose fiber have improvements of 46% in elastic modulus and 148% in tensile strength [25].

Electrospinning is an efficient and versatile [26] process to fabricate highly porous membranes. It is a straightforward technique to fabricate continuous fibers at nanoscale. The spun fibers are collected in ranges of micro- and nano- meters. Simply, a high electric potential is applied to a spinneret (or needle), which is connected to a polymer solution syringe. Polymer solution is fed by a syringe pump and spun in the electric field. The charged spun solution is elongated to a fiber-like jet, and then collected on a collector (grounded substrate). The

electrospinning process has been studied for many applications, such as biomaterials [27]–[29], batteries [30]–[32], capacitors [33]–[35], catalysts [36], [37] and filtration [38], [39].

Poly(Bisphenol-A-co-Epichlorohydrin) *PBE* is a copolymer of bisphenol a with epichlorohydrin. PBE is also known as poly(hydroxyl ether of bisphenol-A) or phenoxy resin. It is ductile, tough and miscible with various polymers due to the presence of a pedant hydroxyl group (proton donor with appropriate functional groups) in the repeating unit [40]–[43]. PBE is a widely used thermoplastic resin. It has been shown to increase glass transition temperature of functional polymer blends [41], [44], such as in thermal-responsive shape memory applications [45]. PBE has been used as additive in thermoplastic to increase tensile strength and elongation [46], [47], elastic modulus [48], and flexural strength [49]. PBE composites and its blends with carbon nanotube have shown an improvement of storage modulus [50], [51]. PBE is also used for increasing of the fracture toughness as polymer matrix and modifier for cryogenic applications [52], [53]. PBE matrix exhibits significant dispersion of organic modified red mud and enhanced overall thermal stability of the organic - inorganic composites [54]. In addition to being a vital component in polymer blends and composites, PBE based materials are used as coating agents and binders to improve interfacial adhesion of carbon fiber-reinforce thermoplastic composites [55]–[57] and have gained interest as high-performance composites for aerospace applications.

Herein, PBE was selected as a model thermoplastic resin due to its wide range applications. PBE porous membrane was created with the electrospinning process. Various microstructures with corresponding density, elastic modulus and tensile strength were obtained by adjusting the polymer-solution concentration, solvent system and process parameters. Membrane morphology, mechanical and thermal properties were studied by scanning electron microscopy, tensile testing, thermogravimetric analysis and differential scanning calorimetry, respectively.

## 2. MATERIAL AND METHODS

### 2.1 Materials

Poly(Bisphenol A-co-Epichlorohydrin) PBE (Mw ~ 40,000 pellets), acetone (laboratory standard) and *N,N*-dimethylformamide DMF (anhydrous, 99.8%) were purchased from Sigma-Aldrich and used as received.

### 2.2 Experiments

PBE was dissolved in different solvent ratios of acetone:DMF to concentrations of 0.125, 0.150, 0.175, 0.200, 0.225 and 0.250 g/mL. DMF was gradually added to acetone with an increment of 10% (acetone:DMF in v/v%), then stirred until obtained a homogeneous solution. The solution was loaded into a 10 mL syringe (1/10 mL graduation) equipped with a stainless steel gauge 18 blunt-tip needle (0.838 mm, inner diameter). The polymer solution was fed with a feeding rate of 0.3 mL/h. High acceleration voltages of 20 and 25 kV were applied at the needle-tip. Aluminum foil collector was set up at 15 cm (tip-to-collector distance) from the needle-tip. Electrospinning experiments were conducted at room temperature (25 °C) and 50 - 55% relative humidity.

### 2.3 Characterizations

Surface micrographs were obtained by a field emission scanning electron microscope (FE-SEM JEOL 7000F), operated at 2 kV. Average density for each solution concentration was calculated by the average of individual weight and volume of three electrospun samples with a diameter of 7/32 inch (0.56 cm). Tensile strengths were measured by a universal testing machine (UTM Instron 5567A) with a crosshead speed of 0.2 mm/min. In order to avoid imperfection of standard dog-bone sample preparations, each electrospun membrane was cut into a strip of 0.25 inches (5.71 cm) width and 1 inch (2.54 cm) length with 0.5 inches (1.27 cm) gauge-length. Thermal stability and thermal decomposition temperature were obtained thermogravimetric analysis (TGA, TA Instrument Q50), scanned from 35 °C – 700 °C at a heating rate of 10 °C/min. Glass transition temperature $T_g$ and melting temperature $T_m$ were

determined by differential scanning calorimetry method (DSC, TA Instrument Q20), scanned from 35 °C – 600 °C at a heating rate of 10 °C/min. Average sample mass for thermal analysis was approximately 2 mg.

## 3. RESULTS AND DISCUSSION

### 3.1 Solvent Composition Affects Morphology

Solution with a concentration of 0.200 g/mL with different amounts of DMF in the mixed acetone was spun under an acceleration voltage of 25 kV. DMF was gradually added into acetone to dissolve PBE and increase the dielectric constant $\epsilon$ with an increment of 10% by volume. The minimum volume of DMF to dissolve PBE into a homogeneous solution is 20%. A higher dielectric constant result in thicker fibers and more deposition on the collector because of more charges on the spinning jet. O. Kolling experimentally determined and calculated (Equation 1) the dielectric constants of acetone:DMF system at 25 °C [58].

$$\epsilon = 36.69 - 15.99 \mathcal{X} \tag{5}$$

where $\mathcal{X}$ is mole fraction of acetone. Porous structures of the electrospun PBE membrane were present with the amounts of DMF up to 60% (Figure 2). The maximum corresponding dielectric constant obtained for the fiber structure is about 27 (Table 1). The boiling points of acetone and DMF at room temperature are 56 °C and 153 °C, respectively. Although a homogeneous solution cannot be obtained with pure acetone, acetone is required as a mechanism to control the morphology because it evaporates faster than DMF and so reduces the diameter of the spinning jets prior to being collected on the grounded substrate. Excess volume of spinning jets reached the collector and lost the porous structure when the amount of acetone is less than 40%. Fine and consistent fiber structure (Figure 2) was obtained with acetone:DMF ratio of 60:40 (%, v/v).

Table 6 Dielectric constant of mixed solvents with different ratios of acetone:DMF [58]

| Solvent ratio Acetone:DMF (%, v/v) | Volume (mL) | | Moles of solvent (mol) | | Mole fraction of acetone | Dielectric constant |
|---|---|---|---|---|---|---|
| | Acetone | DMF | Acetone | DMF | | |
| 80:20 | 8 | 2 | 107.989 | 27.199 | 0.799 | 23.917 |
| 70:30 | 7 | 3 | 94.490 | 40.799 | 0.698 | 25.522 |
| 60:40 | 6 | 4 | 80.992 | 54.399 | 0.598 | 27.125 |
| 50:50 | 5 | 5 | 67.493 | 67.998 | 0.498 | 28.725 |
| 40:60 | 4 | 6 | 53.994 | 81.598 | 0.398 | 30.323 |
| 30:70 | 3 | 7 | 40.496 | 95.198 | 0.298 | 31.918 |
| 20:80 | 2 | 8 | 26.997 | 108.797 | 0.199 | 33.511 |
| 10:90 | 1 | 9 | 13.499 | 122.397 | 0.099 | 35.102 |
| 0:100 | 0 | 10 | 0 | 135.997 | 0 | 36.690 |
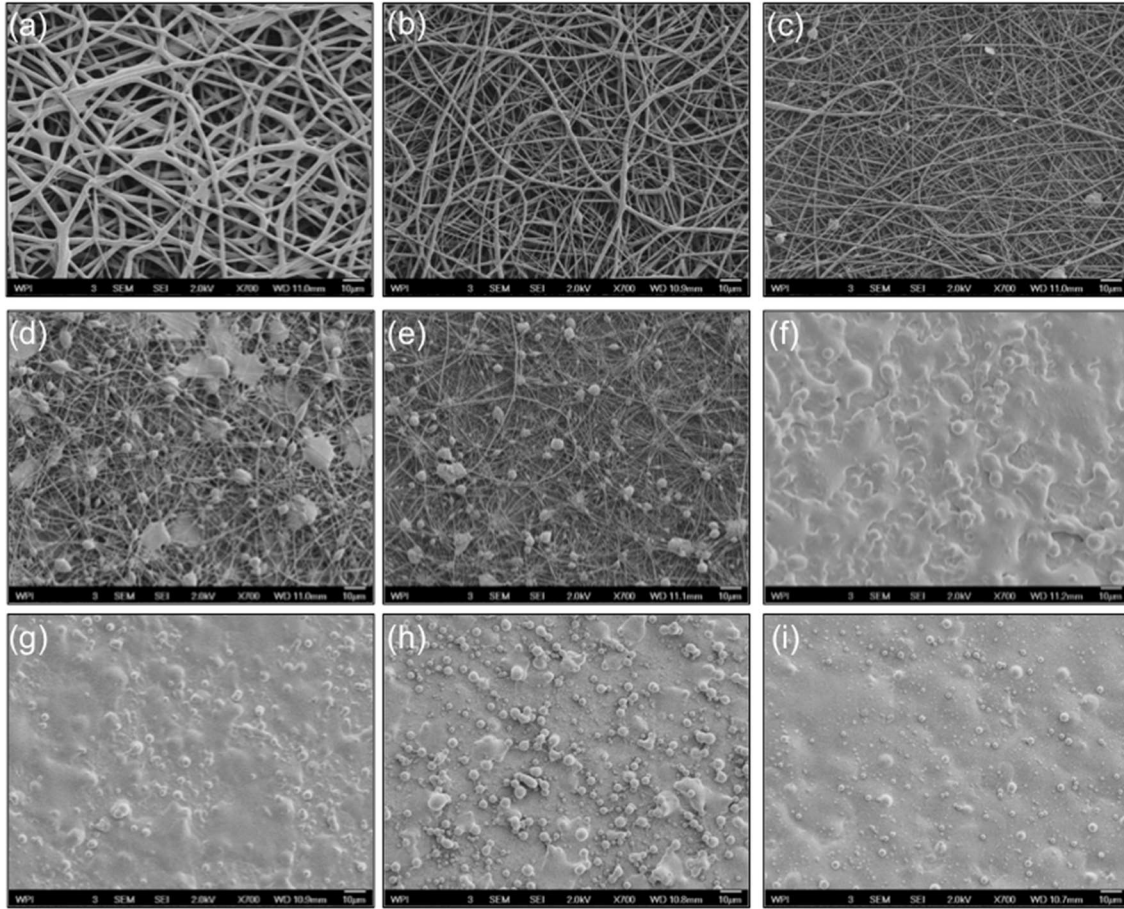
Figure 31 Effect of solvent composition to morphology of electrospun PBE membrane,

(a) 80:20, (b) 70:30, (c) 60:40, (d) 50:50, (e) 40:60, (f) 30:70, (g) 20:80,

(h) 10:90 and (i) 0:100 of acetone:DMF (%, v/v)

(Scale bar = 10 μm, magnification ×700)

## 3.2 Concentrations and Acceleration Voltages Affect Surface Morphology

Structures of the electrospun membranes with the mixed solvent of 60:40 acetone:DMF (%, v/v) are either bead-fiber or fiber structure (Figure 3). Beads domination of bead-fiber structure was obtained at low concentrations, 0.125 - 0.175 g/mL. Beads were decreasing while concentrations were increasing. Fiber structure was obtained at the concentrations of 0.200 - 0.250 g/mL. Only the concentration of 0.200 g/mL yielded fine and consistent fibers. At 0.250 g/mL, fibers are slightly inconsistent and much larger than those of 0.200 g/mL. Although the concentration of 0.125 g/mL was able to be electrospun, the sample was powder-like and was not able to be peeled off from the collector. Thus, this concentration will not be used for further characterizations. Morphology of the electrospun membrane was also affected by the acceleration voltage. Lower acceleration voltage decreases the strength of the electric field. Hence, the charged solution jets at lower acceleration voltage were spun slower with less volume in each spun solution jet. This provided sufficient time for the solution jets to elongate during the flight and allow the solvents to evaporate. A mismatch of the solvents evaporation and spun volumes of the solution jet resulted in dry fibers (less fiber entanglement), excess wet fibers or electrospray.

Scale bar ⊢ = 1 μm

Acceleration voltages:
(I) 25 kV, (II) 20 kV, (III) 15 kV

Concentrations:
(a) 0.125 g/mL,
(b) 0.150 g/mL,
(c) 0.175 g/mL,
(d) 0.200 g/mL,
(e) 0.225 g/mL,
(f) 0.250 g/mL
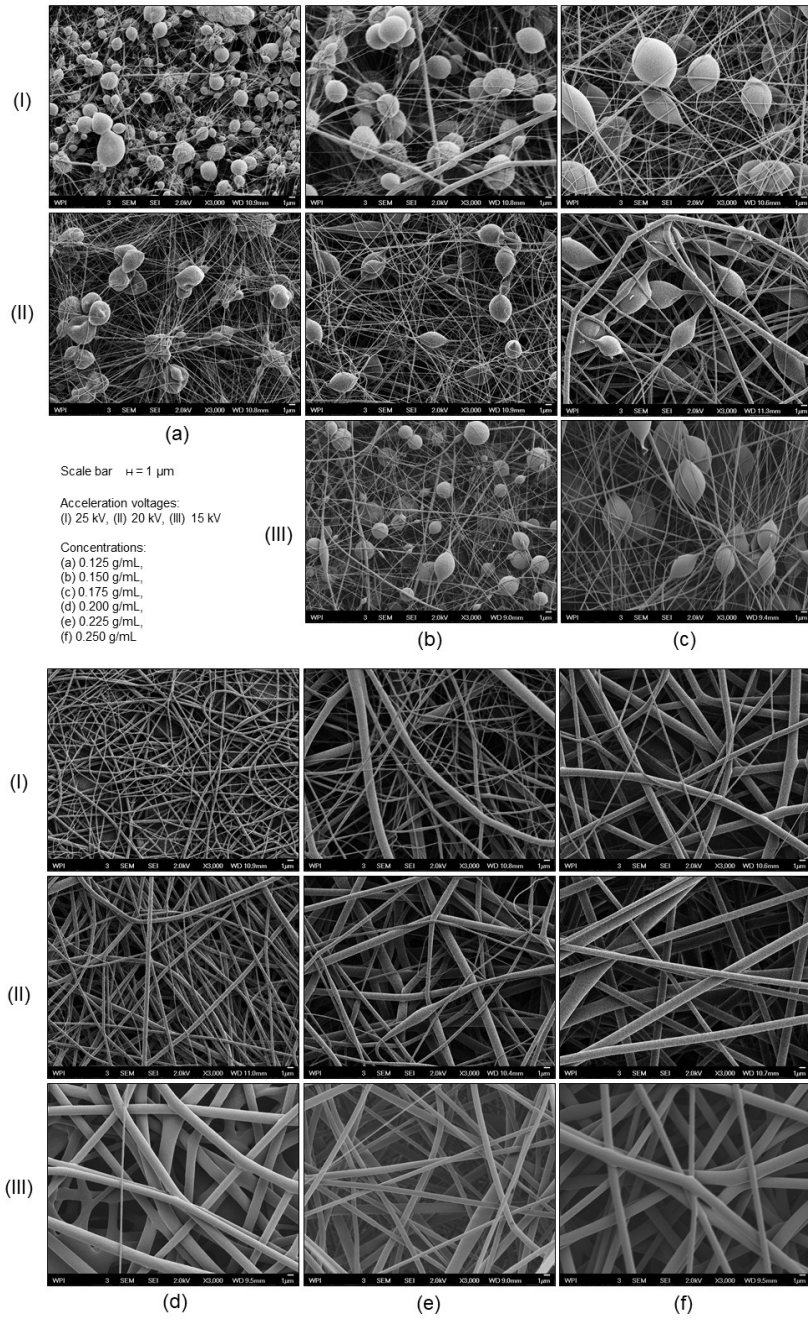
Figure 32 Effects of concentration (a - f) and acceleration voltage (row I, II and III) to morphology, (a) 0.125 g/mL, (b) 0.150 g/mL, (c) 0.175 g/mL, (d) 0.200 g/mL, (e) 0.225 g/mL and (f) 0.250 g/mL; (row I) 25 kV, (row II) 20 kV and (row III) 15 kV

(Scale bar = 1 μm, magnification ×3,000)

Table 7 Average density of electrospun samples corresponds to different solution concentrations with an acceleration voltage of 20 kV

| Concentration of electrospun sample (g/mL) | Average density (mg/cm³) |
|:---:|:---:|
| 0.150 | 0.034 ± 0.003 |
| 0.175 | 0.026 ± 0.002 |
| 0.200 | 0.043 ± 0.006 |
| 0.225 | 0.040 ± 0.005 |
| 0.250 | 0.030 ± 0.001 |
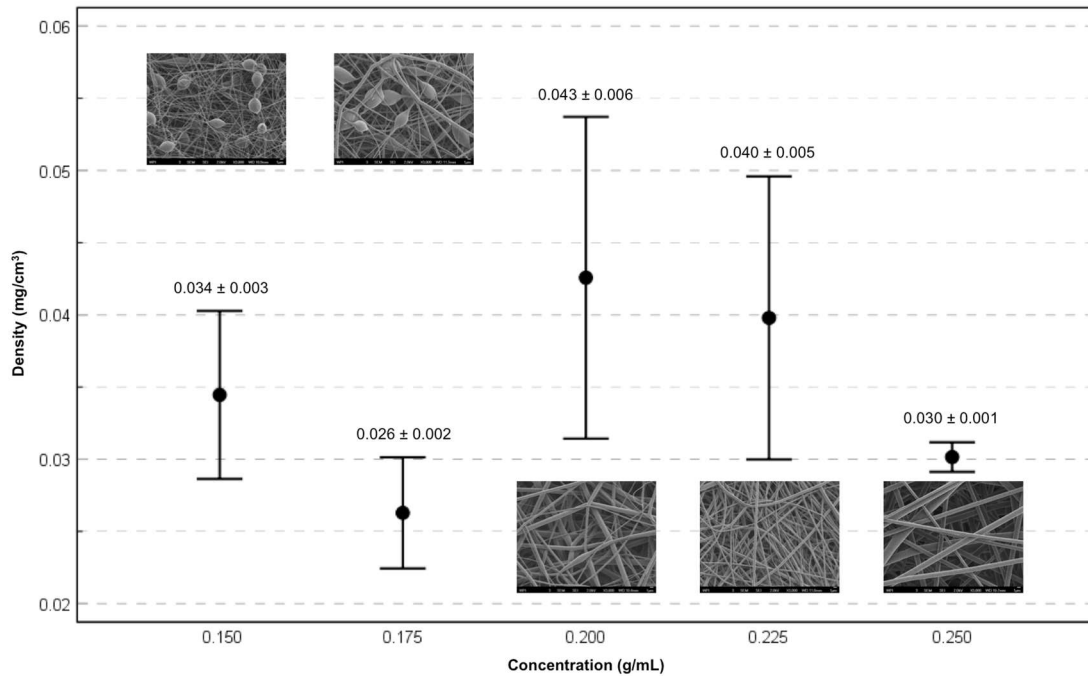


Figure 33 Average density corresponds to different concentrations of electrospun membrane (Acceleration voltage = 20 kV)

Average densities of the electrospun sample decrease while the solution concentrations increase because of the morphology changes from bead dominant to fiber dominant of the mixed bead-fiber structure (Figure 33 *b and c*: density = $0.034 \pm 0.003$ mg/cm³ with the concentration of 0.150 g/mL and density = $0.026 \pm 0.002$ mg/cm³ with the concentration of

0.175 g/mL). For the fiber structure, the electrospun sample with a solution concentration of 0.200 g/mL (consistent fiber structure) has the highest density ($0.040 \pm 0.006$ mg/cm$^3$). The densities decrease at higher solution concentrations due to inconsistent fiber structure.

According to the study of the process and solution parameters, the morphology can be manipulated by adjusting the concentration while keeping certain parameters of the solvent composition and the acceleration voltage. In this study, the lower acceleration voltage (20 kV) is suitable to control the structure.

**3.3 Thermal Study of Electrospun PBE Membrane**

Figure 34 shows the TGA thermogram corresponding to the electrospun PBE membranes and PBE pellet. The electrospun PBE membranes do not have significant weight changes until ~ 370°C (thermal decomposition temperature) and decreases about 70% up to 450 °C which indicates its outstanding resistance ability to elevated temperatures. Glass transition temperature $T_g$ is taken at the midpoint of the changes in slopes for heat capacity from a DSC thermogram (Figure 35). Melting temperature $T_m$ is indicated by the endothermic peak of the DSC thermogram (Figure 36). The glass transition and melting temperatures are in ranges of 65–75 °C and 200-210 °C, respectively.
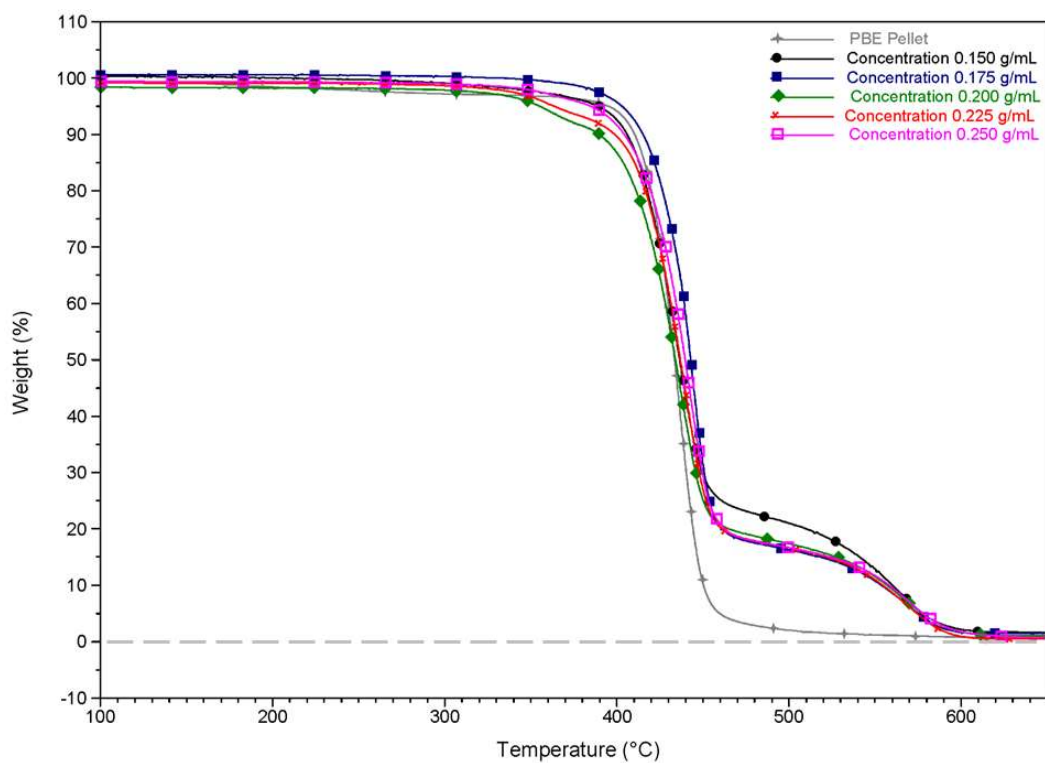
Figure 34 TGA thermogram shows thermal stability and thermal decomposition
temperatures

Table 8 Glass transition temperature $T_g$ and melting temperatures $T_m$ of electrospun sample

| Concentration of electrospun sample (g/mL) | Glass transition temperature $T_g$ (ºC) |
|---|---|
| PBE pellets | 68.50 |
| 0.150 | 67.20 |
| 0.175 | 71.49 |
| 0.200 | 78.00 |
| 0.225 | 74.27 |
| 0.250 | 74.49 |
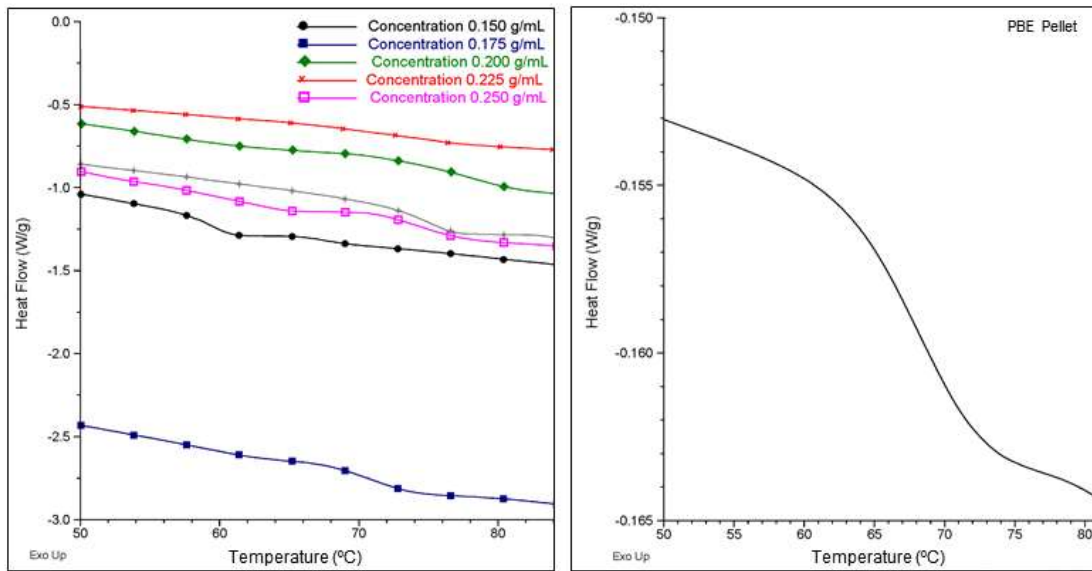
Figure 35 DSC Thermogram shows glass transition temperature $T_g$
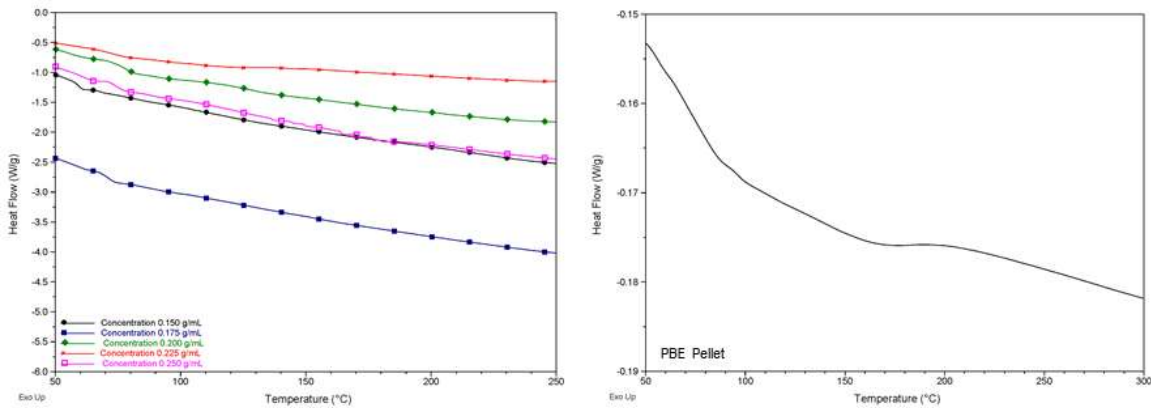


Figure 36 DSC Thermogram shows melting temperatures $T_m$ (~200-210 ºC)

## 3.4 Mechanical Property

Three electrospun samples for each concentration were used as tensile specimens. Elastic modulus and tensile strength are shown in Table 9, Figure 37 and

Figure 38. The electrospun membrane with a concentration of 0.200 g/mL (average density = 0.043 ± 0.006 mg/cm$^3$) has relatively higher elastic modulus, tensile strength and more consistent morphology than other concentrations. As shown in

Figure 38, membranes with the mixed bead-fiber structure (concentrations < 0.200 g/mL) have lower tensile strength than the fiber structure (concentrations ≥ 0.200 g/mL). Although the tensile strengths of membranes with fiber structure are similar to those of 0.200 g/mL, only consistent fiber structure provides the highest elastic modulus.

Table 9 Elastic modulus and tensile strength corresponding to concentrations

| Polymer concentration of the electrospun sample (g/mL) | Elastic modulus (GPa) | Tensile strength (MPa) |
| :---: | :---: | :---: |
| 0.150 | 1.129 ± 0.746 | 0.135 ± 0.065 |
| 0.175 | 3.322 ± 0.736 | 0.294 ± 0.022 |
| 0.200 | 9.125 ± 2.573 | 1.260 ± 0.195 |
| 0.225 | 2.229 ± 0.994 | 1.055 ± 0.353 |
| 0.250 | 5.019 ± 2.309 | 1.271 ± 0.112 |
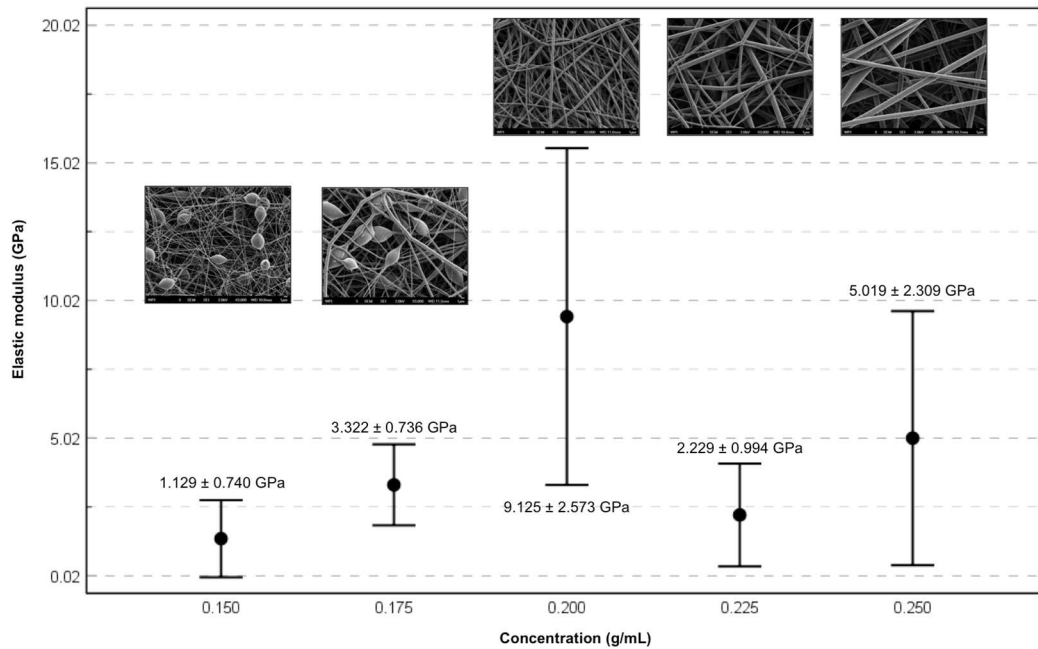


Figure 37 Elastic modulus (GPa) of the electrospun membranes corresponds to the solution concentration (g/mL)
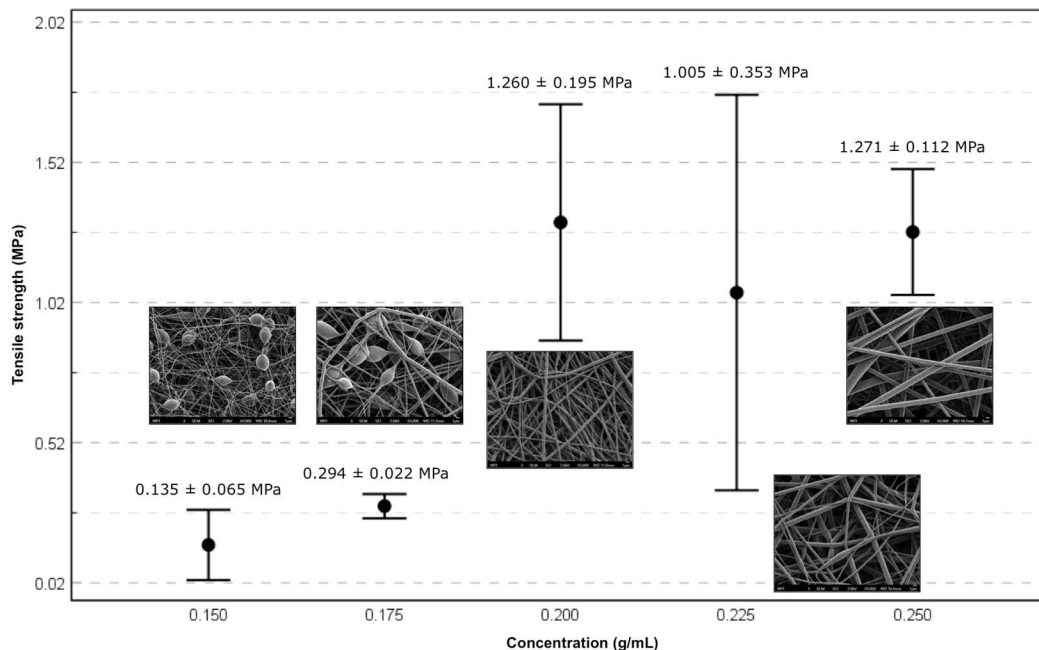
Figure 38. Tensile strength (MPa) of the electrospun membranes corresponds to the solution concentration (g/mL)

## 4. CONCLUSION

In this report, porous PBE membranes were created by an electrospinning process. Glass transition, melting and thermal decomposition temperatures of the electrospun samples have insignificant changes to the PBE pellets. In this study, membrane density, tensile strength and elastic modulus vary corresponding to the morphology. The consistent fiber morphology is an important characteristic to create the electrospun membrane with high tensile strength and elastic modulus. Polymer concentration, solvent system and acceleration voltage are regulated in order to control the morphology. Dielectric constant and acceleration voltage simultaneously affect the spinning rate of solution jets. The higher dielectric constants or acceleration voltage result in higher spin rates, more elongation of the spun jets and more deposition on the grounded collector. Mismatch of dielectric constants and acceleration voltages could lose the porous structure or turn the process to electrospray. Solvent systems are not only used for adjusting the dielectric constant but are also an important parameter for the spun jets to form the desired morphology due to the boiling point. Hence, the fast evaporation of acetone makes solution jets thinner during the flight but the slower evaporation

of DMF makes the deposited fibers entangle. This study does not only present the process controls and corresponding properties of the electrospinning PBE, but also a form of porous PBE membranes for further applications.

## COMPETING INTERESTS

Authors have declared that no competing interests exist.

## AUTHORS' CONTRIBUTIONS

This work was carried out in collaboration between all authors. Keaswejjareansuk conducted the experiments, characterizations and analyzed data. Prof. Wang provided hands-on experiences on the electrospinning during the experiment design. Prof. Sisson contributed comments and suggestions on thermal characterizations. Prof. Liang and Prof. Wang supervised the findings of this work, discussed the results and commented on the manuscript. All authors read and approved the final manuscripts.

## REFERENCES

[1]     X. Pang, X. Zhuang, Z. Tang, and X. Chen, "Polylactic acid (PLA): Research, development and industrialization," *Biotechnol. J.*, vol. 5, no. 11, pp. 1125–1136, Nov. 2010.

[2]     U. Ali, K. J. B. A. Karim, and N. A. Buang, "A Review of the Properties and Applications of Poly (Methyl Methacrylate) (PMMA)," *Polym. Rev.*, vol. 55, no. 4, pp. 678–705, 2015.

[3]     H. Guerrero, J. Zoido, J. L. Escudero, and E. Bernabeu, "Characterization and sensor applications of polycarbonate optical fibers," *Fiber Integr. Opt.*, vol. 12, no. 3, pp. 257–268, Jan. 1993.

[4]     M. Khayet and T. Matsuura, "Application of surface modifying macromolecules for the preparation of membranes for membrane distillation," *Desalination*, vol. 158, no. 1–3, pp. 51–56, Aug. 2003.

[5]     S. Kaliaguine, M. . Guiver, S. M. . Zaidi, S. . Mikhailenko, and G. . Robertson, "Proton conducting composite membranes from polyether ether ketone and heteropolyacids for

fuel cell applications," *J. Memb. Sci.*, vol. 173, no. 1, pp. 17–34, Jul. 2002.

[6]     S. Ayyaru and S. Dharmalingam, "Development of MFC using sulphonated polyether ether ketone (SPEEK) membrane for electricity generation from waste water," *Bioresour. Technol.*, vol. 102, no. 24, pp. 11167–11171, Dec. 2011.

[7]     D. Almasi, N. Iqbal, M. Sadeghi, I. Sudin, M. R. Abdul Kadir, and T. Kamarul, "Preparation Methods for Improving PEEK's Bioactivity for Orthopedic and Dental Application: A Review," *Int. J. Biomater.*, vol. 2016, pp. 1–12, Apr. 2016.

[8]     A. Abdelrasoul, H. Doan, A. Lohi, and C.-H. Cheng, "Morphology Control of Polysulfone Membranes in Filtration Processes: a Critical Review," *ChemBioEng Rev.*, vol. 2, no. 1, pp. 22–43, Feb. 2015.

[9]     S. S. Lane, R. L. Lindstrom, P. A. Williams, and C. W. Lindstrom, "Polysulfone Intracorneal Lenses," *J. Refract. Surg.*, vol. 1, no. 5, pp. 207–216, Nov. 1985.

[10]    K. Hamad, M. Kaseem, H. W. Yang, F. Deri, and Y. G. Ko, "Properties and medical applications of polylactic acid: A review," *Express Polym. Lett.*, vol. 9, no. 6, pp. 435–455, 2015.

[11]    A. B. Fuertes and T. A. Centeno, "Carbon molecular sieve membranes from polyetherimide," *Microporous Mesoporous Mater.*, vol. 26, no. 1–3, pp. 23–26, Dec. 1998.

[12]    P. Appendini and J. H. Hotchkiss, "Review of antimicrobial food packaging," *Innov. Food Sci. Emerg. Technol.*, vol. 3, no. 2, pp. 113–126, Jun. 2002.

[13]    P. Kannan, J. J. Biernacki, and D. P. Visco, "A review of physical and kinetic models of thermal degradation of expanded polystyrene foam and their application to the lost foam casting process," *J. Anal. Appl. Pyrolysis*, vol. 78, no. 1, pp. 162–171, Jan. 2007.

[14]    J. Nart, J. D. Sanz-Moliner, J. M. Carbonell, A. Pujol, A. Santos, and I. S. Martín, "High-density polytetrafluoroethylene membranes in guided bone and tissue regeneration procedures: a literature review," *Int. J. Oral Maxillofac. Surg.*, vol. 43, no. 1, pp. 75–84, Jan. 2013.

[15]    D. J. Kim, M. J. Jo, and S. Y. Nam, "A review of polymer-nanocomposite electrolyte membranes for fuel cell application," *Journal of Industrial and Engineering Chemistry*, vol. 21. Elsevier, pp. 36–52, 25-Jan-2015.

[16]    H. R. Gallantree, "Review of transducer applications of polyvinylidene fluoride," *IEE Proc. I Solid State Electron Devices*, vol. 130, no. 5, p. 219, 2010.

[17]  S. Wang *et al.*, "The use of polyvinylidene fluoride (PVDF) films as sensors for vibration measurement: A brief review," *Ferroelectrics*, vol. 502, no. 1, pp. 28–42, 2016.

[18]  G. Harsanyi, "Polymer films in sensor applications: A review of present uses and future possibilities," *Sens. Rev.*, vol. 20, no. 2, pp. 98–105, 2000.

[19]  G. dong Kang and Y. ming Cao, "Application and modification of poly(vinylidene fluoride) (PVDF) membranes - A review," *Journal of Membrane Science*, vol. 463. Elsevier, pp. 145–165, 01-Aug-2014.

[20]  N. Wanasekara, V. Chalivendra, and P. Calvert, "Sub-micron scale mechanical properties of polypropylene fibers exposed to ultraviolet and thermal degradation," *Polym. Degrad. Stab.*, vol. 96, no. 4, pp. 432–437, 2011.

[21]  J. V. Alexander, J. W. Neely, and E. A. Grulke, "Effect of chemical Functionalization on the mechanical properties of polypropylene hollow fiber membranes," *J. Polym. Sci. Part B Polym. Phys.*, vol. 52, no. 20, pp. 1366–1373, Oct. 2014.

[22]  Z. Ye, S. Zhu, W. J. Wang, H. Alsyouri, and Y. S. Lin, "Morphological and mechanical properties of nascent polyethylene fibers produced via ethylene extrusion polymerization with a metallocene catalyst supported on MCM-41 particles," *J. Polym. Sci. Part B Polym. Phys.*, vol. 41, no. 20, pp. 2433–2443, Oct. 2003.

[23]  F. Zhang, T. Endo, W. Qiu, L. Yang, and T. Hirotsu, "Preparation and mechanical properties of composite of fibrous cellulose and maleated polyethylene," *J. Appl. Polym. Sci.*, vol. 84, no. 11, pp. 1971–1980, Jun. 2002.

[24]  Q. T. H. Shubhra, A. K. M. M. Alam, and M. A. Quaiyyum, "Mechanical properties of polypropylene composites: A review," *Journal of Thermoplastic Composite Materials*, vol. 26, no. 3. pp. 362–391, 2013.

[25]  A. K. Bledzki, A. Jaszkiewicz, and D. Scherzer, "Mechanical properties of PLA composites with man-made cellulose and abaca fibres," *Compos. Part A Appl. Sci. Manuf.*, vol. 40, no. 4, pp. 404–412, Apr. 2009.

[26]  D. H. Reneker and I. Chun, "Nanometre diameter fibres of polymer, produced by electrospinning," *Nanotechnology*, vol. 7, no. 3, pp. 216–223, 1996.

[27]  H. Yoshimoto, Y. M. Shin, H. Terai, and J. P. Vacanti, "A biodegradable nanofiber scaffold by electrospinning and its potential for bone tissue engineering," *Biomaterials*, vol. 24, no. 12, pp. 2077–2082, May 2003.

[28]  Z. M. Huang, Y. Z. Zhang, S. Ramakrishna, and C. T. Lim, "Electrospinning and mechanical characterization of gelatin nanofibers," *Polymer (Guildf).*, vol. 45, no. 15, pp. 5361–5368, Jul. 2004.

[29]  J. A. Matthews, G. E. Wnek, D. G. Simpson, and G. L. Bowlin, "Electrospinning of collagen nanofibers," *Biomacromolecules*, vol. 3, no. 2, pp. 232–238, 2002.

[30]  J.-W. Jung, C.-L. Lee, S. Yu, and I.-D. Kim, "Electrospun nanofibers as a platform for advanced secondary batteries: a comprehensive review," *J. Mater. Chem. A*, vol. 4, no. 3, pp. 703–750, 2016.

[31]  Y.-T. Peng and C.-T. Lo, "Electrospun porous carbon nanofibers as lithium ion battery anodes," *J. Solid State Electrochem.*, vol. 19, no. 11, pp. 3401–3410, Nov. 2015.

[32]  S. W. Choi, S. M. Jo, W. S. Lee, and Y. R. Kim, "An electrospun poly(vinylidene fluoride) nanofibrous membrane and its battery applications," *Adv. Mater.*, vol. 15, no. 23, pp. 2027–2032, Dec. 2003.

[33]  S. Hosogai and H. Tsutsumi, "Electrospun nickel oxide/polymer fibrous electrodes for electrochemical capacitors and effect of heat treatment process on their performance," *J. Power Sources*, vol. 194, no. 2, pp. 1213–1217, Dec. 2009.

[34]  F. Zhang, C. Yuan, J. Zhu, J. Wang, X. Zhang, and X. W. Lou, "Flexible films derived from electrospun carbon nanofibers incorporated with Co3O4hollow nanoparticles as self-supported electrodes for electrochemical capacitors," *Adv. Funct. Mater.*, vol. 23, no. 31, pp. 3909–3915, Aug. 2013.

[35]  P. Ramakrishnan and S. Shanmugam, "Electrochemical Performance of Carbon Nanorods with Embedded Cobalt Metal Nanoparticles as an Electrode Material for Electrochemical Capacitors," *Electrochim. Acta*, vol. 125, pp. 232–240, Apr. 2014.

[36]  A. C. Patel, S. Li, C. Wang, W. Zhang, and Y. Wei, "Electrospinning of porous silica nanofibers containing silver nanoparticles for catalytic applications," *Chem. Mater.*, vol. 19, no. 6, pp. 1231–1238, 2007.

[37]  E. Formo, E. Lee, D. Campbell, and Y. Xia, "Functionalization of electrospun TiO 2 nanofibers with Pt nanoparticles and nanowires for catalytic applications," *Nano Lett.*, vol. 8, no. 2, pp. 668–672, 2008.

[38]  R. Gopal, S. Kaur, Z. Ma, C. Chan, S. Ramakrishna, and T. Matsuura, "Electrospun nanofibrous filtration membrane," *J. Memb. Sci.*, vol. 281, no. 1–2, pp. 581–586, Sep. 2006.

[39]  X. H. Qin and S. Y. Wang, "Filtration properties of electrospinning nanofibers," *J. Appl. Polym. Sci.*, vol. 102, no. 2, pp. 1285–1290, Oct. 2006.

[40]  M. A. Iriarte, J. J. Iruin, and J. I. Eguiazábal, "Thermal decomposition of miscible phenoxy/poly(ethylene oxide) blends," *J. Mater. Sci.*, vol. 24, no. 3, pp. 1021–1024, Mar. 1989.

[41]  R. Zhang, X. Luo, and D. Ma, "Miscibility of polyhydroxy ether of bisphenol-A with ethylene terephthalate-caprolactone copolyesters," *Eur. Polym. J.*, vol. 31, no. 10, pp. 1011–1014, Oct. 1995.

[42]  B. K. Kim and C. H. Choi, "Melt blends of poly(methyl methacrylate) with a phenoxy," *Polymer (Guildf).*, vol. 37, no. 5, pp. 807–812, Jan. 1996.

[43]  M. A. Corres, M. Zubitur, M. Cortazar, and A. Múgica, "Thermal and thermo-oxidative degradation of poly(hydroxy ether of bisphenol-A) studied by TGA/FTIR and TGA/MS," *J. Anal. Appl. Pyrolysis*, vol. 92, no. 2, pp. 407–416, 2011.

[44]  Q. Guo, "Effect of curing agent on the phase behaviour of epoxy resin/phenoxy blends," *Polymer (Guildf).*, vol. 36, no. 25, pp. 4753–4760, Jan. 1995.

[45]  H. M. Jeong, B. K. Ahn, and B. K. Kim, "Miscibility and shape memory effect of thermoplastic polyurethane blends with phenoxy resin," *Eur. Polym. J.*, vol. 37, no. 11, pp. 2245–2252, Nov. 2001.

[46]  T. Yilmaz, Ö. Özarslan, E. Yildiz, A. Kuyulu, E. Ekinci, and A. Güngör, "Effects of nonreactive resins on the properties of a UV-curable methacrylated urethane resin," *J. Appl. Polym. Sci.*, vol. 69, no. 9, pp. 1837–1845, Aug. 1998.

[47]  G. Qipeng, H. Jinyu, L. Binyao, C. Tianlu, Z. Hongfang, and F. Zhiliu, "Blends of phenolphthalein poly(ether ether ketone) with phenoxy and epoxy resin," *Polymer (Guildf).*, vol. 32, no. 1, pp. 58–65, Jan. 1991.

[48]  G. D. Choi, S. H. Kim, W. H. Jo, and M. S. Rhim, "The morphology and mechanical properties of phenoxy/liquid crystalline polymer blends and the effect of transesterification," *J. Appl. Polym. Sci.*, vol. 55, no. 4, pp. 561–569, Jan. 1995.

[49]  H. Wu, C. M. Ma, and J. Lin, "Processability and Properties of Phenoxy Resin Toughened Phenolic Resin Composites," *J. Appl. Polym. Sci.*, vol. 63, no. March 1996, pp. 911–917, Feb. 1997.

[50]  B.-X. Yang, J.-H. Shi, K. P. Pramoda, and S. H. Goh, "Enhancement of stiffness, strength, ductility and toughness of poly(ethylene oxide) using phenoxy-grafted

multiwalled carbon nanotubes," *Nanotechnology*, vol. 18, no. 12, p. 125606, Mar. 2007.

[51] H. W. Goh, S. H. Goh, G. Q. Xu, K. P. Pramoda, and W. D. Zhang, "Dynamic mechanical behavior of in situ functionalized multi-walled carbon nanotube/phenoxy resin composite," *Chem. Phys. Lett.*, vol. 373, no. 3–4, pp. 277–283, May 2003.

[52] T. Ueki, K. Nojima, K. Asano, S. Nishijima, and T. Okada, "Toughening of Epoxy Resin Systems for Cryogenic Use," in *Advances in Cryogenic Engineering Materials*, Boston, MA: Springer US, 1998, pp. 277–283.

[53] T. Ueki, S. Nishijima, and Y. Izumi, "Designing of epoxy resin systems for cryogenic use," *Cryogenics (Guildf).*, vol. 45, no. 2, pp. 141–148, Feb. 2005.

[54] C. Capela, S. E. Oliveira, and J. A. M. Ferreira, "Mechanical behavior of high dosage short carbon fiber reinforced epoxy composites," *Fibers Polym.*, vol. 18, no. 6, pp. 1200–1207, Jun. 2017.

[55] C. Capela, S. E. Oliveira, J. Pestana, and J. A. M. Ferreira, "Effect of fiber length on the mechanical properties of high dosage carbon reinforced," *Procedia Struct. Integr.*, vol. 5, pp. 539–546, Jan. 2017.

[56] M. A. Fernández-Ruiz, L. M. Gil-Martín, J. F. Carbonell-Márquez, and E. Hernández-Montes, "Epoxy resin and ground tyre rubber replacement for cement in concrete: Compressive behaviour and durability properties," *Constr. Build. Mater.*, vol. 173, pp. 49–57, Jun. 2018.

[57] A. H. Bhat, H. P. S. Abdul Khalil, I. U. H. Bhat, and A. K. Banthia, "Development and characterization of novel modified red mud nanocomposites based on poly(hydroxy ether) of bisphenol A," *J. Appl. Polym. Sci.*, vol. 119, no. 1, pp. 515–522, Jan. 2011.

[58] J. W. Yi *et al.*, "Effect of phenoxy-based coating resin for reinforcing pitch carbon fibers on the interlaminar shear strength of PA6 composites," *Compos. Part A Appl. Sci. Manuf.*, vol. 87, pp. 212–219, Aug. 2016.

[59] U. Beier, J. K. W. Sandler, V. Altstädt, H. Spanner, and C. Weimer, "Mechanical performance of carbon fibre-reinforced composites based on stitched and bindered preforms," *Compos. Part A Appl. Sci. Manuf.*, vol. 40, no. 11, pp. 1756–1763, Nov. 2009.

[60] U. Beier *et al.*, "Mechanical performance of carbon fibre-reinforced composites based on preforms stitched with innovative low-melting temperature and matrix soluble

thermoplastic yarns," *Compos. Part A Appl. Sci. Manuf.*, vol. 39, no. 9, pp. 1572–1581, Sep. 2008.

[61]    O. W. Kolling, "Dielectric Characterization of Cosolvents Containing N,N-Dimethylformamide," *Trans. Kansas Acad. Sci.*, vol. 97, no. 3/4, p. 88, Oct. 1994.

# CHAPTER 4 ELECTROSPUN LAYER-BY-LAYER POLYMER SEPARATOR

**Paper 2: Fabrication of Electrospun Layer-by-Layer PVdF-HFP/PEO Separator for Structural Battery Applications**

Wisawat Keaswejjareansuk, Cesar Guerrero, Richard D. Sisson Jr., Jianyu Liang*
*Worcester Polytechnic Institute, Worcester, MA, USA*

*Corresponding author.
Address: Worcester Polytechnic Institute 100 Institute Road, Materials Science and Engineering, Mechanical Engineering Department. Worcester, MA 01609
E-mail address: jianyul@wpi.edu

## ABSTRACT

In this paper, non-woven mats of layer-by-layer PVDF-HFP/PEO and PVDF-HFP were created by electrospinning process. In corresponding to the demands of energy, structural battery concept is being realized using carbon fibers as electrode materials with conventional polymer separators such as polypropylene porous membrane. This work uses the electrospinning to create layer-by-layer PVdF-HFP/PEO separator with fiber structure. Thermal characteristics of electrospun layer-by-layer membrane is similar to those of the electrospun PVdF-HFP. Ionic conductivity of the electrospun layer-by-layer separator is ~90% higher than the conventional polypropylene separator. Owing the characteristics of electrospun non-woven mats and material properties of PVdF-HFP and PEO, the electrospun layer-by-layer PVdF-HFP/PEO has high tensile strength (~25 MPa), high melting temperature (~145 ℃) and excellent thermal stability (up to ~400 ℃).

# 1. INTRODUCTION

Lithium-ion batteries (LIBs) dominate the consumer electronics with higher energy density operating voltage compared to other commercial rechargeable battery system. LIBs consist of anode, cathode and separator soaked with electrolyte. Separator is a porous polymer membrane that be allowing ions transportation but electrically insulating. Separator is a crucial component to prevent physical contact between electrodes. High mass contribution of LIBs makes size and weight limitations in many applications (i.e. mobile phone, wearable device or hybrid electric vehicle). Structural battery is the battery with multifunctional materials, which simultaneously serves as power source and part of the structure. Prior works on structural battery have been focused on electrode materials, for example utilize carbon fiber reinforced polymers (CFRP). While the carbon fiber (CF) or CF-composites with high tensile strength and tensile stiffness-to-weight ratio are progressively developed, glass-fiber [1][2][3], polymer membrane [4] or polymer matrix [5] are being use as the separator or separator/electrolyte for the structural battery system. In addition to the nature of separator materials having relatively low mechanical integrity to the system, the electrochemical and the mechanical performances have a trade-off relationship with each other. According to the progress of structural battery, fiber is an ideal form to the realization of structural battery [6]. Electrospinning is a facile process to create continuous nano- to micro-diameter fibers, ~40-2,000 nm [7]. Polymer solution is loaded into a syringe equipped with the high electric potential at the tip of stainless steel needle. The syringe is then setup on a syringe pump. A ground substrate (collector) is, then, placed at a certain distance from the needle tip of the solution syringe (tip-to-collector distance).  Polymer solution is spun in a form of solution jets into an electric field and collected as non-woven mats at the collector. Solvent evaporates while the solution jets are travelling in the electric field thus decreasing in the jets diameter and increasing in the surface charge density. Prior to solution jets deposition, the solution jets are whipping and stretching due to bending instability. Electrospun solution jets are loosely deposited on the top of prior deposited fibers, thus surface morphology is the same as the morphology though out the membrane. Because pore size is an important characteristic of separator in preventing all active materials to transport through it, consistent fiber morphology is required to control the pore formation of the electrospun membranes. The solidified electrospun fibers deposit on the collector having bead, bead-fiber or fiber morphology. The surface morphology can be customized by controlling: 1) solution parameters, which are property of polymer, solution concentration and solvent system and 2) process parameters, includes electric potential, solution feed rate and tip-to-collector distance.

Thermal characteristic of the electrospun membranes is the properties of polymer. Both polymer properties and membrane morphology affect mechanical integrity.

Poly(vinylidene fluoride-co-hexafluoropropylene) PVdF-HFP is a promising materials for lithium-ion battery separators due to high chemical resistance, relative high dielectric constant ($\varepsilon \sim 8.4$-10.6) [8][9], high solubility in various organic solvent, low crystallinity and glass transition temperatures [10], and high anodic stability. Crystalline VdF unit provides mechanical integrity, while amorphous HFP unit capable to traps large amounts of liquid electrolyte, offers higher ionic conduction and superior hydrophobicity [11] to the crystalline VdF. PVdF-HFP has good chemical and mechanical stabilities, thus, suitable for long-term performance of lithium-ion battery. Many prior works on PVdF-HFP composites have been studied for structural performances. For examples, Sohn *et al.* [12] studied PVdF-HFP/PMMA coated the commercial polyethylene separator with high ionic conductivity of $1.69 \times 10^{-3}$ S/cm and electrochemically stable up to 5 V by linear sweep voltammetry. Chen et al. [13] created electrospun PVdF-HFP/PI. PVdF-HFP is used as bonding fiber and shutdown function due to relatively lower melting temperature than the heat resistant polyimide (PI).

Poly(ethylene oxide) (PEO) is a semi-crystalline polymer that has high dielectric constant and high $Li^+$ donor number. Amorphous phase of PEO promotes ion transportation due to its chain flexibility [14]. Beside liquid LIBs system, PEO is attractive as blends/additives in gel- and solid- electrolytes LIBs. Prior studies of solid polymer PEO electrolyte show ionic conductivity in a range of $10^{-6}$-$10^{-4}$ S/cm [15]–[17] at room temperature. On other studies, gel polymer PEO electrolyte has the ionic conductivity in an order of $10^{-4}$-$10^{-3}$ S/cm [18]–[26]. Because of its high ionic conductivity and able to easily be dissolved in various solvents (i.e. water, ethanol or acetone) at room temperature, PEO is a candidate polymer suitable to creates the fibrous separator for liquid LIBs by the electrospinning process.

In this study, PVdF-HFP and PEO were electrospun with different electrospinning conditions. The aim of this study is to create layer-by-layer of PVdF-HFP and PEO membrane with fiber morphology for structural battery applications. The electrospun membranes were characterized for thermal, mechanical and electrochemical performances using scanning electron microscopy (SEM), differential scanning calorimetry (DSC), thermogravimetric analysis (TGA), tensile testing and electrochemical impedance spectroscopy (EIS).

## 2. EXPERIMENT SECTION

### 2.1 Materials

Poly(vinylidene fluoride-co-hexafluoropropylene) PVdF-HFP (Mw ~ 400,000), poly(ethylene oxide) PEO (Mw ~100,000), acetone (laboratory standard), ethanol (laboratory reagent, 96%) and *N,N*-dimethylformamide DMF (anhydrous, 99.8%) were purchased from Sigma-Aldrich and used as received.

### 2.2 Experiments

PVdF-HFP was dried in vacuum at 60 °C for 24 h, then dissolved in mixed solvents of acetone:DMF (6:4 v/v %) to concentration of 0.25 and 0.15 g/mL. PEO with a molecular weight of 100,000 was dissolved in ethanol:DI water to a concentration of 0.18 and 0.2 g/mL. Ethanol was gradually added into DI water then stirred until obtained a homogeneous solution. The solution was loaded into a 10mL syringe equipped with a stainless steel blunt-tip needle (18-gauge, 0.838 mm inner diameter). The polymer solution was fed at a feeding rate of 0.3 mL/h into an electric field with high acceleration voltages of 15 and 25 kV. A grounded collector (aluminum foil) was placed at 15 cm from the needle tip. Electrospinning experiment were conducted at a room temperature (25 °C) and 50-55% relative humidity.

### 2.3 Characterizations

Surface micrographs were taken at 2kV using a field emission scanning electron microscopy (FE-SEM JEOL 7000F). Tensile strength was measured by a micro-tensile tester (Instron 5848 MicroTester) with a strain rate of $5 \times 10^{-4}$ 1/s (speed of gauge portion = 6 mm/min). The electrospun membrane was cut into a strip of 0.5 cm width and 4 cm length with 2 cm gauge-length to avoid imperfection of standard dog-bone sample preparation. Ionic conductivity was measured by electrochemical impedance spectroscopy (EIS) using potentiostats/galvanostats (Bio-Logic VSP mVMP Model 1). Circular electrospun membranes (1.6 cm diameter) were sandwiched between symmetrical stainless steel discs (1.58 cm diameter), then fabricated the coin cells CR2032 in a glove box. EIS was performed over the frequency ranging from $2 \times 10^{-3}$ to $2 \times 10^{5}$ Hz at AC amplitude of 100 mV. Thermal stability and melting temperature $T_m$ were determined by thermogravimetric analysis (TGA, TA Instrument Q50) and differential scanning calorimetry (DSC, TA Instrument

Q20), respectively, at a heating rate of 10 °C/min. Average mass of sample for thermal analysis is ~ 2mg.

# 3. RESULTS AND DISCUSSION

## 3.1 Morphology studies

*Surface morphology of electrospun PVdF-HFP* Surface morphology of the electrospun PVdF-HFP with corresponding solution concentrations (0.15 and 0.20 g/mL) and acceleration potentials (15 and 25 kV) are presented in Table 10 and Figure 39. The electrospun jets were spun faster as the jets stretching, reducing jet diameters (thinner) and increasing surface charges at higher acceleration potentials (15 kV in Figure 39a vs 25 kV in Figure 39b). Beads present in both acceleration potentials due to low concentration of the polymer solution (0.15 g/mL), hence drops of the polymer solution were also being collected on the fibers at the grounded collector. Approximately 33% higher concentration (0.20 g/mL, Figure 39 c and d), fiber structure was able to obtain for both acceleration potentials.

Table 10 Surface morphology of electrospun PVdF-HFP with different concentrations and acceleration potentials

| | Acceleration potential (kV) | |
|---|---|---|
| **Solution concentration $c$ (g/mL)** | **15** | **25** |
| c = 0.15 | Bead-fiber, bead dominant | Bead-fiber, fiber dominant |
| c = 0.20 | Fiber | Fiber |
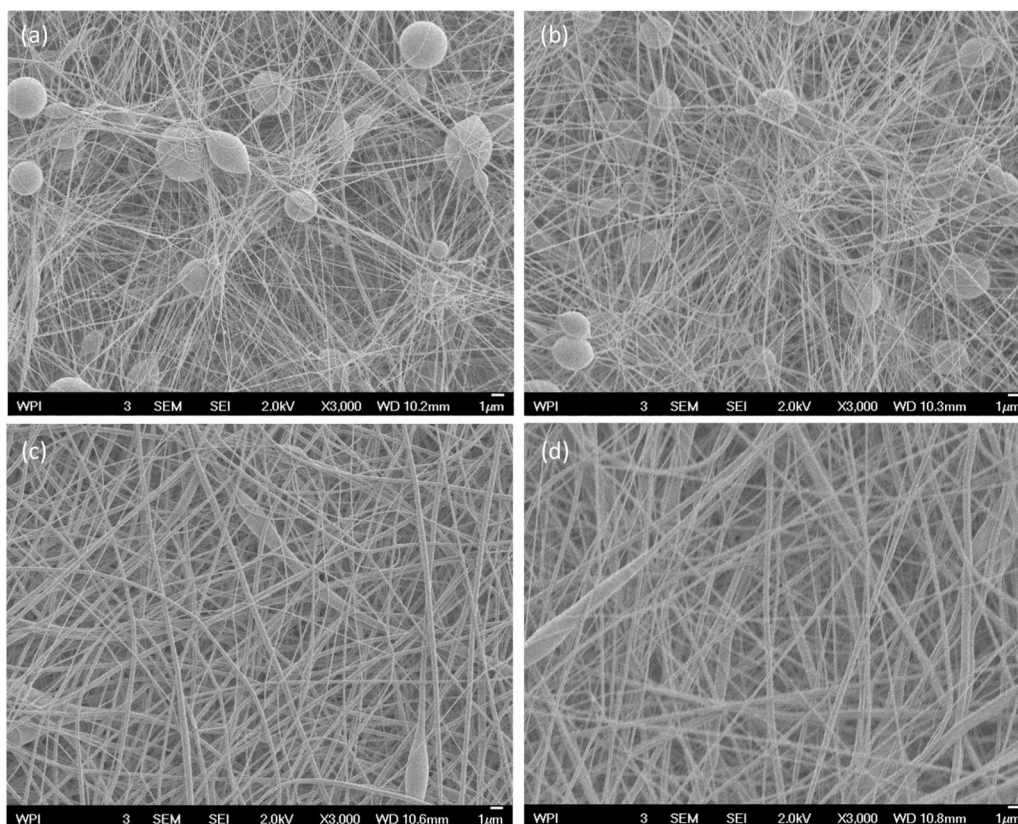
Figure 39 surface morphology of electrospun PVdF-HFP with different concentrations (0.15 g/mL a and b; 0.20 g/mL c and d) and acceleration potentials (15 kV a and c; 25 kV b and d) (Scale bar = 1 μm, magnification ×3,000)

*Surface morphology of electrospun PEO* Surface morphology of electrospun fiber structure with PEO membranes is illustrated in Figure 40 and Figure 41 for the concentration of 0.18 g/mL and 0.20 g/mL, respectively. Although both solution concentrations produced fibers structure, higher concentration (0.20 g/mL) deposited more dense fibers. Solvents system is an influent factor in forming morphology of the electrospun membrane. Properties of solvent (such as boiling point and dielectric constant) make the solution jets stretching, decreasing jets diameter and increasing surface charge. Mixed solvents with 4:6, 1:1 and 6:4 of ethanol:DI water (v/v %) were examined. The morphology of the electrospun membranes was less controllable with a solvents ratio of 4:6 (ethanol:DI water v/v %) under a specific solution feed rate and tip-to-collector distance (Figure 40 a and d; Figure 41 a and d). In addition to the effect of solvent properties to the electrospinning process, PEO dissolves in ethanol at ~70 °C which higher than the room temperature [27], a ratio

of 1:1 ethanol:DI water (v/v %) provided an ease of polymer solution preparations at the room temperature.
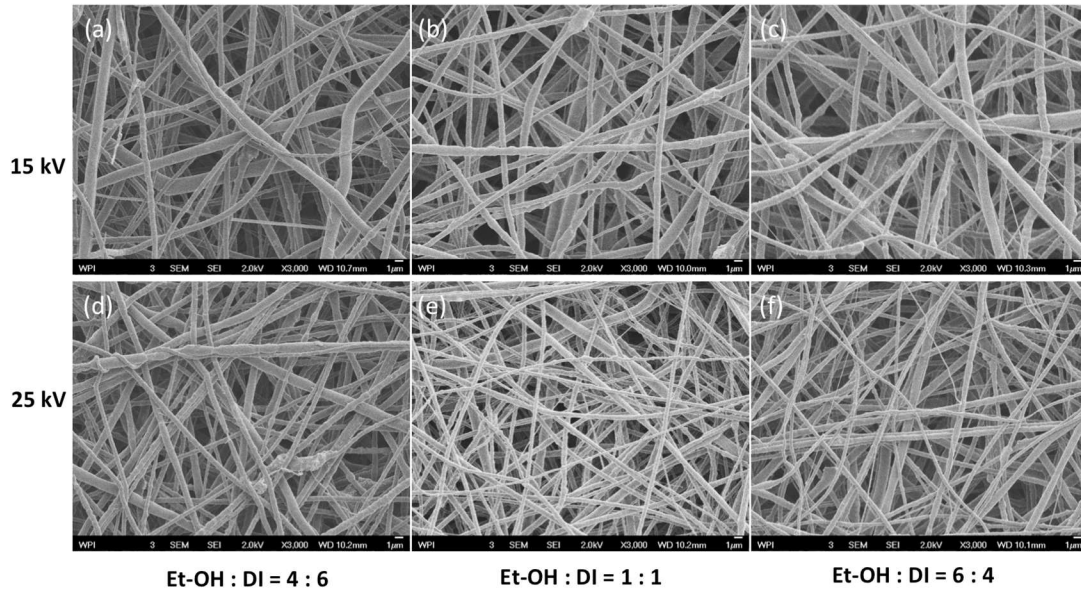


Et-OH : DI = 4 : 6          Et-OH : DI = 1 : 1          Et-OH : DI = 6 : 4

Figure 40 electrospun PEO with a solution concentration of 0.18 g/mL

(Scale bar = 1 μm, magnification ×3,000)

**15 kV**

(a) (b) (c)

**25 kV**

(d) (e) (f)

Et-OH : DI = 4 : 6          Et-OH : DI = 1 : 1          Et-OH : DI = 6 : 4
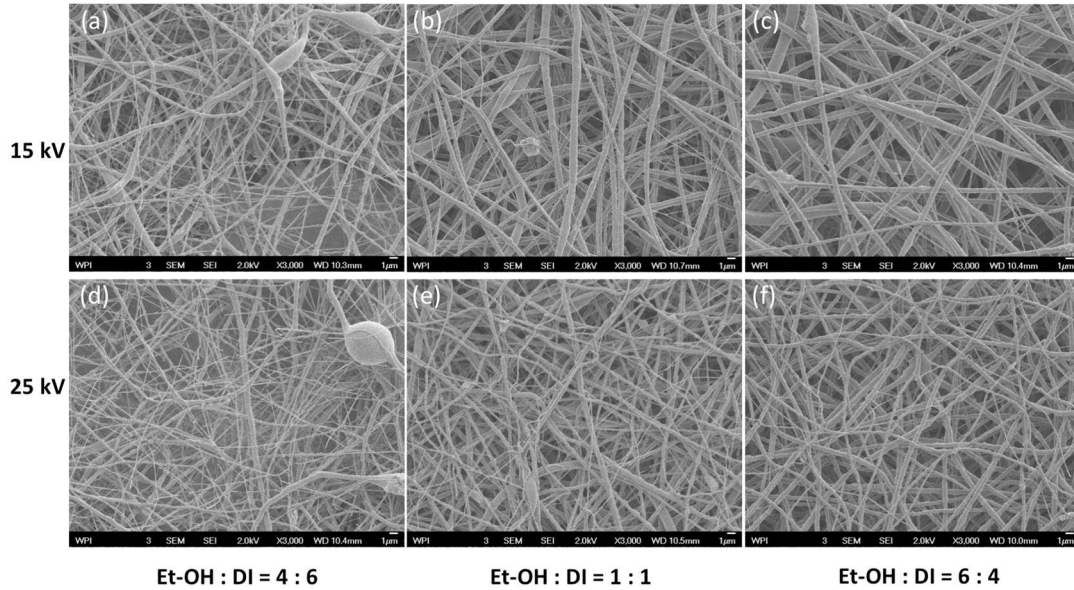
Figure 41 electrospun PEO with a solution concentration of 0.20 g/mL

(Scale bar = 1 μm, magnification ×3,000)

*Electrospun layer-by-layer of PVdF-HFP/PEO* In realization of using the electrospinning process to creates the layer-by-layer membrane, both PVdF-HFP and PEO were electrospun under the same conditions (acceleration potential = 25 kV and tip-to-collector distance = 15 cm). Thickness of the electrospun membranes was controlled by thermal press using iron (~60 °C) with spacers. Thermal press is not only making the loose deposited fibers dense together, but also thermally fusing the fibers together. Figure 42 shows the electrospun PVdF-HFP and electrospun layer-by-layer PVdF-HFP/PEO before and after thermal press. All further characterizations were performed on thermally pressed samples.
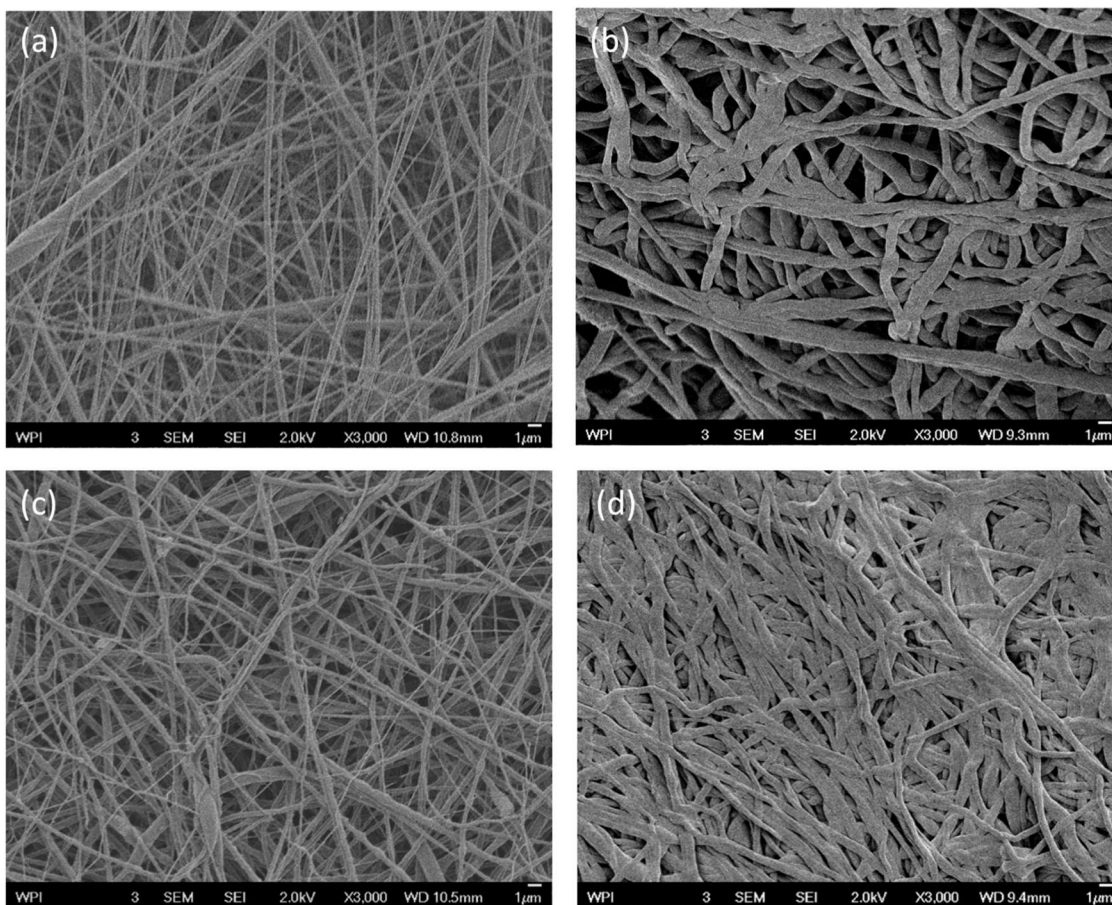
Figure 42 electrospun PVdF-HFP (a - as spun; b - thermal pressed) and layer-by-layer PVdF-HFP/PEO (c - as spun; d - thermal pressed)

(Scale bar = 1 μm, magnification ×3,000)

**3.2 Ionic conductivity**

Bulk resistance of the electrospun polymer membrane was obtained from a real-axis interception of the electrochemical impedance spectra in high frequency region (Figure 43). Ionic conductivity $\sigma$ was then calculated per unit length of the membrane thickness by an Equation 6,

$$\sigma = \frac{d}{R_b A} \qquad \text{Equation 6}$$

where d, $R_b$ and A are thickness (cm), bulk resistance (ohm) and cross-sectional area (cm$^2$), respectively. The bulk resistance $R_b$ corresponding to membrane's thickness and calculated ionic conductivity $\sigma$ are presented in Table 11. The ionic conductivity of the electrospun PVdF-HFP and electrospun layer-by-layer PVdF-HFP/PEO membranes is ~78% and ~90% higher than that of the polypropylene commercial separator.
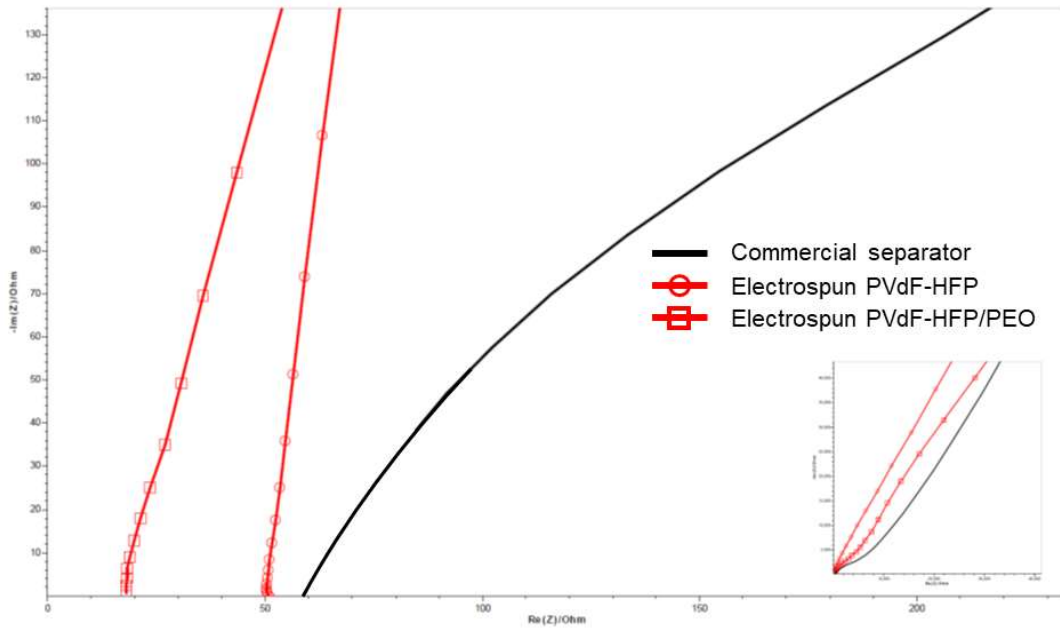


Figure 43 electrochemical impedance spectra of electrospun PVdF-HFP and electrospun layer-by-layer PVdF-HFP/PEO

Table 11 Ionic conductivity of electrospun PVdF-HFP and electrospun layer-by-layer PVdF-HFP/PEO at room temperature

|  | Thickness (µm) | Bulk resistance (Ω) | Ionic conductivity (S/cm) |
|---|---|---|---|
| Polypropylene commercial separator (Celgard 2400) | 25 | 58 | $0.22 \times 10^{-4}$ |
| Electrospun PVdF-HFP | 100 | 50 | $1.02 \times 10^{-4}$ |
| Electrospun layer-by-layer PVdF-HFP/PEO | 80 | 18 | $2.27 \times 10^{-4}$ |

## 3.3 Thermal studies of electrospun PVdF-HFP and electrospun layer-by-layer PVdF-HFP/PEO

Excellent thermal stability of the separator is required for the safety of LIBs. Typical charging and discharging temperatures of LIBs are 0 to 45 °C and -20 to 60 °C, respectively. The thermal stability of the electrospun membranes was studied with thermogravimetric analysis (TGA). Figure 44 illustrates the thermogravimetric analysis of the electrospun layer-by-layer PVdF-HFP/PEO and the electrospun PVdF-HFP. Both membranes do not have significant weight change until 400 °C and decrease approximately 81% up to 490 °C with residual mass of 19% corresponds to thermal degradation of polymer. Figure 45 demonstrates the DSC analysis. An endothermic peak of the electrospun PVdF-HFP appears at ~145 °C which the melting temperature of material. The electrospun layer-by-layer PVdF-HFP/PEO shows two endothermic peaks at 65 °C and 143 °C which reflect the melting temperature of PEO and PVdF-HFP, respectively. High thermal stability and much higher melting temperatures than the operating temperatures of the electrospun membranes indicate its outstanding resistance ability to elevated temperatures.
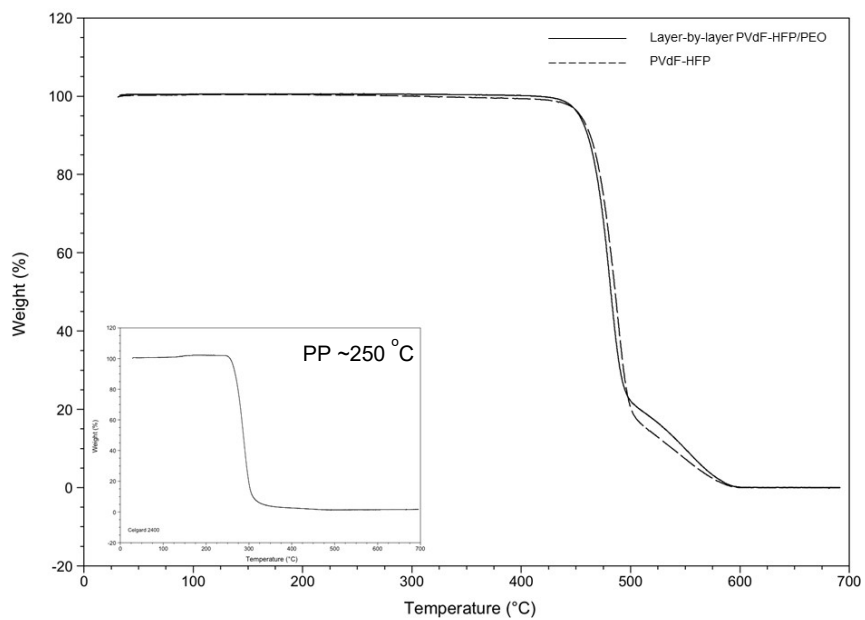
Figure 44 TGA thermogram of electrospun layer-by-layer PVdF-HFP/PEO and electrospun
PVdF-HFP (inset: polypropylene commercial separator)
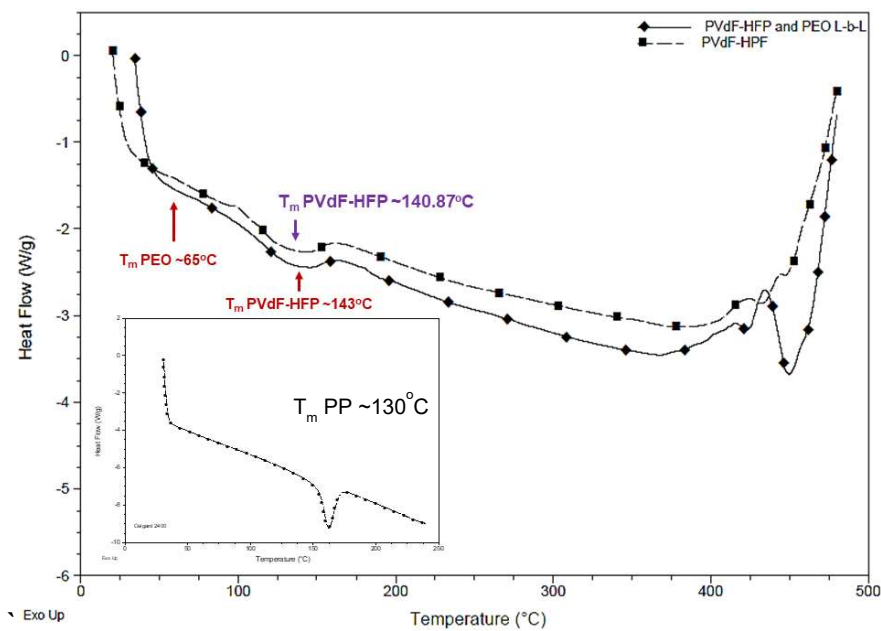


Figure 45 DSC thermogram of electrospun layer-by-layer PVdF-HFP/PEO and electrospun
PVdF-HFP (inset: polypropylene commercial separator)

## 3.4 Mechanical property

Tensile strength and elongation-to-break are simultaneously important mechanical property for separator. In addition to the high tensile strength, the separator should able to withstands deformation to ensure safety of battery. Because the electrospun fibers are randomly deposited on the collector then formed the non-woven porous membrane with a certain thickness, the fiber diameter contributes to the mechanical property of the membrane. Prior studies on size dependent mechanical property of the electrospun fiber with various types of polymer fibers show the mechanical property is not significantly changes with the fibers those have the diameters larger than 600 nm [28]–[33]. In this experiment, the fiber diameters of the thermally pressed electrospun PVdF-HFP and the electrospun layer-by-layer PVdF-HFP/PEO are approximately 1 μm or larger (Figure 42 *b* and *d*). The electrospun layer-by-layer PVdF-HFP/PEO membranes exhibit tensile strength as good as the electrospun PVdF-HFP (>20 MPa, Figure 46). The electrospun layer-by-layer PVdF-HFP/PEO with a thickness of 80 μm has elongation-to-break ~50% higher than the electrospun PVdF-HFP. Although the electrospun layer-by-layer PVdF-HFP/PEO has high tensile strength and elongation-to-break, the membrane with a thickness of 65 μm (~18.75% thinner) shows the decrease of the elongation-to-break ~29% while sustains the tensile strength and elastic modulus (Table 12). In comparison with polypropylene commercial separator i.e. Celgard 2400, tensile strength of the electrospun membranes approximately doubles to those of Celgard 2400 in transverse direction.

Table 12 Tensile stress and tensile strain of electrospun PVdF-HFP and electrospun layer-by-layer PVdF-HFP/PEO

*Symbols:* [a] machine direction (MD). [b] transverse direction (TD); [*] anisotropy

| Separator | Tensile strength (MPa) | Elongation-to-break (%) | Elastic modulus (GPa) |
|---|---|---|---|
| Polypropylene commercial separator (Celgard 2400[*]) [34] | 168±10.07 (MD[a])/ 11±4.7 (TD[b]) | 33±0.9 (MD)/ 315±20.4 (TD) | NA |
| Electrospun PVdF-HFP (thickness = 100 μm) | 21.93±7.95 | 87.89±14.77 | 0.25±0.03 |
| Electrospun layer-by-layer PVdF-HFP/PEO (thickness = 80 μm) | 25.87±5.79 | 192.81±19.07 | 0.21±0.06 |
| Electrospun layer-by-layer PVdF-HFP/PEO (thickness = 65 μm) | 23.51±6.91 | 136.91±28.47 | 0.20±0.05 |

\
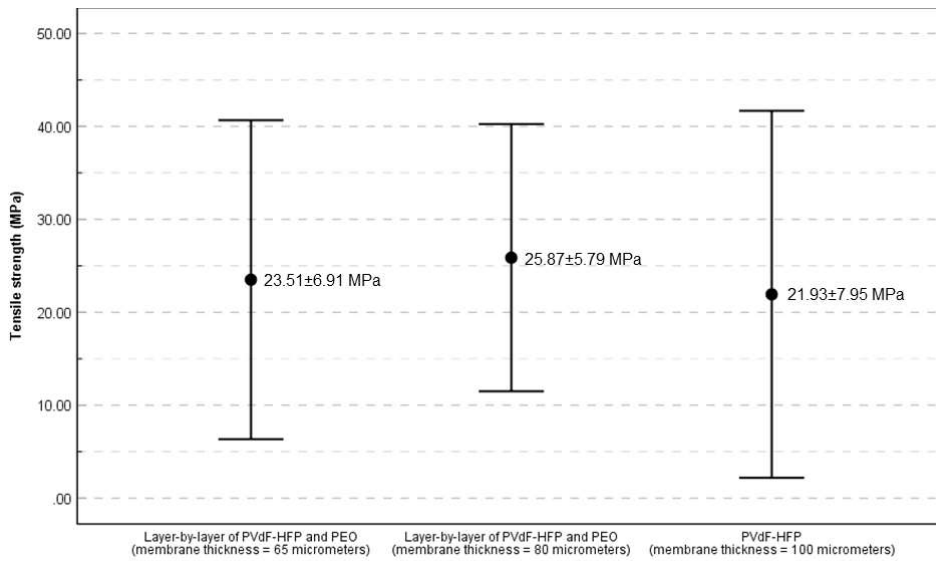


Figure 46 Tensile strength of the electrospun layer-by-layer PVdF-HFP/PEO and the electrospun PVdF-HFP
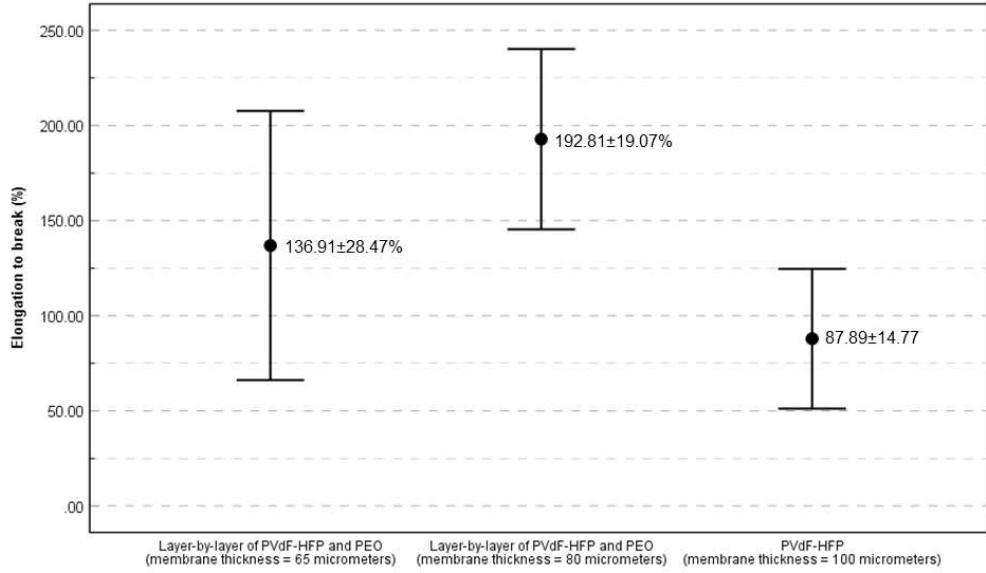
Figure 47 Elongation to break of the electrospun layer-by-layer PVdF-HFP/PEO and the electrospun PVdF-HFP
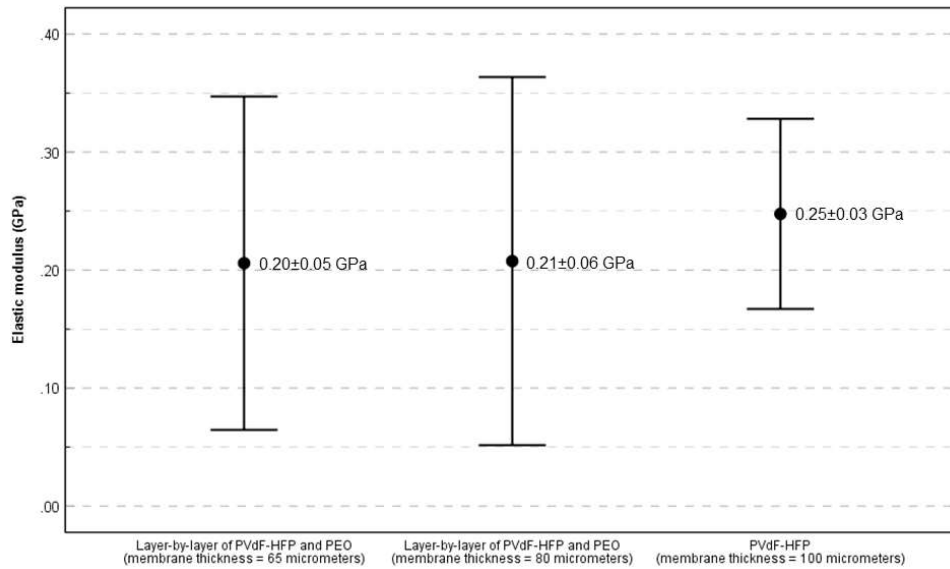


Figure 48 Elastic modulus of the electrospun layer-by-layer PVdF-HFP/PEO and electrospun PVdF-HFP

## 4. CONCLUSIONS

The non-woven mats of PVdF-HFP and layer-by-layer PVdF-HFP/PEO were created by electrospinning process. Although fiber morphology can be obtained with various acceleration potentials and ratios of the mixed solvents (for both PVdF-HFP and PEO), the acceleration potential of 25 kV, 0.25 g/mL PVdF-HFP/6:4 acetone:DMF (v/v %) and 0.20 g/mL /1:1 ethanol:DI water (%, v/v) are suitable to create the layer-by-layer of electrospun PVdF-HFP/PEO. Owing the characteristics of electrospun non-woven mats, the electrospun layer-by-layer can be used as separator with high tensile strength (~25 MPa) and high elongation-to-break (~190%). Ionic conductivity and thermal characteristics of both electrospun PVdF-HFP and the electrospun layer-by-layer PVdF-HFP/PEO are similar, in a range of $1$-$2\times10^{-4}$ S/cm. The decreasing of membrane's characteristic is also a common trade-off among thermal, mechanical and electrochemical performances of the separators, the electrospun separators in this study exhibit improvements in mechanical property and ionic conductivity while sustain the thermal characteristics.

## COMPETING INTERESTS

Authors have declared that no competing interests exist.

## AUTHORS' CONTRIBUTIONS

This work was carried out in collaboration between all authors. Keaswejjareansuk conducted the experiments, characterizations and analyzed data. Guerrero assisted with micro-tensile tests. Prof. Sisson contributed advices on thermal studies. Prof. Liang supervised the findings of this work, discussed the results and commented on the manuscript. All authors read and approved the final manuscripts.

## REFERENCES

[1]     E. Jacques, M. H. Kjell, D. Zenkert, and G. Lindbergh, "The effect of lithium-intercalation on the mechanical properties of carbon fibres," *Carbon N. Y.*, vol. 68, pp. 725–733, 2014.

[2]     N. Ihrner, W. Johannisson, F. Sieland, D. Zenkert, and M. Johansson, "Structural lithium ion battery electrolytes: Via reaction induced phase-separation," *J. Mater. Chem. A*, vol. 5, no. 48, pp. 25652–25659, Dec. 2017.

[3]     J. Hagberg *et al.*, "Lithium iron phosphate coated carbon fiber electrodes for structural lithium ion batteries," *Compos. Sci. Technol.*, vol. 162, pp. 235–243, Jul. 2018.

[4]     D. J. Noelle, M. Wang, and Y. Qiao, "Improved safety and mechanical characterizations of thick lithium-ion battery electrodes structured with porous metal current collectors," *J. Power Sources*, vol. 399, pp. 125–132, Sep. 2018.

[5]     T. C. Nirmale, I. Karbhal, R. S. Kalubarme, M. V. Shelke, A. J. Varma, and B. B. Kale, "Facile Synthesis of Unique Cellulose Triacetate Based Flexible and High Performance Gel Polymer Electrolyte for Lithium Ion Batteries," *ACS Appl. Mater. Interfaces*, p. acsami.7b07020, 2017.

[6]     A. Rahman, M. Rashid, A. K. M. Mohiuddin, and H. Moktar, "The prospects of panel style nano-battery technology for EV/HEV," in *IEEE International Conference on Industrial Engineering and Engineering Management*, 2016, vol. 2016–Janua, pp. 1531–1535.

[7]     D. H. Reneker and I. Chun, "Nanometre diameter fibres of polymer, produced by electrospinning," *Nanotechnology*, vol. 7, no. 3, pp. 216–223, 1996.

[8]     A. M. S. K. S. N. M. A. K. G. R. J.Wilson, "Poly(vinylidene fluoride-hexafluoropropylene) (PVdF-HFP) based composite electrolytes for lithium batteries," *Eur. Polym. J.*, vol. 42, no. 8, pp. 1728–1734, Sep. 2006.

[9]     C. W. Liew, Y. S. Ong, J. Y. Lim, C. S. Lim, K. H. Teoh, and S. Ramesh, "Effect Of Ionic Liquid On Semi – crystalline Poly ( vinylidene fluoride – co – hexafluoropropylene ) Solid Copolymer Electrolytes," *Int. J. Electrochem. Sci.*, vol. 8, pp. 7779–7794, 2013.

[10]    H. Xie, Z. Tang, Z. Li, Y. He, Y. Liu, and H. Wang, "PVDF-HFP composite polymer electrolyte with excellent electrochemical properties for Li-ion batteries," *J. Solid State Electrochem.*, vol. 12, no. 11, pp. 1497–1502, Nov. 2008.

[11]    B. S. Lalia, E. Guillen-Burrieza, H. A. Arafat, and R. Hashaikeh, "Fabrication and characterization of polyvinylidenefluoride-co-hexafluoropropylene (PVDF-HFP) electrospun membranes for direct contact membrane distillation," *J. Memb. Sci.*, vol. 428, pp. 104–115, 2013.

[12]    J. Y. Sohn, J. S. Im, J. Shin, and Y. C. Nho, "PVDF-HFP/PMMA-coated PE separator for lithium ion battery," *J. Solid State Electrochem.*, vol. 16, no. 2, pp. 551–556, 2012.

[13]    W. Chen, Y. Liu, Y. Ma, J. Liu, and X. Liu, "Improved performance of PVdF-HFP/PI nanofiber membrane for lithium ion battery separator prepared by a bicomponent cross-electrospinning method," *Mater. Lett.*, vol. 133, pp. 67–70, Oct. 2014.

[14]    Z. Xue, D. He, and X. Xie, "Poly(ethylene oxide)-based electrolytes for lithium-ion batteries," *J. Mater. Chem. A*, vol. 3, no. 38, pp. 19218–19253, 2015.

[15]  B. Chen *et al.*, "A new composite solid electrolyte PEO/Li10GeP2S12/SN for all-solid-state lithium battery," *Electrochim. Acta*, vol. 210, pp. 905–914, Aug. 2016.

[16]  M. Jaipal Reddy, J. Siva Kumar, U. V. Subba Rao, and P. P. Chu, "Structural and ionic conductivity of PEO blend PEG solid polymer electrolyte," *Solid State Ionics*, vol. 177, no. 3–4, pp. 253–256, Jan. 2006.

[17]  E. Quartarone, P. Mustarelli, and A. Magistris, "PEO-based composite polymer electrolytes," *Solid State Ionics*, vol. 110, no. 1–2, pp. 1–14, Jul. 1998.

[18]  I. Basumallick, P. Roy, A. Chatterjee, A. Bhattacharya, S. Chatterjee, and S. Ghosh, "Organic polymer gel electrolyte for Li-ion batteries," *J. Power Sources*, vol. 162, no. 2 SPEC. ISS., pp. 797–799, Nov. 2006.

[19]  B. Choi, "Lithium ion conduction in PEO–salt electrolytes gelled with PAN," *Solid State Ionics*, vol. 113–115, no. 1–2, pp. 123–127, Dec. 2002.

[20]  Q. Lu, J. Yang, J. Wang, Y. Nuli, J. Fang, and R. Miao, "Novel cross-linked copolymer gel electrolyte supported by hydrophilic polytetrafluoroethylene for rechargeable lithium batteries," *J. Memb. Sci.*, vol. 449, pp. 176–183, Jan. 2013.

[21]  W. Li, Y. Pang, J. Liu, G. Liu, Y. Wang, and Y. Xia, "A PEO-based gel polymer electrolyte for lithium ion batteries," *RSC Adv.*, vol. 7, no. 38, pp. 23494–23501, Apr. 2017.

[22]  H. Li, X. T. Ma, J. L. Shi, Z. K. Yao, B. K. Zhu, and L. P. Zhu, "Preparation and properties of poly(ethylene oxide) gel filled polypropylene separators and their corresponding gel polymer electrolytes for Li-ion batteries," *Electrochim. Acta*, vol. 56, no. 6, pp. 2641–2647, Feb. 2011.

[23]  M. Egashira, H. Todo, N. Yoshimoto, and M. Morita, "Lithium ion conduction in ionic liquid-based gel polymer electrolyte," *J. Power Sources*, vol. 178, no. 2, pp. 729–735, Apr. 2008.

[24]  B. K. Choi, Y. W. Kim, and H. K. Shin, "Ionic conduction in PEO-PAN blend polymer electrolytes," *Electrochim. Acta*, vol. 45, no. 8, pp. 1371–1374, Jan. 2000.

[25]  L. Balo, Shalu, H. Gupta, V. Kumar Singh, and R. Kumar Singh, "Flexible gel polymer electrolyte based on ionic liquid EMIMTFSI for rechargeable battery application," *Electrochim. Acta*, vol. 230, pp. 123–131, Mar. 2017.

[26]  Y. Aihara, G. B. Appetecchi, and B. Scrosati, "A New Concept for the Formation of Homogeneous, Poly(ethylene oxide) based, Gel-Type Polymer Electrolyte," *J. Electrochem. Soc.*, vol. 149, no. 7, p. A849, Jul. 2002.

[27]  D. L. Ho, B. Hammouda, S. R. Kline, and W. R. Chen, "Unusual phase behavior in mixtures of poly(ethylene oxide) and ethyl alcohol," *J. Polym. Sci. Part B Polym. Phys.*, vol. 44, no.

3, pp. 557–564, 2006.

[28]  M. Cai *et al.*, "A Parallel Bicomponent TPU/PI Membrane with Mechanical Strength Enhanced Isotropic Interfaces Used as Polymer Electrolyte for Lithium-Ion Battery," *Polymers (Basel).*, vol. 11, no. 1, p. 185, Jan. 2019.

[29]  U. Stachewicz, R. J. Bailey, W. Wang, and A. H. Barber, "Size dependent mechanical properties of electrospun polymer fibers from a composite structure," *Polymer (Guildf).*, vol. 53, no. 22, pp. 5132–5137, Oct. 2012.

[30]  J. Pelipenko, J. Kristl, B. Janković, S. Baumgartner, and P. Kocbek, "The impact of relative humidity during electrospinning on the morphology and mechanical properties of nanofibers," *Int. J. Pharm.*, vol. 456, no. 1, pp. 125–134, Nov. 2013.

[31]  A. Arinstein and E. Zussman, "Electrospun polymer nanofibers: Mechanical and thermodynamic perspectives," *J. Polym. Sci. Part B Polym. Phys.*, vol. 49, no. 10, pp. 691–707, May 2011.

[32]  G. Ico *et al.*, "Size-dependent piezoelectric and mechanical properties of electrospun P(VDF-TrFE) nanofibers for enhanced energy harvesting," *J. Mater. Chem. A*, vol. 4, no. 6, pp. 2293–2304, Feb. 2016.

[33]  S. Y. Chew, T. C. Hufnagel, C. T. Lim, and K. W. Leong, "Mechanical properties of single electrospun drug-encapsulated nanofibres," *Nanotechnology*, vol. 17, no. 15, pp. 3880–3891, Aug. 2006.

[34]  M. J. Lee *et al.*, "Highly lithium-ion conductive battery separators from thermally rearranged polybenzoxazole," *Chem. Commun.*, vol. 51, no. 11, pp. 2068–2071, 2015.

# CHAPTER 5 ELECTROSPUN POLYMER-METAL OXIDE COMPOSITE SEPARATOR

## Paper 3: Electrospun Composite Separator with TiO$_2$ Nanoparticles for Structural Lithium-ion Battery

Wisawat Keaswejjareansuk, Yehong Chen, Cesar Guerrero, Richard D. Sisson Jr., Jianyu Liang*

*Worcester Polytechnic Institute, Worcester, MA, USA*

*Corresponding author.

Address: Worcester Polytechnic Institute 100 Institute Road, Materials Science and Engineering, Mechanical Engineering Department. Worcester, MA 01609

E-mail address: jianyul@wpi.edu

## ABSTRACT

In this paper, non-woven fiber structure, PVdF-HFP/TiO$_2$ composite separator were created by electrospinning process. TiO$_2$ nanoparticles (NPs) were simply dispersed to form suspension used in the electrospinning experiment. At 9 wt.% loadings of TiO$_2$ NPs, the electrospun composite separator has a tensile strength and elastic modulus as high as 40.47 MPa and 0.47 GPa. Thermal characteristics of electrospun composite are similar to those of the electrospun PVdF-HFP. Ionic conductivity of the electrospun composite separator is 79% and 95% higher than the electrospun PVdF-HFP and conventional polypropylene separator. The electrospun composite separators exhibit high melting temperature (~133-140 °C) and excellent thermal stability (up to ~310 °C).

# 1. INTRODUCTION

Structural battery is introduced as multifunctional materials and structures, which have capability to perform energy storage and more functions, simultaneously [1]. The structural battery was first proposed as Nickel-hydrogen battery in 1998 by NASA for its nano-satellite technology development [2]. The structural battery concept was then re-introduced as Lithium-ion battery (LIB) along with structural capacitor and structural fuel cell in 2006 [3][4]. In 2009, Liu *et al.* demonstrated the structural lithium-ion battery consists of (1) structural polymer, cathode active material and carbon fiber together as cathode, (2) anode active material and carbon fiber as anode, and (3) insulating fibers/glass as separator [5]. Since then, progress of the structural battery to date has been focusing on electrode materials, especially using carbon fiber [6]-[19]. Unlike the electrode, separator materials for the structural battery have been slowly advancements. Snyder *et al.* investigated the first solid polymer electrolyte that exhibits both ionic conductivity and mechanical integrity for the structural battery purpose in 2007 [20]. Later in 2017, Ihrner *et al.* fabricated composite laminar of thermoset matrix with carbon fiber as structural battery electrolyte [21], and Trupti *et al.* developed flexible cellulose-based gel polymer electrolyte with good mechanical strength and ionic conductivity [22]. Beside the structural battery development, the advancement of separator in conventional lithium ion battery is relatively slow than those of electrode materials (Figure 49). An ionic conductivity of the separator in the conventional lithium-ion battery is in an order of $10^{-4}$-$10^{-3}$ S/cm [23].
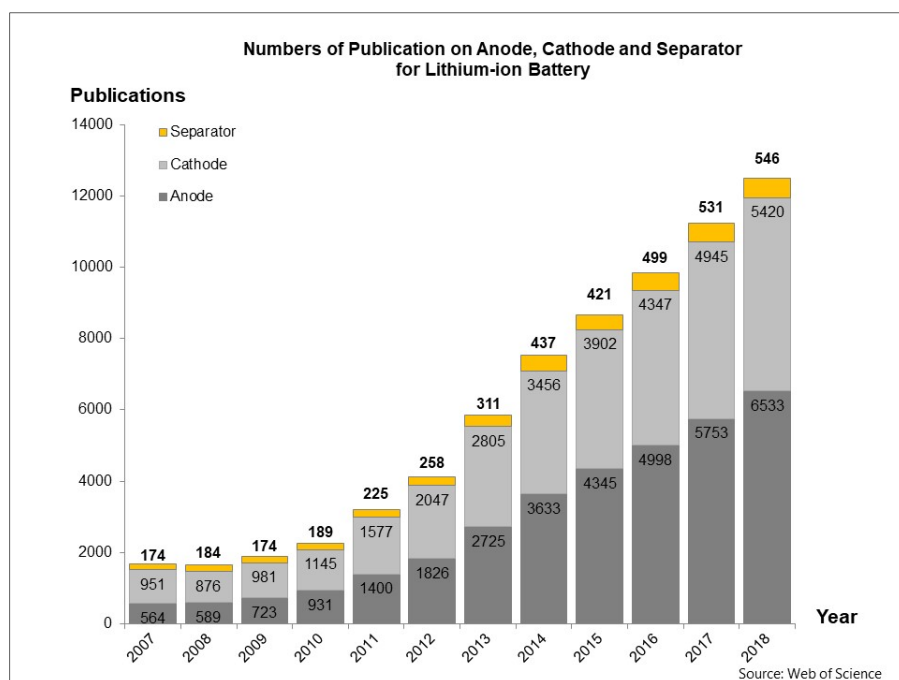
Figure 49 Research trends by the number of publication on conventional lithium-ion battery development from 2007-2018 (source: Web of Science)

According to prior works on structural electrode, lightweight fiber structured materials are preferred for the separator [24][12][19][13]. The fiber structure offers mechanical integrity, high porosity and high surface area per volume that enhance electrolyte uptake. Electrospinning is known for a simple process to create continuous, micro- and nano- diameter fibers. Polymer solution is loaded into a syringe equipped with metallic spinneret (needle). The solution syringe is setup on a syringe-pump at a distance from a ground substrate (collector). High electric potential is connected at a spinneret to generate an electric field between the spinneret and the substrate. Polymer solution is ejected into the electric field and randomly collected on the substrate. The morphology of the electrospun membranes is controlled by adjusting the polymer solution (concentration and solvent system) and the electrospinning process parameters (acceleration potential, solution feed rate and tip-to-collector distance).

Regardless of fabrication process, an addition of $TiO_2$ nanoparticles (NPs) to organic phase demonstrates improvement in mechanical properties in various types of polymer. Natural rubber in an experiment of Meera *et al.* increases its tensile strength ~39% with 10 wt.% loading of NPs [25]. Polu *et al.* added 8 wt.% of $TiO_2$ NPs to PEO-based polymer with 33% increasing in tensile strength

[26]. Thiolene nanocomposites were studied by Schechtel *et al.* exhibit monotonically increment in elastic modulus from 6.2 to 37.5 GPa by adding NPs from 0 to 90 wt.% [27]. Bayani *et al.* investigated the epoxy composite that has an increment of flexural strength ~41.2% with 5 wt.% of NPs [28]. Interestingly, the nanocomposites mentioned above have higher thermal conductivity than the neat polymers.

Poly(vinylidene fluoride-hexafluoropropylene) (PVdF-HFP) has been studied in many liquid and solid system because of its high dielectric constant ($\varepsilon = 8.4$ [29]), amorphous phase promotes $Li^+$ transportation and crystalline phases provides mechanical support [30][31][32]. In prior studies, the composite PVdF-HFP membranes with $TiO_2$ micro- [33] and nano-particles [34] those were created by phase inversion and casting methods demonstrate the improvements of tensile strength, ionic conductivity and interfacial stability. Study of Chen *et al.* shows that PI/PVdF-HFP composite separator with $TiO_2$ nanofillers has much improvement in tensile strength (~78%) and ionic conductivity (~25%) with only 2 wt.% of nanofiller [35]. Hence, the $TiO_2$ nanoparticle was anticipated to improve the ionic conductivity and mechanical property of the separator.

Herein, fiber structured PVdF-HFP/$TiO_2$ composite membranes were created by dispersion of nanoparticles to form a suspension for the electrospinning process. The aim of this work is to create a non-woven separator with improvements in mechanical property and ionic conductivity for structural battery applications. Structure of the electrospun separator was visualized by SEM. mechanical property was tested with micro-tensile tester. Ionic conductivity and thermal characteristics were studied by EIS and DSC/TGA, respectively.

## 2. EXPERIMENTS

### 2.1 Materials

Poly(vinylidene fluoride-co-hexafluoropropylene) PVdF-HFP (Mw ~ 400,000), Titanium dioxide nanopowder (anatase, particle size < 25nm), acetone (laboratory standard), and *N,N-*dimethylformamide DMF (anhydrous, 99.8%) were purchased from Sigma-Aldrich and used as received.

## 2.2 Experiments

PVdF-HFP and $TiO_2$ NPs were dried in vacuum furnace at 60 °C for 24 h. $TiO_2$ NPs (5, 7 and 9 wt.% of polymer) was dispersed in acetone by sonication for 30 minutes. DMF was then gradually added to the suspension to achieves a ratio of acetone:DMF = 6:4 (v/v). PVdF-HFP was dissolved into the suspension to a concentration of 0.20 g/mL. The suspension was loaded into a 10 mL syringe equipped with a stainless steel blunt-tip-needle (18-gauge, 0.838 mm inner diameter). A stationary aluminum foil collector was setup at 15 cm. from the needle-tip. The prepared suspension was fed with a feeding rate of 0.3 mL/h into an electric field with high acceleration potential of 25 kV. Electrospinning experiments were conducted at room temperature (25 °C) and 50-55 % relative humidity. Prior to characterizations, the electrospun samples were dried in vacuum furnace at 60 °C for 48 h.

## 2.3 Characterizations

Structure of the electrospun membranes was visualized by a field emission scanning electron microscopy (FE-SEM JEOL 7000F) with an operating voltage of 2kV. PVdF-HFP/$TiO_2$ nanoparticles composite membranes were examined by X-ray diffraction method (Malvern PANanalytical Empyrean X-ray Diffractometer) with Cu-$K_\alpha$ radiation ($\lambda$=1.54060 Å) over a scanning range of 15-80° ($2\theta$). Circular electrospun samples (1.6 cm diameter), sandwiched between symmetrical stainless steel discs (1.58 cm diameter) were fabricated a coin cell CR2032 in a glove box for an ionic conductivity measurement. The ionic conductivity was measured by electrochemical impedance spectroscopy (EIS, Bio-Logic VSP mVMP Model 1 potentiostats/galvanostats). EIS was performed over a frequency ranging from $2\times10^{-3}$ to $2\times10^5$ Hz at an AC amplitude of 100 mV. Thermal stability and melting temperature $T_m$ were determined by thermogravimetric analysis (TGA, TA Instrument Q50 over 25-700 °C) and differential scanning calorimetry (DSC, TA Instrument Q20 over 35-480 °C) at a heating rate of 15 °C/min. An average mass of samples for thermal analysis is ~ 2 mg. Mechanical property was characterized by a micro-tensile tester (Instron 5848 MicroTester) with a strain rate of $5\times10^{-4}$ 1/s (speed of gauge portion = 6 mm/min). The electrospun membrane was cut into a strip of 0.5 cm width and 4 cm length with 2 cm gauge-length for tensile testing.

## 3. RESULTS AND DISCUSSION

### 3.1 Morphology studies

Surface morphology of the electrospun PVdF-HFP/TiO2 composites are presented in Figure 50. The electrospun samples have consistent fibers with diameters in a range of 100-400 nm. The XRD spectra of $TiO_2$ NPs (2a), pristine electrospun PVdF-HFP (2b) and electrospun PVdF-HFP/$TiO_2$ composites (2c-2e) were acquired to confirm the loading of $TiO_2$ NPs into the electrospun fibers, Figure 51. Peaks of $TiO_2$ present at $2\theta = 26^o$ and $2\theta = 48^o$ with higher amount of $TiO_2$ NPs.
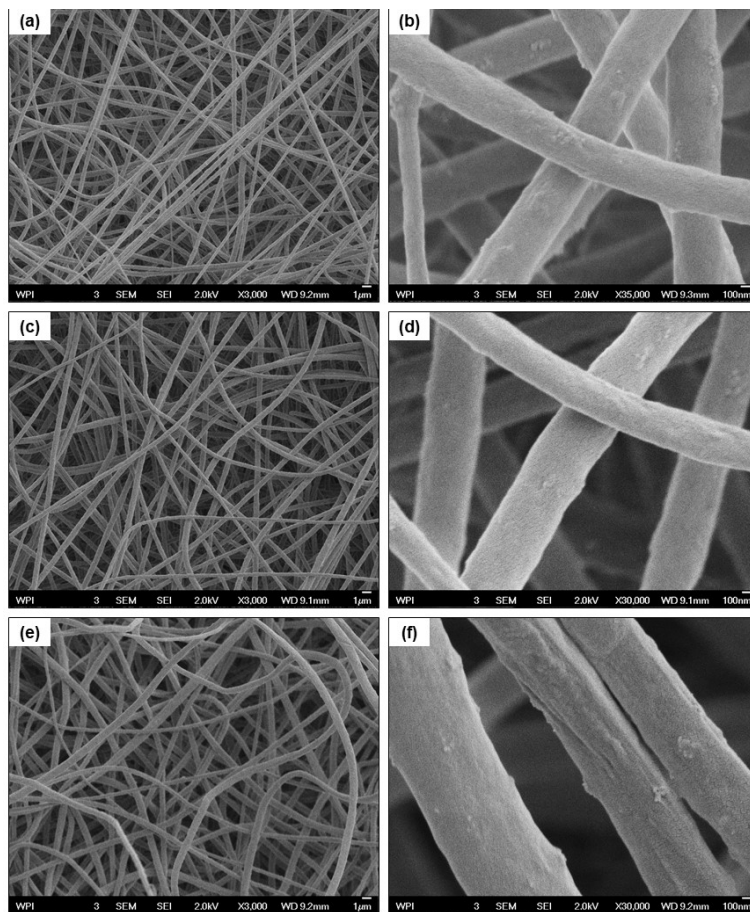


Figure 50 Morphology of electrospun PVdF-HFP/$TiO_2$ composite separators

(a) - (b) 5 wt.%, (c) - (d) 7 wt.% and (e) - (f) 9 wt.%

Scale bar (a), (c), and (e) = 1μm, magnification ×3,000

Scale bar (b), (d), and (f) = 100 nm, magnification ×30,000
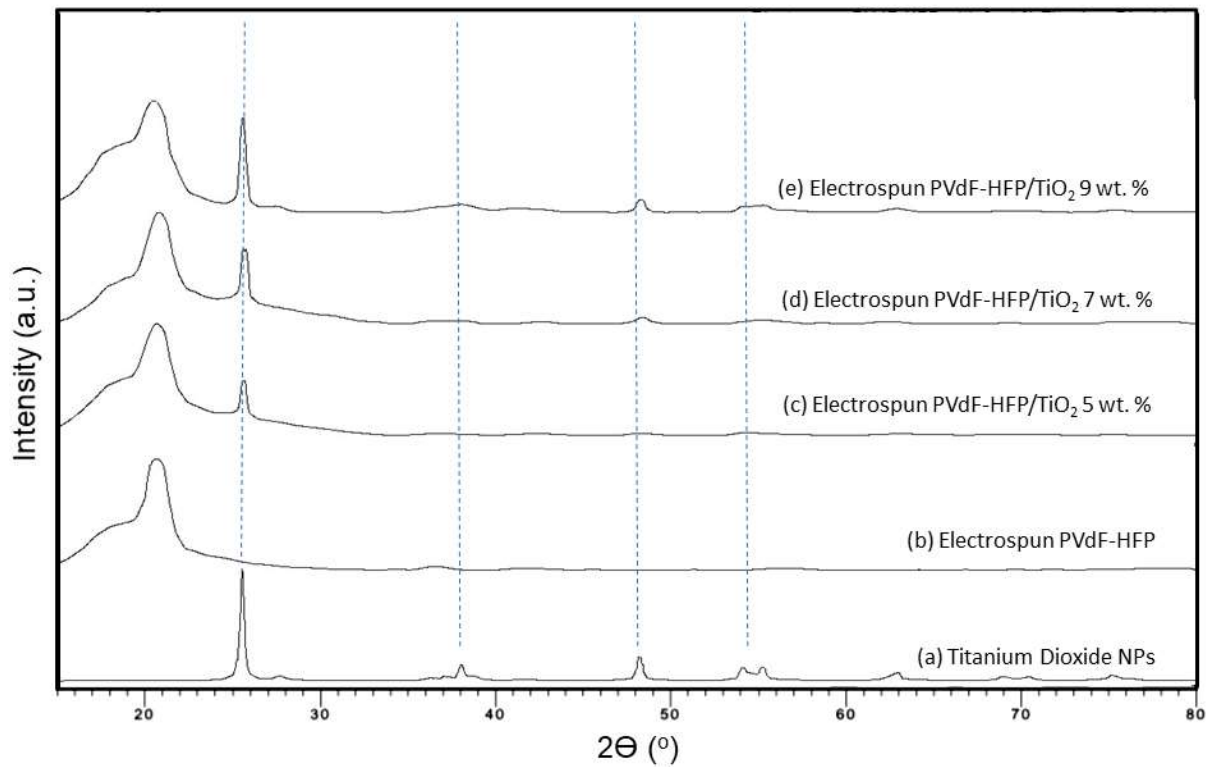
Figure 51 XRD spectra of electrospun PVdF-HFP/TiO$_2$ composites

## 3.2 Ionic conductivity

Bulk resistance of the electrospun polymer membrane was obtained from the interceptions on a real-axis of the electrochemical impedance spectra (Figure 52). Ionic conductivity $\sigma$ was then calculated per unit length of the membrane thickness by Equation 6,

$$\sigma = \frac{d}{R_b A}$$
<div align="right">Equation 7</div>

where d, $R_b$ and A are thickness (cm), bulk resistance (ohm) and cross-sectional area (cm$^2$), respectively. The bulk resistance $R_b$ corresponding to the thickness and calculated ionic conductivity $\sigma$ are presented in

Table 11. The electrospun composites have ionic conductivity 89-95 % higher than that of the polypropylene commercial separator. The highest ionic conductivity in this study is $4.94 \times 10^{-4}$ S/cm (95.5% higher than the polypropylene separator) corresponding to 9 wt.% loadings.
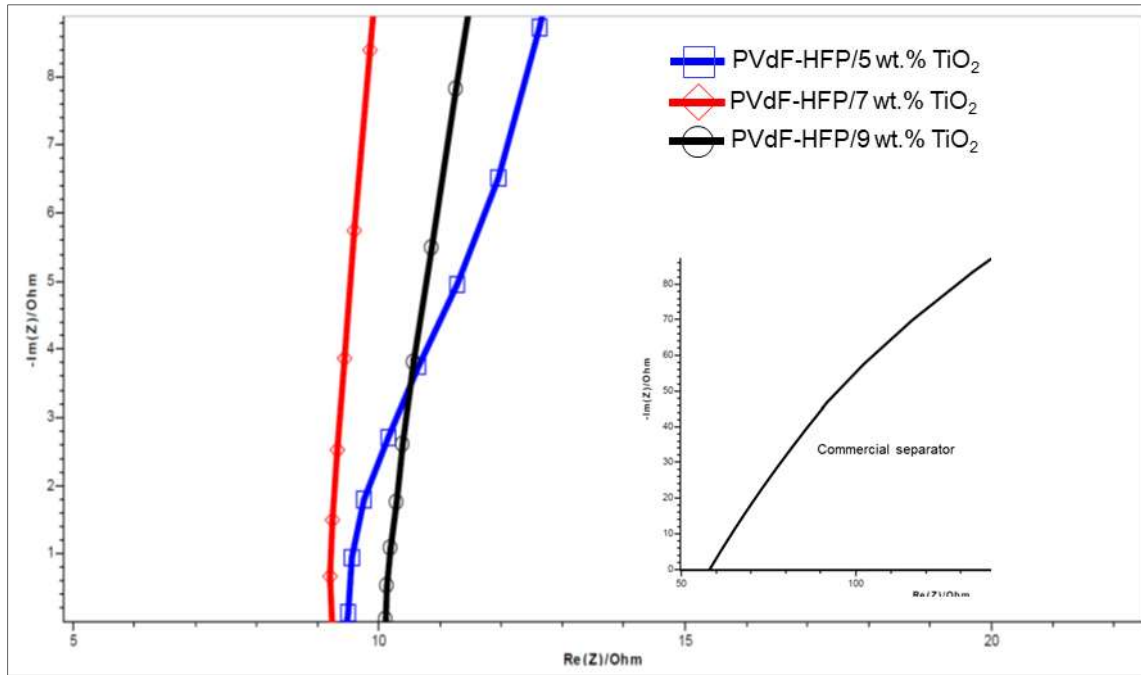


Figure 52 electrochemical impedance spectra of electrospun PVdF-HFP/TiO$_2$ composites (inset: polypropylene commercial separator)

Table 13 Ionic conductivity of electrospun PVdF-HFP/TiO$_2$ composites at room temperature

| Electrospun samples | Thickness (μm) | Bulk resistance (Ω) | Ionic conductivity (S/cm) |
|---|---|---|---|
| PVdF-HFP/TiO$_2$ 5 wt.% | 80 | 9.5 | $4.30 \times 10^{-4}$ |
| PVdF-HFP/TiO$_2$ 7 wt.% | 81 | 10.2 | $4.05 \times 10^{-4}$ |
| PVdF-HFP/TiO$_2$ 9 wt.% | 90 | 9.3 | $4.94 \times 10^{-4}$ |
| Polypropylene commercial separator, Celgard 2400 (inset) | 25 | 58 | $0.22 \times 10^{-4}$ |

## 3.3 Thermal studies

In thermogravimetric analysis, the composite separators are decomposed by heat which cause bonds within the molecules to be broken. Weight of the sample decreases slowly as begins, then decreases rapidly over short temperature range until the material become spent. Thermal decomposition temperatures of the composite separators start at ~300 °C. Temperatures at 50% weight loss are ~410-440 °C, Figure 53. Unlike the composite separator, electrospun pristine PVdF-HFP has the thermal decomposition temperature and temperature at 50% weight loss at approximately 420 °C and 490 °C, respectively. Melting temperatures $T_m$ of the composite membranes from the DSC thermogram (Figure 54) are 145-147 °C, slightly higher than that of electrospun PVdF-HFP.

Table 14 Melting temperature of the electrospun PVdF-HFP/TiO$_2$ composites

| Separator | Melting Temperature $T_m$ (°C) |
|---|---|
| Composite separator with TiO$_2$ NPs loading 5 wt. % | 146.41 |
| Composite separator with TiO$_2$ NPs loading 7 wt. % | 147.12 |
| Composite separator with TiO$_2$ NPs loading 9 wt. % | 145.08 |
| Polypropylene commercial separator (Celgard 2400[*]) | 161.93 |
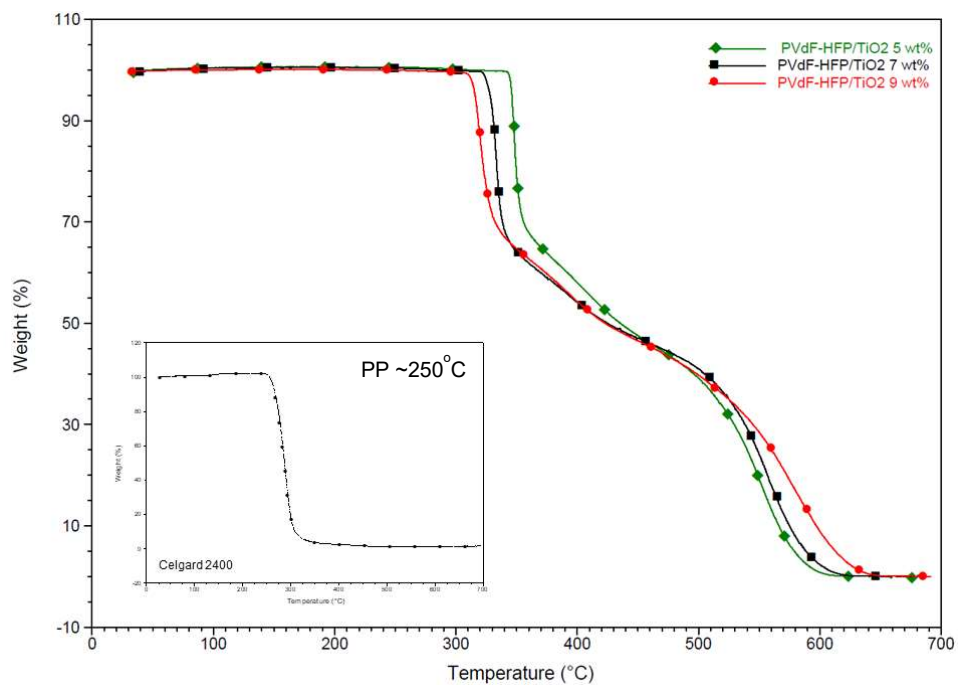
Figure 53 TGA thermogram of electrospun PVdF-HFP/TiO$_2$ composite separators
(inset: polypropylene commercial separator)
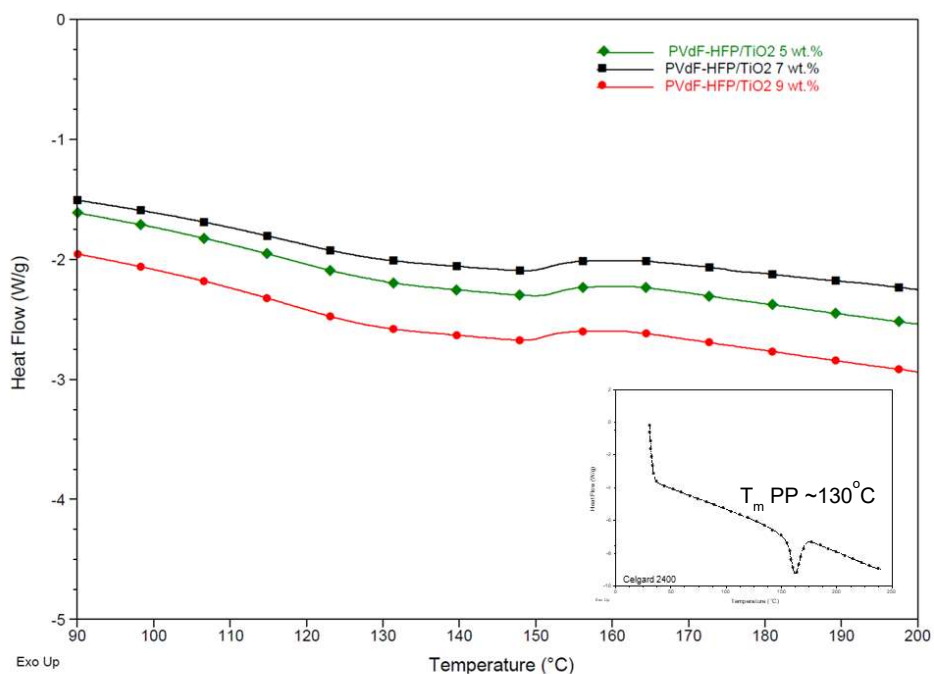


Figure 54 DSC thermogram of electrospun PVdF-HFP/TiO$_2$ composite separators
(inset: polypropylene commercial separator)

## 3.4 Mechanical property

Elastic modulus and tensile strength increase with increasing amounts of nanoparticles. At higher $TiO_2$ NPs loadings, the elastic modulus and tensile strength are 86-93% and 84-92% higher than the unloaded electrospun sample, respectively. The electrospun composite separator with 9 wt.% NPs loading has the highest elastic modulus (0.47 GPa) and tensile strength (40.44 MPa). Although strain at the tensile strength is expected to decrease, the electrospun sample with 9 wt.% addition of $TiO_2$ has the highest strain of 127%. In comparison with polypropylene commercial separator, for example Celgard 2400, tensile strengths of electrospun composite separator are higher than those of Celgard 2400 in transverse direction.

Table 15 Tensile strength and elastic modulus of the electrospun PVdF-HFP/$TiO_2$ composite separator

| Electrospun Sample | Elastic modulus (GPa) | Tensile strength (MPa) | Strain at tensile strength (%) |
|---|---|---|---|
| PVdF-HFP/$TiO_2$ 5 wt.% | 0.22 | 19.59 | 87.00 |
| PVdF-HFP/$TiO_2$ 7 wt.% | 0.46 | 34.00 | 85.00 |
| PVdF-HFP/$TiO_2$ 9 wt.% | 0.47 | 40.44 | 127.00 |
| Polypropylene commercial separator (Celgard 2400[*]) [36] | NA | 168 (MD[a])/ 11 (TD[b]) | NA |

[a] machine direction (MD). [b] transverse direction (TD); [*] anisotropy
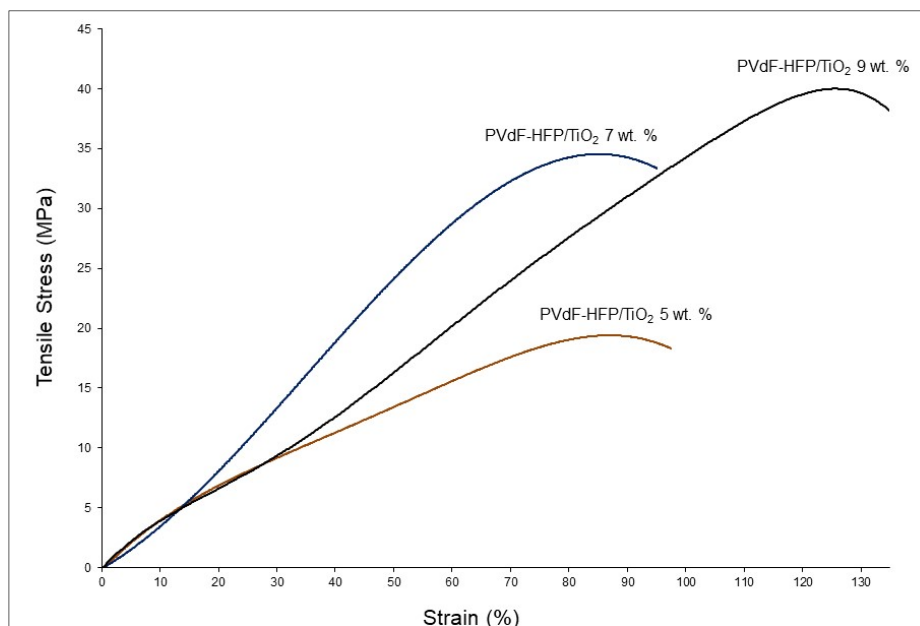
Figure 55 Tensile stress-strain curves of the electrospun PVdF-HFP/TiO$_2$ composite separators

## 4. CONCLUSIONS

Non-woven composite PVdF-HFP/TiO$_2$ separators were simply fabricated by dispersion of TiO$_2$ NPs to form the suspension, then used the electrospinning method to create the fiber structured membrane. The electrospun composite separators have melting temperatures ~133-140 ℃ and its structure stables up to 300 ℃. As expectation, the composite separators show improvements in mechanical property and ionic conductivity. The crystallinity of the electrospun composite separators increases with NPs loadings. Although the amorphous phase of PVdF-HFP is known to promote the ion transportation, the highest ionic conductivity in this study is 4.94×10$^{-4}$ S/cm (9 wt.% NPs loading) which is ~96% higher than that of the polypropylene commercial separators. The composite separator with 9 wt.% TiO$_2$ NPs loading also has the highest tensile strength (40.44 MPa), elastic modus (0.47 GPa), and strain at the tensile strength (127%).

**COMPETING INTERESTS**

Authors have declared that no competing interests exist.

**AUTHORS' CONTRIBUTIONS**

This work was carried out in collaboration between all authors. Keaswejjareansuk conducted the experiments, characterizations and analyzed data. Chen assisted with data collection for DSC and TGA analysis. Guerrero performed the micro-tensile tests. Prof. Sisson provided feedback on thermal characterizations. Prof. Liang supervised the findings of this work, discussed the results and commented on the manuscript. All authors read and approved the final manuscripts.

**REFERENCES**

[1]  S. Shalouf, J. Zhang, C. Wang, and L. Wackett, "THE EFFECTS OF MECHANICAL DEFORMATION ON THE PERFORMANCE OF COMPOSITE STRUCTURES EMBEDDED WITH POLYMER BATTERIES," in *International Conference on Composite Materials-ICCM19*, 2003.

[2]  P. V. Panetta *et al.*, "NASA-GSFC Nano-Satellite Technology Development," Logan, 1998.

[3]  E. D. Wetzel, D. J. O. Brien, J. F. Snyder, R. H. Carter, and J. T. South, "Multifunctional Structural Power and Energy Composites for U.S Army Applications," *Multifunct. Struct. / Integr. Sensors Antennas*, no. 2006, pp. 2–14, 2006.

[4]  J. F. Snyder *et al.*, "Multifunctional Structural Composite Batteries," Aberdeen Proving Ground, 2007.

[5]  P. Liu, E. Sherman, and A. Jacobsen, "Design and fabrication of multifunctional structural batteries," *J. Power Sources*, vol. 189, no. 1, pp. 646–650, 2009.

[6]  P. V. Panetta *et al.*, "NASA-GSFC Nano-Satellite Technology Development," Logan, 1998.

[7]  E. D. Wetzel, D. J. O. Brien, J. F. Snyder, R. H. Carter, and J. T. South, "Multifunctional Structural Power and Energy Composites for U.S Army Applications," *Multifunct. Struct. / Integr. Sensors Antennas*, no. 2006, pp. 2–14, 2006.

[8]  J. F. Snyder *et al.*, "Multifunctional Structural Composite Batteries," Aberdeen Proving Ground, 2007.

[9]  E. L. Wong, D. M. Baechle, K. Xu, R. H. Carter, J. F. Snyder, and E. D. Wetzel, "Design and Processing of Structural Composite Batteries," Aberdeen Proving Ground, 2007.

[10] T. Pereira, Z. Guo, S. Nieh, J. Arias, and H. T. Hahn, "Embedding thin-film lithium energy

cells in structural composites," *Compos. Sci. Technol.*, vol. 68, no. 7–8, pp. 1935–1941, 2008.

[11]    A. Rahman, M. Rashid, A. K. M. Mohiuddin, and H. Moktar, "The prospects of panel style nano-battery technology for EV/HEV," in *IEEE International Conference on Industrial Engineering and Engineering Management*, 2016, vol. 2016–Janua, pp. 1531–1535.

[12]    Y. Yu and B. Zhang, "MULTIFUNCTIONAL STRUCTURAL BATTERIES BASED ON CARBON FIBER REINFORCED PLASTIC COMPOSITES: INVESTIGATION ON MECHANICAL AND ELECTROCHEMICAL PROPERTIES," in *21st International Conference on Composite Materials*, 2017.

[13]    J. Hagberg *et al.*, "Lithium iron phosphate coated carbon fiber electrodes for structural lithium ion batteries," *Compos. Sci. Technol.*, vol. 162, pp. 235–243, Jul. 2018.

[14]    M. Y. Park, J. H. Kim, D. K. Kim, and C. G. Kim, "Perspective on Carbon Fiber Woven Fabric Electrodes for Structural Batteries," *Fibers Polym.*, vol. 19, no. 3, pp. 599–606, 2018.

[15]    A. Javaid and M. Z. Ali, "Multifunctional structural lithium ion batteries for electrical energy storage applications," *Mater. Res. Express*, vol. 5, no. 5, p. 55701, 2018.

[16]    G. Fredi *et al.*, "Graphitic microstructure and performance of carbon fibre Li-ion structural battery electrodes," *Multifunct. Mater.*, vol. 1, pp. 1–32, 2018.

[17]    T. J. Adam *et al.*, "Multifunctional composites for future energy storage in aerospace structures," *Energies*, vol. 11, no. 2, p. 335, Feb. 2018.

[18]    J. Wallenstein *et al.*, "Graphitic microstructure and performance of carbon fibre Li-ion structural battery electrodes," *Multifunct. Mater.*, vol. 1, no. 1, p. 015003, Aug. 2018.

[19]    W. Johannisson *et al.*, "Multifunctional properties of a carbon fiber UD lamina structural battery electrode," *Compos. Sci. Technol.*, Aug. 2018.

[20]    J. F. Snyder, R. H. Carter, and E. D. Wetzel, "Electrochemical and mechanical behavior in mechanically robust solid polymer electrolytes for use in multifunctional structural batteries," *Chem. Mater.*, vol. 19, no. 15, pp. 3793–3801, 2007.

[21]    N. Ihrner, W. Johannisson, F. Sieland, D. Zenkert, and M. Johansson, "Structural lithium ion battery electrolytes: Via reaction induced phase-separation," *J. Mater. Chem. A*, vol. 5, no. 48, pp. 25652–25659, Dec. 2017.

[22]    T. C. Nirmale, I. Karbhal, R. S. Kalubarme, M. V. Shelke, A. J. Varma, and B. B. Kale, "Facile Synthesis of Unique Cellulose Triacetate Based Flexible and High Performance Gel Polymer Electrolyte for Lithium Ion Batteries," *ACS Appl. Mater. Interfaces*, p. acsami.7b07020, 2017.

[23]    S. J. Lue, K.-L. Tung, A. Huang, J. F. Soesanto, and K. K. Jana, "Separator Membranes for

High Energy-Density Batteries," *ChemBioEng Rev.*, vol. 5, no. 6, pp. 346–371, Dec. 2018.

[24]    M. H. Kjell, E. Jacques, D. Zenkert, M. Behm, and G. Lindbergh, "PAN-based carbon fibers for structural lithium-ion batteries," *ECCM 2012 - Compos. Venice, Proc. 15th Eur. Conf. Compos. Mater.*, no. June, pp. 24–28, 2012.

[25]    A. P. Meera *et al.*, "Thermophysical and mechanical properties of TiO 2 and silica nanoparticle-filled natural rubber composites," *J. Elastomers Plast.*, vol. 44, no. 4, pp. 369–382, 2012.

[26]    A. R. Polu and H. W. Rhee, "Effect of TiO2 nanoparticles on structural, thermal, mechanical and ionic conductivity studies of PEO12-LiTDI solid polymer electrolyte," *J. Ind. Eng. Chem.*, vol. 37, pp. 347–353, May 2016.

[27]    E. Schechtel *et al.*, "Elastic Modulus and Thermal Conductivity of Thiolene/TiO2 Nanocomposites," *J. Phys. Chem. C*, vol. 121, no. 45, pp. 25568–25575, 2017.

[28]    M. Bayani, M. Ehsani, H. A. Khonakdar, J. Seyfi, and M. H. HosseinAbadi-Ghaeni, "An investigation of TiO2 nanoparticles effect on morphology, thermal, and mechanical properties of epoxy/silica composites," *J. Vinyl Addit. Technol.*, vol. 23, pp. E216–E221, Sep. 2017.

[29]    H. Xie, Z. Tang, Z. Li, Y. He, Y. Liu, and H. Wang, "PVDF-HFP composite polymer electrolyte with excellent electrochemical properties for Li-ion batteries," *J. Solid State Electrochem.*, vol. 12, no. 11, pp. 1497–1502, Nov. 2008.

[30]    J. H. Cao, B. K. Zhu, and Y. Y. Xu, "Structure and ionic conductivity of porous polymer electrolytes based on PVDF-HFP copolymer membranes," *J. Memb. Sci.*, vol. 281, no. 1–2, pp. 446–453, Sep. 2006.

[31]    A. Du Pasquier, P. C. Warren, D. Culver, A. S. Gozdz, G. G. Amatucci, and J. M. Tarascon, "Plastic PVDF-HFP electrolyte laminates prepared by a phase-inversion process," *Solid State Ionics*, vol. 135, no. 1–4, pp. 249–257, Nov. 2000.

[32]    H. Wang, Y. Liu, H. Xie, Z. Tang, Z. Li, and Y. He, "PVDF-HFP composite polymer electrolyte with excellent electrochemical properties for Li-ion batteries," *J. Solid State Electrochem.*, vol. 12, no. 11, pp. 1497–1502, 2008.

[33]    R. Miao *et al.*, "PVDF-HFP-based porous polymer electrolyte membranes for lithium-ion batteries," *J. Power Sources*, vol. 184, no. 2, pp. 420–426, Oct. 2008.

[34]    K. M. Kim, N. G. Park, K. S. Ryu, and S. H. Chang, "Characteristics of PVdF-HFP/TiO2 composite membrane electrolytes prepared by phase inversion and conventional casting methods," *Electrochim. Acta*, vol. 51, no. 26, pp. 5636–5644, Aug. 2006.

[35]    W. Chen, Y. Liu, Y. Ma, and W. Yang, "Improved performance of lithium ion battery

separator enabled by co-electrospinnig polyimide/poly(vinylidene fluoride-co-hexafluoropropylene) and the incorporation of TiO2-(2-hydroxyethyl methacrylate)," *J. Power Sources*, vol. 273, pp. 1127–1135, Jan. 2015.

[36]  J. H. Kim *et al.*, "Highly lithium-ion conductive battery separators from thermally rearranged polybenzoxazole," *Chem. Commun.*, vol. 51, no. 11, pp. 2068–2071, 2014.

# CHAPTER 6 CONCLUSIONS AND FUTURE WORKS OF ELECTROSPUN SEPARATOR FOR STRUCTURAL BATTERY APPLICATIONS

## Conclusions

This dissertation presents a series of experimental studies on electrospinning process and membrane fabrication as separator in lithium-ion battery for structural applications. The electrospun layer-by-layer (l-b-l) of PVdF-HFP/PEO/PVdF-HFP separator was fabricated with the same process parameters. The l-b-l PVdF-HFP/PEO/PVdF-HFP separator has the ionic conductivity $\sim$1-2 $\times10^{-4}$ S/cm and tensile strength $\sim$25 MPa. The electrospun PVdF-HFP/TiO$_2$ composite separator was prepared by direct dispersions of nanoparticles into the polymer solution. The polymer-metal oxide composites have the improved tensile strength in a range of 19.59-40.44 MPa and ionic conductivity of 4.05-4.94 $\times10^{-4}$ S/cm. Melting temperature of the electrospun layer-by-layer separator and the electrospun polymer-metal oxide composite separator are dominated by the property of polymer, PVdF-HFP ($T_m \sim$133-140 $^o$C).

Conclusion remarks are making follow:

1. The electrospinning process has been utilizing in many applications, thus the knowledge related to the electrospinning has been already established. In this study, the electrospinning process was controlled by adjusting the material and process parameters, for examples solution concentration, acceleration potentials and solution feeding rate. Effects of the solutions' dielectric constant and solvent compositions under the accelerated electric field were also studied. At higher dielectric constant, the solution jets tend to spin faster. For example, this study used a mixed solvent of acetone and DMF because of the physical properties of each constitution. Although PVdF-HFP could be dissolved in DMF, acetone was used as a mechanism to control the depositing fibers because of its relatively low boiling point to the room temperature. While the solution jets were spun in the electric field, acetone was continuously evaporated. Hence, diameter of the spun jets decreased, and the spun jets further elongated because of high surface charges.

2. Electrospun membrane for LIB separator has specified requirements, such as high melting temperature, high thermal decomposition temperature and high dimensional stable those to be able to withstand the service temperatures of the battery, decent mechanical strength and moderate to high ionic conductivity. Because thermal characteristics and ionic conductivity are dominated by the material itself, selecting of polymer is as important as controlling the solution and process parameters. Mechanical property can be customized by controlling the membrane structure. Post electrospinning treatment, such as thermal treats and hot-pressing is performed to enhances the structural integration and mechanical property. A quick hot-pressing is preferred because the post treatment membrane still maintains its fiber structure. On another hand, fiber structure may melt due to high treating temperature and/or long treatment time.

**Future works**

*Characterizations*

Electrochemical characterization with half-cell configuration and dielectric/conductivity behaviors studies will allow more understand the performance of the electrospun separator.

- Unlike the ionic conductivity measured by set up the electrospun separator between *stainless steel plates* in the EIS studied, the EIS test with the *half-cell configuration* will provides interfacial resistance between electrode and the electrospun separator. In addition to the EIS method, charge-discharge test with the half-cell configuration will provides cycling performance and rate capability of the LIB.

- In this study, the reported ionic conductivity was measured at the room temperature. Charge and discharge temperatures of LIB are 0-45ºC and -20-60ºC, respectively. Study on dielectric/conductivity behaviors in the range of operating temperatures will obtains the performance information at different temperatures.

*Electrospinning strategy*

Possible electrospinning strategy is coating (dip coat or vacuum filtration) the electrospun membrane with ionic polymers to create core-shell structure. The electrospun fibers function as the core with mechanical integrity. The coated layer of ionic polymers functions as the shell promoting ionic conductivity.

# APPENDIX 1 – LIST OF PUBLICATIONS

1. **W. Keaswejjareansuk**, X. Wang and J. Liang, "Electrospun Poly(Bisphenol-A-co-Epichlorohydrin) membrane", *to be submitted to Polymers for Advanced Technologies*

2. **W. Keaswejjareansuk**, C. Guerrero, R.D. Sisson and J. Liang, "Fabrication of Electrospun Layer-by-Layer PVdF-HFP/PEO Separator for structural Battery Applications", *to be submitted to Journal of Polymer Science, Part B: Polymer Physics*

3. **W. Keaswejjareansuk**, Y. Chen, C. Guerrero, R.D. Sisson and J. Liang, "Electrospun Composite Separator with $TiO_2$ Nanoparticle for Structural Lithium-ion Battery", *to be submitted to Polymer*

# APPENDIX 2 – PRESENTATIONS

**W. Keaswejjareansuk** and J. Liang. "Multifunctional Electrospun Multilayered Separator for Flexible Battery Applications." Poster presented at symposium of Materials-to-Devices for Integrated Wearable System-Energy Harvesting and Storage, Sensors/Actuators and Integration – the Materials Research Society Fall Meeting, Boston, Massachusetts, November 29, 2018

**W. Keaswejjareansuk**, X. Wang and J. Liang. "Electrospinning Process for Lithium-ion Battery Separator." Oral presented at symposium of Advanced Processing and Manufacturing for Energy Conversion, Storage and Harvesting Devices – the Materials Research Society Fall Meeting, Boston, Massachusetts, November 28, 2018.

**W. Keaswejjareansuk** and J. Liang. "Electrospun Polymer-Ceramic Composite Separator for Structural Battery Applications." Poster presented at symposium of Application of Nanoscale Phenomena and Materials to Practical Electrochemical Energy Storage and Conversion – the Materials Research Society Fall Meeting, Boston, Massachusetts, November 27, 2018.

**W. Keaswejjareansuk**, R.D. Sisson, X. Wang, J. Liang. "Multifunctional Electrospun Separators for Structural Battery Applications." Poster presented at Nano2018 – the 14th International Conference on Nanostructured Materials, Kowloon, Hong Kong SAR, June 24-29, 2018.

**W. Keaswejjareansuk**, J. Liang. "Multifunctional Electrospun Separators for Structural Battery Applications." Poster presented at WPI Science Soldier Research symposium, Worcester, Massachusetts, February 26, 2018.

**W. Keaswejjareansuk**, J. Liang. "Multifunctional Electrospun Separators for Structural Battery Applications." Oral presented at symposium of Battery and Energy Technology Joint General Session – the 232nd ECS Meeting, National Harbor, Maryland, October 5, 2017.

**W. Keaswejjareansuk**, J. Liang. "Multifunctional Electrospun Separators for Structural Battery Applications." Oral presented at New England Energy Research Forum – Materials and Processes for Clean Energy, Worcester, Massachusetts, June 28, 2017.

**W. Keaswejjareansuk**, J. Liang. "Electrospun Separator for Structural Battery Applications." Oral presented at Spring 2017 Meeting of APS New England section, Worcester, Massachusetts, April 15, 2017.

**W. Keaswejjareansuk**, J. Liang. "Electrospun Separator for Structural Battery Applications." Oral presented at symposium of Advanced Materials for Energy Conversion and Storage – the TMS 2017 Conference, San Diego, California, March 2, 2017.

**W. Keaswejjareansuk**, J. Liang, X. Wang. "Electrospun Separator for Structural Battery Applications." Poster presented at the Materials Research Society Fall Meeting, Boston, Massachusetts, December 1, 2016.

**W. Keaswejjareansuk**, J. Liang, X. Wang. "Electrospun Separator for Structural Battery Applications." Poster presented at Cabot 2016 Students Materials Research Forum, Billerica, Massachusetts, June 2, 2016.

**W. Keaswejjareansuk**, J. Liang, X. Wang. "Electrospun Separator for Structural Battery Applications." Poster presented at the 2016 American Society for Engineering Education – Northeast Conference, Kingston, Rhode Island, April 28, 2016.

**W. Keaswejjareansuk**, J. Liang, X. Wang. "Electrospun Separator for Structural Battery Applications." Poster presented at the WPI 8th Annual Sustainability Project Competition: Envisioning Sustainable Futures, Worcester, Massachusetts, April 20, 2016.

**W. Keaswejjareansuk**, J. Liang, X. Wang. "Electrospun Separator for Structural Battery Applications." Poster presented at the WPI Annual Graduate Research Innovation Exchange, Worcester, Massachusetts, February 3, 2016.

# APPENDIX 3 - CHEMICAL ABBREVIATIONS

CA – cellulose acetate

CF – carbon fiber

CNT – carbon nanotube

DA – dophamine

DEGBA – bisphenol A diglycidyl ether

DMC – dimethyl carbonate

EC – ethylene carbonate

$LiClO_4$ – lithium perchlorate

$LiFePO_4$ – lithium iron phosphate

GO – graphene oxide

OPSZ – organopolysilazane

PAA – polyamic acid

PAN-polyacrylonitrile

PBS – poly(butylene succinate)

PC – propylene carbonate

PEO – polyethylene oxide

PEI – polyethyleniminepd

PPESK – Poly(phthalazinone ether sulfone ketone)

PES – poly(ethersulfone)

PI – polyimide

PLA – poly(lactic acid)

PMDA – pyromellitic diahydride

PMIA – poly-m-phenylene isophthalamide

PMMA – poly(methyl methacrylate)

PTFE - Polytetrafluoroethylene

PU – polyurethane

PVdF – polyvinyllidene difluoride

PVdF-HFP – poly(vinylidene fluoride-co-hexafluoropropylene)

PVP – polyvinylpyrrolidone

TBAC – tetrabutylammonium chloride

TEGDA – tri(ethylene glycol) diacrylate